2019

STUDIES OF OXIDATIVE DAMAGE, BRAIN PROTEOME, AND NEUROCHEMICAL METABOLITES IN COGNITIVE AND NEURODEGENERATIVE DISORDERS: (1) CHEMOTHERAPY-INDUCED COGNITIVE IMPAIRMENT; (2) PARKINSON DISEASE RAT MODEL

Xiaojia Ren
University of Kentucky, xj.ren.work@gmail.com
Digital Object Identifier: https://doi.org/10.13023/etd.2020.024

STUDENT AGREEMENT:

I represent that my thesis or dissertation and abstract are my original work. Proper attribution has been given to all outside sources. I understand that I am solely responsible for obtaining any needed copyright permissions. I have obtained needed written permission statement(s) from the owner(s) of each third-party copyrighted matter to be included in my work, allowing electronic distribution (if such use is not permitted by the fair use doctrine) which will be submitted to UKnowledge as Additional File.

I hereby grant to The University of Kentucky and its agents the irrevocable, non-exclusive, and royalty-free license to archive and make accessible my work in whole or in part in all forms of media, now or hereafter known. I agree that the document mentioned above may be made available immediately for worldwide access unless an embargo applies.

I retain all other ownership rights to the copyright of my work. I also retain the right to use in future works (such as articles or books) all or part of my work. I understand that I am free to register the copyright to my work.

REVIEW, APPROVAL AND ACCEPTANCE

The document mentioned above has been reviewed and accepted by the student's advisor, on behalf of the advisory committee, and by the Director of Graduate Studies (DGS), on behalf of the program; we verify that this is the final, approved version of the student's thesis including all changes required by the advisory committee. The undersigned agree to abide by the statements above.

Xiaojia Ren, Student

Dr. D. Allan Butterfield, Major Professor

Dr. Yinan Wei, Director of Graduate Studies

STUDIES OF OXIDATIVE DAMAGE, BRAIN PROTEOME, AND NEUROCHEMICAL METABOLITES IN COGNITIVE AND NEURODEGENERATIVE DISORDERS: (1) CHEMOTHERAPY-INDUCED COGNITIVE IMPAIRMENT; (2) PARKINSON DISEASE RAT MODEL

DISSERTATION

A dissertation submitted in partial fulfillment of the
requirements for the degree of Doctor of Philosophy in the
College of Arts and Sciences
at the University of Kentucky

By

Xiaojia Ren

Lexington, Kentucky

Director: Dr. D. Allan Butterfield, Professor of Chemistry

Lexington, Kentucky

2019

ABSTRACT OF DISSERTATION

STUDIES OF OXIDATIVE DAMAGE, BRAIN PROTEOME, AND NEUROCHEMICAL METABOLITES IN COGNITIVE AND NEURODEGENERATIVE DISORDERS: (1) CHEMOTHERAPY-INDUCED COGNITIVE IMPAIRMENT; (2) PARKINSON DISEASE RAT MODEL

The rate of cancer patients is increasing as the development of science and technology. Twenty million cancer survivors are estimated living in the United States by 2025. However, many cancer survivors show cognitive dysfunction, negatively affecting the quality of life. These cognitive impairments are recognized as chemotherapy-induced cognitive impairment (CICI), also called "chemo brain" by cancer survivors, including the diminished ability of memory and learning, hard to concentrate and focus, as well as diminution of executive function and processing speed. The etiologies and pathologies of CICI are complicated, especially in most cases the anti-cancer drug cannot cross the blood-brain barrier (BBB).

One of the significant candidate mechanisms underlying CICI is chemotherapy-induced, oxidative damage-mediated tumor necrosis factor-alpha (TNF-a) elevation. One of the prototypes of reactive oxygen species (ROS)-generating chemotherapeutic agents is Doxorubicin, normally used as part of multi-drug chemotherapeutic regimens to treat solid tumors and lymphomas. In this dissertation, TNF-a null (TNFKO) mice were used to investigate the role of TNF-a in Dox-induced, oxidative damage-mediated alterations in brain. Dox-induced oxidative damage in brain is ameliorated and brain mitochondrial function is preserved in brains of TNFKO mice. Both Dox-decreased levels of hippocampal choline-containing compounds and activities of brain phospholipases are partially protected in the TNFKO group. It is shown in this dissertation that Dox-targeted mitochondrial damage and the levels of brain choline-containing metabolites, as well as the activities of phosphatidylcholine-specific phospholipase C (PC-PLC) and phospholipase D (PLD), are decreased in the CNS and associated with oxidative damage mediated by TNF-a. The results are discussed with respect to identifying a potential therapeutic target to protect against cognitive problems after chemotherapy and thereby improve the quality of life of cancer survivors.

We also tested the effect of a chemotherapy drug adjuvant, 2-mercaptoethane sulfonate sodium (MESNA), on CICI in this dissertation research. In this dissertation research, MESNA ameliorates Dox-induced oxidative protein damage in plasma and decreases subsequent oxidative damage in brain of Dox-treated mice. MESNA also is demonstrated to rescue the memory deficits caused by Dox in the novel object recognition test. The activity of PC-PLC is preserved when MESNA was co-administered with Dox. This study demonstrates the protective effects of MESNA on Dox-related protein oxidation, cognitive decline, phosphocholine levels, and PC-PLC activity in brain and suggests novel potential therapeutic targets and strategies to mitigate CICI.

Parkinson Disease (PD) is considered as the second most neurodegenerative disease, associated with aging and gender. Although the detailed mechanisms remain unknown, inflammation and oxidative damage are two main etiological factors of PD. Certain genetic factors have been discovered related to this disease. Thus, using rodent models with relative gene mutations are the main strategies to investigate PD. However, an ideal rodent model of PD, showing same clinical and biochemical features of PD, has not been found. PTEN-induced putative kinase -1 (PINK1) knockout (KO) rat is the rodent model investigated in this dissertation research. The oxidative damage in the brain of PINK1 KO rats, the ventricle sizes, and neurochemical metabolite profiles in these rats as a function of age and gender were measured. Distinct gender- and age-related alterations were found, many consistent with those in PD. The proteome of brain of PINK1 KO rat as a function of age also was studied. Based on the collected data, the suitability of this unique rat as a faithful model of known characteristics of PD is discussed.

KEYWORDS: Oxidative Damage, MRS, Parkinson Disease, PINK1, Doxorubicin, Chemotherapy-induced Cognitive Impairment (CICI)

Xiaojia Ren

(Name of Student)

12.18.2019

Date

STUDIES OF OXIDATIVE DAMAGE, BRAIN PROTEOME, AND NEUROCHEMICAL METABOLITES IN COGNITIVE AND NEURODEGENERATIVE DISORDERS: (1) CHEMOTHERAPY-INDUCED COGNITIVE IMPAIRMENT; (2) PARKINSON DISEASE RAT MODEL

By
Xiaojia Ren

Dr. D. Allan Butterfield
Director of Dissertation

Dr. Yinan Wei
Director of Graduate Studies

12.18.2019
Date

To
my parents,
my husband Ning, my daughter Taole,
and my Ph.D. professor Dr. Butterfield.

ACKNOWLEDGMENTS

I would first like to extend my deepest gratitude to my Ph.D. professor, Dr. D. Allan Butterfield. Without his knowledge, guidance, support, and mentorship, I would not have become the scientist that I am today. No word can express how thankful I am to Dr. Butterfield. I wish to offer my sincerest thanks to my Ph.D. advisory committee (Dr. Yinan Wei, Dr. Bert Lynn, and Dr. Chuang-guo Zhan, and Dr. Elizabeth Head) for their time, patient guidance, and encouragement. The suggestion and comments from them made me more successful in Ph.D. studies. I would also like to thank my outside examiner of my defense, Dr. Tadahide Izumi, for his valuable comments for my dissertation and future studies.

I am also very grateful to past group members, including Dr. Rukhsana Sultana, Dr. Jeriel Keeney, Dr. Judy Triplett, Dr. Aaron Swomely, Dr. Sarah Förster, and Dr. Antonella Tramutola, for their willingness to teach me new experimental techniques and to help me learn how to troubleshoot experiments. I want to thank Shekinah Alfaro, who is always ready with a helping hand. I also would like to thank other members of the Butterfield laboratory for their help in shaping my scientific development, for being there to discuss the science and for their offers of assistance.

I am thankful to the research collaborators, Teresa, Dr. D. St Clair, Dr. D. Powell, Dr. K. Saatman, Dr. S. Barron, Dr. P. Nelson, Dr. J. Cai, Dr. J. Klein, Dr. H. Zhu, Dr. J. Chen and their lab members who have made contributions to the projects in this dissertation research. Specifically, I would like to thank Dr. Cai and Dr. Powell for their generous help and patience for teaching me the MS and MRS associated knowledge. I also wish to thank the University of Kentucky, Department of Chemistry chair, Dr. Meier, and

the directors of graduate studies, Dr. Anthony, Dr. Yang, Dr. Lovell, and Dr. Wei, and to all of the faculty and staff who have helped me along the way to achieving my goals. Especially thank Art Sebesta for his help with the instruments. Thanks chemistry department offered me research challenge trust funds.

Importantly, I want to extend my gratitude to friends and family who have believed in me and offered their unconditional support. Thanks for my mother Hongjun and my father Dr. Ren. They gave me endless supports on both life and study. Thanks to my husband, Ning. I cannot achieve success without his support and understanding. Thanks to my daughter, Taole. She brings light to my life. Thanks for the time I spent with Dr. Lei and Dr. Shuang. They made my Ph.D. life more enjoyable, and happy and always think of me. I miss the days I stayed with them. Thank Mr. Y.L. Zhu and Mr. Y. Liu. Their attitudes for work and life spirited me always to be kind, gentle, and responsible, and endeavor to do what should be done.

TABLE OF CONTENTS

ACKNOWLEDGMENTS iii

LIST OF TABLES viii

LIST OF FIGURES ix

CHAPTER 1. INTRODUCTION 1

CHAPTER 2. BACKGROUND 4

2.1 Oxidative damages and neurodegeneration 4
2.1.1 Protein carbonyls (PC) 4
2.1.2 Tyrosine nitration (3-NT) 5
2.1.3 Lipid peroxidation and 4-hydroxy-2-trans-nonenal (HNE) 5

2.2 Chemotherapy-induced cognitive impairment (CICI) 6
2.2.1 Candidate mechanisms of CICI 6
2.2.2 Dox and MESNA 10
2.2.2.1 Doxorubicin (Dox) 10
2.2.2.2 2-mercaptoethane sulfonate sodium salt (MESNA) 11

2.3 Parkinson disease (PD) 17

CHAPTER 3. PROTECTION BY MESNA FROM DOXOCUBICIN-INDUCED ELEVATED OXIDATIVE DAMAGE AND NEUROCHEMICAL CHANGES IN BRAIN WITH COGNITIVE DECLINE: INSIGHT INTO MECHANISMS OF CHEMOTHERAPY-INDUCED COGNITIVE IMPAIRMENT (CICI) 20

3.1 Overview 20

3.2 Introduction 21

3.3 Materials and Methods 23
3.3.1 Chemicals 23
3.3.2 Animals 23
3.3.3 Hydrogen magnetic resonance spectroscopy (H^1-MRS) 24
3.3.4 Cognitive function testing: Novel object recognition and open field test 25
3.3.5 Sample collection 26
3.3.6 Sample preparation 26
3.3.7 Slot blot assay 27
3.3.8 Measuring the activity of Phospholipase C and phospholipase D 28

3.4 Results 28
3.4.1 Dox administration results in increases in oxidative damage markers in both brain and plasma 28

3.4.2 Dox administration results in cognitive impairment and decreased locomotor activity31
3.4.3 Dox administration results in a decreased level of choline-containing compounds in the hippocampus 33
3.4.4 Dox administration results in decreased PC-PLC and PLD activity 35
3.5 Discussion 37

CHAPTER 4. THE TRIANGLE OF DEATH OF NEURONS: OXIDATIVE DAMAGE, MITOCHONDRIAL DYSFUNCTION, AND LOSS OF CHOLINE-CONTAINING BIOMOLECULES IN BRAINS OF MICE TREATED WITH DOXORUBICIN: ADVANCED INSIGHTS INTO MECHANISMS OF CHEMOTHERAPY-INDUCED COGNITIVE IMPAIRMENT ("CHEMOBRAIN") INVOLVING TNF-A 47

4.1 Overview 47
4.2 Introduction 48
4.3 Methods and Materials 50
4.3.1 Chemicals 50
4.3.2 Animals 50
4.3.3 Hydrogen magnetic resonance spectroscopy (H^1-MRS) 51
4.3.4 Sample collection 52
4.3.5 Sample preparation 52
4.3.6 Slot blot assay 53
4.3.7 Brain mitochondria isolation and bioenergetic analysis 53
4.3.8 Phospholipase C and phospholipase D activity assays 55
4.4 Results 56
4.4.1 Dox administration results in increased oxidative damage markers in brain and plasma of WT mice that is absent in brain of TNFKO mice 56
4.4.2 Dox administration leads to altered oxygen consumption rate in WT mice brain mitochondria that is prevented in TNFKO mice 59
4.4.3 Changes to the neurochemical profile in hippocampus following Dox administration 61
4.4.4 Dox administration to TNFKO mice results in partial preservation of PLD activity63
4.5 Discussion 65

CHAPTER 5. PROFILES OF BRAIN OXIDATIVE DAMAGE, VENTRICULAR ALTERATIONS, NEUROCHEMICAL METABOLITES IN THE STRIATUM, AND BRIAN PROTEOME OF PINK1 KNOCKOUT RATS AS FUNCTIONS OF AGE AND GENDER: RELEVANCE TO PARKINSON DISEASE 71

5.1 Overview 71
5.2 Introduction 71

5.3 Materials and methods 73
5.3.1 Chemicals 73
5.3.2 Animals 74
5.3.3 Hydrogen magnetic resonance spectroscopy 74
5.3.4 Measuring Ventricle sizes of rat's brain on the MRI imaging 75
5.3.5 Sample preparation 76
5.3.6 Slot blot assay 76
5.3.7 Isoelectric focusing (IEF) 77
5.3.8 Two-dimensional polyacrylamide gel electrophoresis (2D-PAGE) 78
5.3.9 Sypro Ruby staining 78
5.3.10 PDQuest image analyses 79
5.3.11 In-gel trypsin digestion 79
5.3.12 Gel-peptide extraction and desalting 80
5.3.13 LC-MS analysis, data interrogation and protein identification 81

5.4 Results 81
5.4.1 Age and gender both affect the oxidative damage in the rat brains. 81
5.4.2 PINK1 KO male rats have larger ventricle size than female PINK1 KO rats at the same age, suggesting more edema occurs in male PINK1 KO rats. 86
5.4.3 Changes in neurochemical metabolites in striatum of rats were observed as age or gender varies. 88
5.4.4 Changes in the brain proteome of PINK1 KO rats associated with age 92

5.5 Discussion 95

CHAPTER 6. CONCLUSIONS AND FUTURE STUDIES 102

6.1 Conclusions and future studies of project 1: CICI 102
6.1.1 Conclusions of CICI project 102
6.1.2 Future studies of CICI 107

6.2 Conclusions and future studies of project 2: PD 107
6.2.1 Conclusions of PD project 107
6.2.2 Future studies for PD 108

APPENDIX 110

REFERENCES 125

VITA 147

LIST OF TABLES

Table 5.1 Proteins with altered expression in brain of *PINK1* KO rats. 93
Table 5.2 Fold changes of the seven identified proteins as age increases in the brain of *PINK1* KO rats. 94

LIST OF FIGURES

Figure 2.1 The candidate mechanisms of chemotherapy-induced cognitive impairment (CICI) 10
Figure 2.2 Structure of Dox and how Dox generate superoxide..... 11
Figure 2.3 Structure of MESNA 12
Figure 3.1 The effects of Dox and MESNA on the levels of PC and protein-bound HNE in brain and plasma. 30
Figure 3.2 The effects of Dox and MESNA in behavioral NOR and open field tests. 32
Figure 3.3 H^1-MRS results of mouse hippocampus..... 34
Figure 3.4 Phosphatidylcholine-specific phospholipase C (PC-PLC) and Phospholipase D (PLD) activity in brain 72 h post-treatment. 36
Figure 3.5 A pictorial summary of the effects of Dox and MESNA in plasma and brain of mice in the current chapter. 38
Figure 3.6 A putative pathway to apoptosis following Dox-induced TNF-α elevation. ... 43
Figure 3.7 A proposed model of the mechanism of CICI and protective effect of MESNA. 45
Figure 4.1 The levels of protein oxidation and lipid peroxidation were presented by the levels of PC and protein-bound HNE. 58
Figure 4.2 Mitochondrial function in brain of mice treated with Dox and Saline. 60
Figure 4.3 Dox-resulted Cho/Cr ratio decreases in hippocampus could be partially protected by the absence of TNF-α. 62
Figure 4.4 PC-PLC and PLD activities in brain of wild-type and TNFKO mice after Dox or saline treatment. 64
Figure 4.5 Schematic illustration of the sequelae of events in brain following Dox treatment of mice and their prevention or modulation in mice lacking the gene for TNF-α. 66
Figure 5.1 The levels of the biomarker of oxidative damage: protein carbonyl, protein-bound HNE, and 3-NT in the brain of WT and *PINK1* KO rats at different ages and genders. 85
Figure 5.2 The ventricle sizes were measured from MRI images. 87
Figure 5.3 H^1-MRS was used to quantify the changes in levels of neurochemical metabolites in the rat striatum. 89
Figure 5.4 H^1-MRS was used to quantify the neurochemical metabolites changes in the rat striatum. 90
Figure 5.5 H^1-MRS was used to quantify the neurochemical metabolites changes in the rat striatum. 91
Figure 6.1 An expanded model of the mechanism of CICI. 106

CHAPTER 1. INTRODUCTION

The studies displayed in this dissertation mainly investigate the biochemical mechanisms of chemotherapy-induced cognitive impairment (CICI) and the second most neurodegenerative disease, Parkinson disease (PD), by exploring the oxidative damage, brain proteome, and potentially subsequent changes of neurochemical metabolites, mitochondria function, and activities of phospholipases in brain of rodent animal. Utilizing the results as evidence, we propose the conceivable factors and implicated proteins contributing to the etiologies, progression, and pathologies of these cognitive and neurodegenerative disorders, as a consequence, providing potential prevention and targets for mitigating the adverse effects from CICI and PD, thereby improving the quality of life of the patients and cancer survivors.

Brain is the organ which consumes the most oxygen in the bodies of human beings. This feature contributes to the fact that brain has a high level of reactive oxygen species (ROS) and resultant oxidative stress. Thus, it is crucial to maintain the antioxidative ability of brain. Increased oxidation products or exposure, and/or decreased levels of antioxidant capacity in the brain could lead to many biochemical and signaling changes including mitochondrial dysfunction and neuronal death, and as the outcome, cognitive impairments. Over fifty percent of FDA-approved chemotherapeutic drugs generate reactive oxygen species. The antioxidant capacity decreases as age increases. It is not unexpected that many cancer survivors and patients with age-associated neurodegenerative disorders share similar symptoms associated with cognitive loss, including diminished abilities in memory, focusing, executive function, and multi-tasking. With the developments of sciences and technologies, longer life with good quality is one of the most expectation in the world.

In the first part of this dissertation research, the ROS-generating anti-cancer drug, Doxorubicin (Dox), was used as the prototype to study the underlying mechanisms of CICI, especially in the cases of the drugs that cannot cross the blood-brain barrier (BBB). The chemotherapy adjuvant drug 2-mercaptoethane sulfonate sodium (MESNA) was used to test the hypothesis that MESNA is an effective adjuvant to prevent CICI. TNF-α knockout (KO) mice were used to examine the consequences of Dox on the brain with the absence of TNF-α.

In the second part, this dissertation research studied the functions of age and gender in the brain of a potential rodent model for PD, PTEN-induced putative kinase 1 (PINK1) knockout (KO) rats. PINK1 is a mitochondrial surveillance kinase that contributes to the processes involved in eliminating damaged mitochondria from cells. By measuring the oxidative damage and proteome in the global brain, the sizes of brain ventricles, and the neurochemical metabolite profiles of the striatum, the suitability of this unique rat as a faithful model that can recapitulate all of the known dominate characteristics of PD was investigated.

The overall hypothesis of this dissertation research is that oxidative damage is one of the critical factors underlying cognitive and neurodegenerative disorders, including CICI and PD, while together with biochemical changes and mitochondrial dysfunctions in brain contribute to the pathological mechanisms of CICI and PD. To support the overall hypothesis, we investigated plausible answers to the following questions through this dissertation research:

1. Will MESNA be a potential preventative intervention of CICI by scavenging the oxidative damage in the periphery?

2. Does the Dox-initiated, oxidative damage-mediated inflammatory factor TNF-α play an essential role in the formation of CICI?

3. Is PINK1 KO rat an ideal animal model for studying the mechanisms of familial PD?

   a. Does the level of oxidative damage in the brain of PINK1 KO rat change as a function of age and gender?

   b. What biochemical and structural changes exist in PINK1 KO rats' brain as a function of age and gender?

   c. Which proteins in the brain may be implicated in the progression of the PD model?

CHAPTER 2. BACKGROUND

2.1 Oxidative damages and neurodegeneration

Neurodegeneration is a pathological condition of neurons with progressive and selective loss of structures and functions that are essential for cognition (Przedborski et al., 2003). Oxidative damages to DNA, protein, and lipids were shown not only in the normal aging process but also in cognitive and neurodegenerative diseases as central characteristics (Ischiropoulos and Beckman, 2003).

Brain is an organ with high oxygen molecule consumption but with a low capacity of antioxidant defense, containing large numbers of polyunsaturated fatty acids (PUFA), which is easy to be attacked by free radicals. Thus, the balance between antioxidants and oxidative damage is crucial to the health of brain. Antioxidant enzymes are essential to protect brain and maintain the redox state from oxidative damage. Many heat shock proteins, superoxide dismutase (SOD), glutathione peroxidase, peroxiredoxins, bilivaerdin reductase, and catalase are common antioxidant enzymes. Meanwhile, some molecules also carry the ability of anti-oxidation, such as glutathione, lipoic acid, and Vitamins C, D and E (Gilgun-Sherki et al., 2001). When the levels of oxidative stress, such as toxic reactive oxygen species (ROS) and reactive nitrogen species (RNS), are greater than the capacity of the brain antioxidant protection, oxidative damage is formed. General ROS and RNS include hydroxyl radicals, hydrogen peroxide, superoxide ($O_2^{-\bullet}$), peroxynitrite, and nitric oxide.

2.1.1 Protein carbonyls (PC)

The most frequently used biomarker for measuring the level of oxidative damage

is PC. As a result of the oxidative protein modification, carbonyl groups can be formed by direct oxidation on the amino acid side chain, glycoxidation, oxidative cleavage of the peptide backbone, or binding of aldehydes formed from lipid peroxidation (Aksenov et al., 2001; Butterfield, 1997; Butterfield et al., 2002).

2.1.2 Tyrosine nitration (3-NT)

3-nitrotyrosine results from the addition of a nitro group at the 3- position of tyrosine. Nitrated tyrosine may trigger proteasomal degradation of proteins hence cause the death of neurons (Gow et al., 1996; Mattson et al., 1997). Furthermore, this extra nitration could affect the phosphorylation of tyrosine, catalyzed by tyrosine kinase, by sterical interference. As a consequence, 3-NT changes the activity of tyrosine kinase (Tangpong et al., 2007).

2.1.3 Lipid peroxidation and 4-hydroxy-2-trans-nonenal (HNE)

As stated above, brain is rich in PUFA. Allylic hydrogen is removed by free radicals from the lipid acyl chain of PUFA, initiating the lipid peroxidation. A carbon-centered radical is formed. This radical can react with oxygen molecules to produce a peroxyl radical. Radical-radical chain reaction propagates the lipid peroxidation via redox cycling, leading to further allylic hydrogens removed from the lipid acyl chain and reactive alkenals. As a result, lipid asymmetry is lost and neuronal apoptosis is triggered (Castegna et al., 2004). When the lipid peroxidation happens on arachidonic acid, HNE is formed. HNE can bind Cys, His, and Lys residues of proteins by Michael's addition reaction, leading to structural and functional changes of proteins (Butterfield et al., 2010).

2.2 Chemotherapy-induced cognitive impairment (CICI)

Increasing numbers of cancer patients survive and live longer than five years after therapy, but very often side effects of cancer treatment arise at the same time. One of the side effects, chemotherapy-induced cognitive impairment (CICI), also called “chemo brain” or “chemofog” by patients, brings enormous challenges to cancer survivors following successful chemotherapeutic treatment. Decreased abilities of learning, memory, attention, executive function, and processing speed in cancer survivors with CICI are some of the challenges that greatly impair survivors’ quality of life. The molecular mechanisms of CICI involve very complicated processes, which have been the subject of investigation over the past decades. Many mechanistic candidates have been studied including disruption of the blood-brain barrier (BBB), DNA damage, telomere shortening, oxidative damage and associated inflammatory response, gene polymorphism of neural repair, altered neurotransmission, and hormone changes. Oxidative damage is considered as a vital mechanism since over 50% of FDA-approved anti-cancer drugs can generate ROS or reactive nitrogen species RNS, which lead to neuronal death.

2.2.1 Candidate mechanisms of CICI

With advances in science and technology for the treatment of cancer, the number of cancer survivors continues to increase. There were more than 15.5 million cancer survivors at the end of 2015, and this number could rise to 20 million in the next 10 years (Miller et al., 2016). Cognitive dysfunction may happen acutely or after a period following chemotherapy. The phenomenon, called CICI, “chemobrain” or “chemofog” can be subtle or severe. CICI can retard recovery to normal life for cancer survivors, and this condition involves loss of memory and learning ability, less attention and concentration, decreased

executive function, and slower processing speed (Ahles and Saykin, 2007; Butterfield, 2014; Hermelink, 2015; Moore, 2014).

As many as 35%-70% of breast cancer survivors reported cognitive impairment after or even during the treatment (Runowicz et al., 2016). Cognitive impairment affects one-third of childhood cancer survivors (Castellino et al., 2014). In a national cross-sectional study, participants who had a cancer history reported memory impairment 40% more than those without cancer (Jean-Pierre et al., 2012). In a recent study, 65% of breast cancer patients experienced acute cognitive impairment, and 61% of them had late cognitive decline, compared to 21% of patients who had cognitive dysfunction before chemotherapy (Wefel et al., 2010). CICI can even last 20 years post-chemotherapy for breast cancer (Koppelmans et al., 2012). Breast cancer survivors who were treated with cyclophosphamide, methotrexate, and fluorouracil about 21 years ago were recruited. Compared to a non-cancer group, the 196 cancer survivors self-reported more memory complaints and poorer performance in neuropsychological examinations including verbal memory, processing speed, executive function and psychomotor speed (Koppelmans et al., 2012). However, although there is strong evidence for CIC, there also are studies showing no significant cognitive changes before and after chemotherapy (Debess et al., 2010; Moore et al., 2014; Vitali et al., 2017).

The central nervous system (CNS) is affected by chemotherapeutic agents, many of which do not cross the blood-brain barrier (BBB) (Chen et al., 2007). Chemotherapy could lead to pathological changes such as reduced brain connectivity (Kesler, 2014; Kesler and Blayney, 2016; Kesler et al., 2015; Wefel et al., 2015). Consistent with this notion, brain structure and function both are altered in CICI. Volume and density changes of white matter

and grey matter of patients who had chemotherapy were determined by MRI (Deprez et al., 2012; McDonald et al., 2010; Conroy et al., 2013; McDonald et al., 2013). Altered prefrontal cortex and hippocampus also are associated with CICI (Barry et al., 2018; Cheng et al., 2017; Groves et al., 2017; Lee et al., 2017; Raffa, 2010). Hippocampus is an area important for learning and memory in brain. Chemotherapy disrupted the structure and function of hippocampus and impaired its neurogenesis, leading to cognitive deficits (Dietrich et al., 2015).

Functional and structural MRI is a strong tool to demonstrate brains in cancer survivors are different from brains of people not treated with chemotherapeutic agents or healthy people with no cancer, especially in the cases of patients who did not show big differences on neuropsychological tests compared to her healthy monozygotic twin, but had self-reported cognitive impairment (Ferguson et al., 2007). Such changes indicate that cancer survivors who had chemotherapy have to activate more areas in the brain and make more efforts to maintain the ability of work, even if they show a normal aspect in neuropsychological tests (Reuter-Lorenz and Cimprich, 2013). PET scanning also revealed abnormal glucose metabolism in brain of cancer survivors who had undergone chemotherapy (Baudino et al., 2012; Ganz et al., 2013).

A better understanding of the molecular mechanisms of CICI is important to reduce or even prevent cognitive dysfunction after cancer treatment, with the goal of improving the quality of life of survivors without changing chemotherapeutic efficacy. This is particularly the case for those childhood patients and adult patients who live longer. However, the mechanisms of CICI still are not fully understood. A complication of CICI is that it is likely multifactorial in origin, and it shares similar appearances and causes with depression,

anxiety, and fatigue, which are commonly associated with cancer treatment and cancer per se (Ahles and Saykin, 2007; Moore, 2014). Lack of education and aging could be other confounders (Ahles et al., 2008; Janelsins et al., 2017).

Neuronal activity is often altered by chemotherapy (Manchon et al., 2016; Liu et al., 2014). Neuronal apoptosis was observed in correlation with cognitive impairments associated with traumatic brain injury, aging, several neurodegenerative disease and chemotherapy (Avila et al., 2017; Butterfield, 2014; Walker and Tesco, 2013). NMDA receptor antagonists, such as memantine, could reverse the cognitive deficits and protect memory functions by blocking NMDA receptors during chemotherapy treatment (Cole et al., 2013; Vijayanathan et al., 2011). Co-administration of the anti-cancer drug, methotrexate, with the NMDA receptor antagonist dextromethorphan reduced the severity of seizures (Drachtman et al., 2002). However, these antagonists can cause significant side effects (Haddad and Dursun, 2008).

As noted above, neuronal death, which underlies CICI symptoms, occurs even though many FDA-approved anti-cancer drugs cannot cross the BBB. Recent studies suggested that decreased integrity of the BBB, low availability of DNA and neural repair processes, decreased antioxidant levels and increased oxidative damage, hormone changes and immune system responses contribute to neurotoxicity, and eventual neuronal death with subsequent cognitive impairments following chemotherapy (Ahles and Saykin, 2007; Butterfield, 2014; Moore, 2014; Seigers et al., 2013). The candidate mechanisms are shown in Fig. 2.1 above.

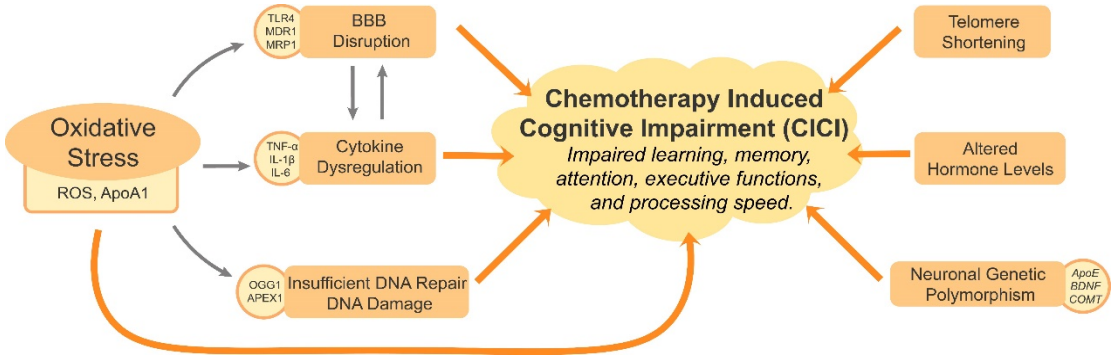

Figure 2.1 The candidate mechanisms of chemotherapy-induced cognitive impairment (CICI)

2.2.2 Dox and MESNA

2.2.2.1 Doxorubicin (Dox)

Dox is an FDA-approved ROS-generating chemotherapeutic drug, prototypically used to treat solid tumors and lymphoma. Dox contains a quinone moiety in its structure. This quinone moiety can be reduced to a semi-quinone (Aluise et al., 2011; Chen et al., 2007) with the presence of NADPH oxidase, Fe^{2+}, Cu^{+} or cytochrome P450 (Butterfield, 2014). Undergoing O_2 oxidation, this semi-quinone is converted back to the quinone structure and produce reactive superoxide, one of the ROS, at the same time (shown in Fig. 2.2). By utilizing the ROS productions, along with inhibiting topoisomerase II and intercalating into DNA, Dox kills cancer cells (Bachur et al., 1977; Chuang and Chuang, 1979; Cummings et al., 1991; Deres et al., 2005; Reich et al., 1979).

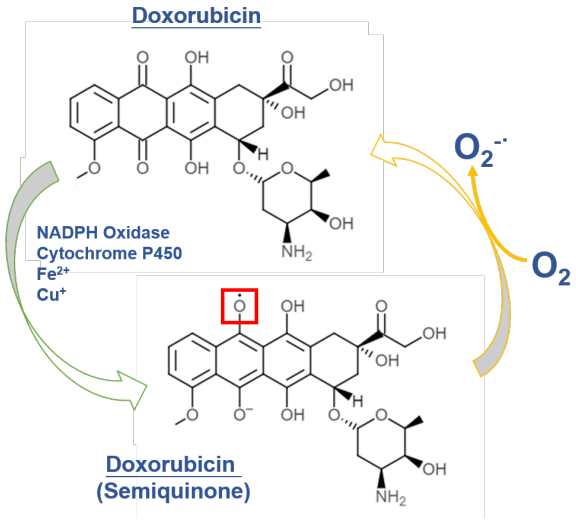

Figure 2.2 Structure of Dox and how Dox generate superoxide

Although in most cases Dox does not cross the BBB, the Butterfield lab in collaborated with the St. Clair lab has provided evidence of that peripheral administration of Dox leads to oxidative damage, dysfunctional mitochondria and elevated TNF-α in brain, prompting brain injury and further cognitive impairments (Joshi et al., 2007; Tangpong et al., 2006, 2007, 2008).

2.2.2.2 2-mercaptoethane sulfonate sodium salt (MESNA)

MESNA is often prescribed for persons being treated with regimens of ifosfamide and/or cyclophosphamide chemotherapy to prevent hemorrhagic cystitis in the bladder by scavenging the metabolic by-product of these drugs, acrolein (Butterfield, 2014; Furlanut and Franceschi, 2003). The free sulfhydryl group of MESNA provides its antioxidant properties. MESNA also is used as an adjuvant shown to suppress lipid peroxidation such as acrolein or HNE in plasma without alleviating cancer drug functions (Zhang et al., 2014) as its negative charge makes MESNA unable to enter cancer cells (Butterfield, 2014). Co-administration of MESNA with Dox can diminish Dox-induced oxidation on

apolipoprotein A-I (ApoA1) (Aluise et al., 2011). The structure of MESNA is shown in Fig. 2.3.

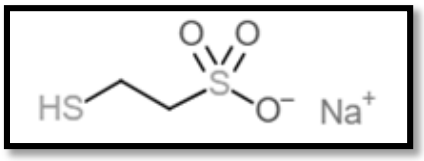

Figure 2.3 Structure of MESNA

2.2.3 Oxidative damage, pro-inflammatory cytokines, and CICI

Oxidative damage and correlated mitochondrial damage often occur in cancer patients or survivors after the treatment of chemotherapeutic agents and are considered as one of the main candidate mechanisms of CICI (Butterfield, 2014; Gaman et al., 2016). Although some cancer patients reportedly may have high levels of oxidative damage and cognitive impairment before chemotherapy, many chemotherapeutic agents are ROS-generating and are associated with DNA and protein damage in both the periphery and brain (Ahles and Saykin, 2007; Butterfield, 2014). Immune responses follow the increase in oxidative damage, increasing pro-inflammatory cytokines locally and activate immune cells in brain. Superoxide ($O_2^{-\bullet}$) can increase the level of oxidative damage markers in mice plasma and activate macrophages with a large production of TNF-α after incubating plasma or macrophage culture with potassium superoxide (Keeney et al., 2015). ROS also is an initiator of BBB disruption, triggering BBB oxidative damage, tight junction modification and matrix metalloproteinase activation (Pun et al., 2009). Dexrazoxane, an iron chelator that can interfere with and decrease free radical formation by its putative antioxidant ability is reportedly cardioprotective when it is administrated with Dox (Bansal et al., 2018; Junjing et al., 2010). This study supports the notion that free oxidative damage is integral

to CICI. Protein oxidation, lipid peroxidation, and dysfunctional BBB make drugs and cytokines easier to enter the brain, the organ which, as noted above, is more vulnerable to oxidative damage due to its high oxygen consumption rate and large presence of unsaturated fatty acid with associated labile allylic hydrogen atoms. Impaired mitochondria in brain secondary to chemotherapy-induced oxidative and nitrosative damage result in elevation of oxidative damage and eventually neuronal death, along with the decreased antioxidant level and glucose dysmetabolism by inactivation of complex I (Tangpong et al., 2006, 2007). Although not relevant to CICI directly since Dox does not cross the BBB, mitochondrial damage was found in Dox-treated neurons (Moruno-Manchon et al., 2016) and is associated with cognitive impairment in aging, traumatic brain injury, or neurodegenerative disorders such as PD or AD (Chaturvedi and Flint Beal, 2013; Liu et al., 2002; Sauerbeck et al., 2011). Accumulation of lipofuscin was also found in brain of Dox-treated mice brain along with altered autophagosomes (Moruno-Manchon et al., 2016).

Superoxide formed via redox cycling produced by Dox led to cardio- and neuro-toxicity. A recent study reported results of rats treated with Dox chronically at a low dose (2mg/kg/week) (El-Agamy et al., 2018). In a step-through passive avoidance test, Dox led to a significantly low memory performance compared to control rats. The number of degenerative hippocampal neurons following Dox correlated with elevated apoptosis, decreased antioxidant glutathione (GSH) levels, diminished activity of catalase, and increased level of the lipid peroxidation product, malondialdehyde (MDA) in hippocampus of treated rats in the same study (El-Agamy et al., 2018). The cognitive impairment and associated neuronal apoptosis were ameliorated by food supplemented with astaxanthin, a carotenoid with antioxidant, anti-apoptotic and anti-inflammatory functions (El-Agamy et

al., 2018). In another study, acute and high dose administration (25mg/kg) of Dox increased oxidative damage indexed by protein-bound HNE and protein carbonyls (PC) in both plasma and brain of mice (Keeney et al., 2018). Novel object cognition (NOR) testing revealed a cognitive impairment of mice 72h after Dox injection. (Keeney et al., 2018). Altered neurochemical profiles in hippocampus and decreased activity of phospholipases in brain also correlated with cognitive impairment (Keeney et al., 2018). All of these deleterious changes were either completely or partially prevented by co-administration of MESNA, an antioxidant drug that scavenges free radicals (Hayslip et al., 2015; Keeney et al., 2018). γ-glutamyl cysteine ethyl ester (GCEkE), a precursor of the antioxidant GSH, restored GSH level and GSH transferase activity in Dox-treated mice brain equivalent to the saline-treated control group, reduced levels of all three oxidative damage markers of protein oxidation and lipid peroxidation in mice brain induced by Dox (Joshi et al., 2007).

BCNU, another name of carmustine [1,3-bis (2-chloroethyl)-1-nitrosourea], is an alkylating chemotherapeutic agent. BCNU-triggered ROS-dependent JNK, and ERK signaling, and apoptosis in neurons could be inhibited by N-acetyl cysteine (NAC) (An et al., 2011). Also, decreased GSH level and glutathione reductase activity were caused by BCNU (An et al., 2011). NAC also protected neurons *in vitro* and rats *in vivo* from cisplatin-induced oxidative damage, mitochondrial dysfunction, and/or cognitive impairment (Lomeli et al., 2017). Dox generated ROS with subsequently elevated peroxisomes in neurons and mice brains (Moruno-Manchon et al., 2018). Maintaining the level of peroxisomes is important to regulate cellular redox homeostasis (Trompier et al., 2014). β-cyclodextrin decreased this Dox-induced ROS production by up-regulating peroxisome-related autophagy (pexophagy) (Moruno-Manchon et al., 2018). Taken

together, all evidence here strongly supports the notion that redox homeostasis is disrupted after many chemotherapeutic agents and that oxidative damage associated with organelle dysfunction plays an important role in CICI.

Antioxidant effectiveness in preventing oxidative damage to brain and other cellular abnormalities following chemotherapy is consistent with the notion of the role of oxidative damage associated with CICI, but this approach normally cannot be pursued in cancer therapy due, in part, to activation of glutathione-S-transferase-mediated coupling of chemotherapeutic agents to reduced GSH and subsequent removal of this complex from the cancer cell by MRP1, thereby decreasing therapeutic efficacy (Jungsuwadee et al., 2009). In contrast, antioxidants that remain and act outside the cancer cells do not interfere with chemotherapy but do scavenge lipid peroxidation products in plasma, preventing inflammatory cytokines from entering the brain parenchyma (Aluise et al., 2011; Butterfield, 2014; Keeney et al., 2018). Moreover, highly redox-active agents that are mitochondrial manganese superoxide dismutase (MnSOD) mimetics, brain-permeable, and selective for mitochondria show great promise of cancer cell death by exacerbating the high oxidative redox state of cancer cells to cause them to undergo apoptosis (Chaiswing et al., 2018).

Oxidative damage mediated CICI is often accompanied by immune response and pro-inflammatory cytokine increase, including IL-1β, IL-6, and TNF-α (Groven et al., 2018; Shi et al., 2018). IL-1β and TNF-α are important to synapse function and neural plasticity (Rizzo et al., 2018). Elevated IL-6 is associated with worsening executive function and poor self-perceived cognitive disturbance in cancer patients (Cheung et al., 2015; Trask et al., 2000). CNS excitability and CICI are associated with peripheral pro-inflammatory

cytokines, modulating functions of neurons and glial cells and neurotransmitter metabolism in brain (Ahles and Saykin, 2007). DNA, synapses and neurites in neurons were also damaged after Dox treatment (Manchon et al., 2016). Chemotherapeutic agents elevate peripheral cytokine levels, which could cross the BBB, leading to immune response, and increase oxidative damage and mitochondria damage in CNS (Butterfield, 2014).

Inflammatory reactions in the CNS are related to activation of the immune cells and originate mainly from microglia (Ransohoff and Perry, 2009). Deficits in hippocampus-based memory ability and highly decreased neurogenesis in brain were found in cyclophosphamide-, cisplatin- or Dox-treated rats, with activated microglia after cyclophosphamide treatment (Christie et al., 2012; Lomeli et al., 2017). The pro-inflammatory enzyme COX-2 also was upregulated with microglia activation and significant cognitive impairment in hippocampus of tumor-bearing mice treated with methotrexate (Yang et al., 2012). Similar results of elevation of COX-2 and prostaglandin E2 were shown in Dox-treated rat hippocampus with increased immunoactivity and glia activation, mediated by the elevated TNF-α (El-Agamy et al., 2018). Activation, death or any status changes of microglia conceivably could lead to more neurological inflammation and neurotoxicity (Santos and Pyter, 2018).

Chemotherapy-induced oxidative damage-mediated TNF-α triggers iNOS production (Tangpong et al., 2007), thereby leading to more oxidative damage and damaged mitochondria. Activated pro-apoptotic proteins p53 and Bax were observed in Dox-treated mice brain associated with TNF-α elevation in both the periphery and the CNS (Tangpong et al., 2006). Apoptotic makers such as released cytochrome c (cyt c) and increased caspase-3 activity have been found in rodent brain after chemotherapy (El-Agamy et al.,

2018; An et al., 2011; Tangpong et al., 2006). The release of cyt c and initiation of apoptotic cascades lead to neuronal death in brain and also to cognitive impairment as consequences (Butterfield, 2014; Keeney et al., 2018; Tangpong et al., 2006).

ApoA1 is possibly one of the key factors in oxidative damage and pro-inflammatory cytokine-mediated CICI. ApoA1 is part of the high-density lipoprotein complex for transporting cholesterol and phospholipids to the liver for degradation. Oxidation and down-regulated expression of ApoA1 were found in a number of neurodegenerative diseases with cognitive deficits, such as AD and PD (Keeney et al., 2013). ApoA1 prevents over-production of IL-1β and TNF-α by interacting with cholesterol transport protein ABCA1 via the JAK2/STAT3 pathway or inhibiting the interaction of monocytes and T-cells (Ren et al., 2017). However, ApoA1 is oxidized by Dox with a concomitant increased TNF-α level and oxidative damage in plasma of cancer patients (Aluise et al., 2011). This result of oxidized ApoA1 correlating with Dox-induced TNF-α elevation also was shown with mice in the same study, and oxidized ApoA1 lost the ability to inhibit TNF-α production in LPS-treated macrophage culture (Aluise et al., 2011).

2.3 Parkinson disease (PD)

Parkinson disease (PD) is the second most common neurodegenerative disease after Alzheimer disease and the most common neurodegenerative movement disorder associated with aging in developed societies. The prevalence of PD is 41 out of 100,000 in people over 40 years old and increases to 1900 out of 100,000 in the eighth decade of life (Cacabelos, 2017). It is estimated that 1,238,000 people over 45 years old in the United State will have PD in 2030 (Marras et al., 2018). Resting tremors, rigidity, postural instability, and bradykinesia constitute important motor symptoms of PD (Cacabelos, 2017;

Jankovic, 2008). Hallucination, anosmia, fatigue, depression, and REM sleep behavior disorder, categorized in non-motor symptoms of PD, may show up years before the onset of motor symptoms (Chaudhuri et al., 2006; Tibar et al., 2018). Gender also affects this disorder of which being male is a risk factor. It was reported that more men than women are diagnosed with PD (Miller and Cronin-Golomb, 2010).

The selective and progressive degeneration of dopaminergic neurons in the substantia nigra pars compacta and aggregation of phosphorylated α-synuclein in Lewy bodies are presented in the PD brain. The exact mechanisms still remain unknown. Brain inflammation and oxidative damage, along with certain environmental factors, and gene mutations, are contemplated as a substantial contribution to the pathologies of PD (Triplett et al., 2015).

2.3.1 Animal Models of PD

Utilizing the animal models with the genetic risk factors of PD is helpful for investigating the roles of these genetic factors in the etiology and pathology of PD. An ideal animal model of PD should display age-associated aspects of defective motor availability, progressive degeneration of dopaminergic neurons, and aberrant pathology of α-synuclein. After studying many-decades in pathogenesis and strategies of therapy of PD with rodent models, an agreement is that a good mouse model to mimic all human PD characteristics does not exist (Dawson et al., 2010). None of the studied models can present all of the dominant clinical and pathological characteristics of PD (Jiang and Dickson, 2017).

2.3.2 PINK1 and *PINK1* knockout rats

PTEN-induced putative kinase -1 (PINK1) is a mitochondrial serine/ threonine-protein kinase, important to monitor the health status of mitochondria. Mutations in the gene for *PINK1* have been shown related to the early onset of autosomal recessive-inherited PD (Kawajiri et al., 2011). With healthy mitochondria, PINK1 is imported to the inner mitochondrial membrane. The N-terminal mitochondrial targeting sequence of PINK1 is cleaved by PARL, a mitochondrial protease. After the cleavage, PINK1 is retro-translocated to the cytosol (Deas et al., 2011). In the case of dysfunctional mitochondria, PINK1 is accumulated on the outer mitochondrial membrane. Parkin, a component of E3 ubiquitin ligase complex, is phosphorylated by PINK1 there. As a result, the ubiquitin-proteasome system is activated to mediate the targeting of proteins for degradation, initiating mitophagy (Matsuda et al., 2010).

The manifestation of the four cardinal motor symptoms, developed α-synuclein in Lewy bodies, and nigrostriatal neurodegeneration, were not observed in *PINK1* KO mice (Glasl et al., 2012). A genetic rat model could have some advantages as a rodent model of PD, including a bigger brain size compared to a knockout mouse model. In this dissertation research, *PINK1* knockout (KO) rats were used, since mutations in *PINK-1* lead to familial PD.

CHAPTER 3. PROTECTION BY MESNA FROM DOXOCUBICIN-INDUCED ELEVATED OXIDATIVE DAMAGE AND NEUROCHEMICAL CHANGES IN BRAIN WITH COGNITIVE DECLINE: INSIGHT INTO MECHANISMS OF CHEMOTHERAPY-INDUCED COGNITIVE IMPAIRMENT (CICI)

3.1 Overview

With the growing number of cancer survivors, chemotherapy-induced cognitive impairment (CICI) is recognized as a real complication after chemotherapy rather than cognitive impairment only from cancer alone. In past studies, doxorubicin (Dox) was used as a prototype of reactive oxygen species (ROS)-generating chemotherapeutic drugs. Administration of Dox caused oxidation of apolipoprotein A-1 (ApoA1) in plasma, leading to tumor necrosis factor-alpha (TNF-α) elevation and oxidative damage in both plasma and brain. The antioxidant drug, 2-mercaptoethane sulfonate sodium (MESNA), was co-administrated with Dox and showed prevention from Dox-induced protein oxidation and increased TNF-α in plasma. In the current chapter, oxidative damage in plasma and brain, respectively, of Dox-treated mice, with or without co-administration of MESNA was measured. The antioxidant ability of MESNA led to ameliorated Dox-induced oxidative protein damage in plasma, which is consistent with our previous works. In addition, the decreased level of Dox-induced oxidative damage in brain also was observed by co-administration of MESNA, along with rescued Dox-caused memory and cognitive deficits examined by novel object recognition (NOR) test. Furthermore, Dox treatment was shown to lead to a significant decline in the level of choline-containing compounds (Cho) in hippocampus of mice by hydrogen magnetic resonance imaging spectroscopy (H^1-MRS) techniques. To better understand results from this MRS observation, the activities of the phospholipases, the enzymes phosphatidylcholine specific phospholipase C (PC-PLC) and phospholipase D (PLD) that catalyze phosphatidylcholine (PtdCho), producing choline and

phosphocholine (PCho), respectively, were measured. We noticed that activities of both PC-PLC and PLD were dramatically diminished in mice brain following Dox injection. Co-administration of MESNA with Dox can preserve the activity of PC-PLC; however, MESNA did not protect the activity of PLD. The studies in this chapter demonstrate the protective effects of MESNA on anti-oxidant defense in both plasma and brain, cognitive function, levels of choline-containing compounds in hippocampus, and PC-PLC activity in brain from Dox administration. The results provide biochemical and functional evidence for the better elucidation of plausible mechanisms of CICI, suggesting novel potential therapeutic targets and strategies to protect against cognitive impairment from chemotherapy.

3.2 Introduction

CICI, called "chemo brain" by cancer survivors, usually is considered an increasingly significant side effect of chemotherapy with impairments in many cognitive and executive functions (McDonald and Saykin, 2013; Simo et al., 2013). The mechanisms of CICI remain unknown. The complexity of cancer and cancer treatments brings out the difficulties of the investigation into mechanisms of CICI, especially because in many cases, the chemotherapeutic drugs cannot get into brain due to the inability to cross the blood-brain barrier (BBB). Perceiving the underlying mechanisms by which CICI occurs is important to bring a good quality of life to cancer survivors by protecting non-targeted tissues against undesired toxicities of anticancer drugs. Peripheral toxic effects induced by the chemotherapeutic drugs, subsequently leading to structural and functional alterations in the brain, are thought to be major pathological factors of CICI. Neuroinflammatory consequences and even changes in levels of neurotransmitters and function are latter

aspects leading to cognitive impairment (Aluise et al., 2011; Joshi et al., 2010; Raffa, 2011; Saykin et al., 2003).

Dox is known as an anthracycline ROS-generating chemotherapeutic drug in many multidrug chemotherapy regimens, commonly used to treat solid tumors and leukemia (Cummings et al., 1991; Gutteridge, 1984; Handa and Sato, 1975). Our lab has shown that administration of Dox led to damaged mitochondria associated with elevated oxidative damage and production of TNF-α in brain, although Dox cannot cross the blood-brain barrier (BBB) (Joshi et al., 2007; Tangpong et al., 2007; Tangpong et al., 2006; Tangpong et al., 2008). The quinone moiety structure of Dox can be converted to a semi-quinone, undergoing one-electron reduction. (Aluise et al., 2011; Chen et al., 2007). Through the redox cycling of this structure back to the quinone *in vivo*, reactive superoxide free radical ($O_2^{-\bullet}$) is formed from oxygen molecule during the process of converting the semi-quinone moiety back to the quinone, producing oxidative damage as a consequence. Previous studies showed that Dox elevated oxidative damage and dysfunctional proteins including ApoA1 in plasma, resulting in disturbances to the central nervous system (Aluise et al., 2011). After being oxidized, ApoA1 lost its ability to restrain TNF-α release in plasma (Aluise et al., 2011).

MESNA is an FDA-approved adjuvant of chemotherapy to prevent bladder cystitis and bleeding caused by neurotoxicity metabolism of cyclophosphamide and ifosfamide to acrolein. The free sulfhydryl group in the structure of MESNA can react with free radicals and lipid peroxidation aldehyde products. With its negative charge, MESNA will not get into cells, thus can decrease the unwanted oxidative toxicities from chemotherapy without interfering with the efficacy of the oxidative effects of anti-cancer drugs in cancer cells

(Bernacki et al., 1987) (Fang et al., 2009). Our lab discovered that co-administration of MESNA can restore ApoA1 and repress subsequent TNF-α elevation in plasma of mice (Aluise et al., 2011).

Hence in this chapter, we tested the hypothesis that MESNA would show protective effects from Dox-induced CICI by measuring the levels of oxidative damage, neurochemical metabolites, and cognitive performance.

3.3 Materials and Methods

3.3.1 Chemicals

General chemicals, protease inhibitors, and antibodies were purchased from Sigma-Aldrich (St. Louis, MO, USA). Pierce™ BCA Protein Assay Kit was purchased from ThermoFisher Scientific (Rockford, IL). The nitrocellulose membrane was purchased from Bio-Rad (Hercules, CA). EnzChek® Direct Phospholipase C Assay Kit and Amplex® Red Phospholipase D Assay Kit were purchased from Invitrogen/Life Technologies (Carlsbad, CA). Doxorubicin HCl was purchased from Bedford Laboratories™, and MESNA was purchased from Baxter Healthcare Corporation.

3.3.2 Animals

All mice were purchased from Jackson Laboratory. The F1 progeny of C57BL/6 x C3H hybrids (B6C3) were used in the current chapter. Each of the mice was 2-3 months old, male, and weighing approximately 30 grams. All mice were housed in the University of Kentucky Animal Facility with standard conditions. The Institutional Animal Care and Use Committee of the University of Kentucky had approved all experimental procedures. Mice were injected using a single intraperitoneal (i.p.) dose of 25 mg/kg Dox or the same

volume of saline control (Desai et al., 2013; Yen et al., 1996). MESNA was administered at 160 mg/kg i.p. 15 min before, 3 h after, and 6 h after DOX treatment. Post-treatment 72 h, mice were processed into MRS study or NOR test, immediately followed with mice sacrifice. The mice were euthanized with CO_2, right followed with blood and tissues collecting for molecular or biochemical experiments.

3.3.3 Hydrogen magnetic resonance spectroscopy (H^1-MRS)

H^1-MRS was employed to identify the amount of the neurochemical metabolites in the mouse hippocampus in this current chapter. 7T Bruker Clinscan horizontal bore system (7.0T, 30cm, 300Hz) was equipped with a triple-axis gradient system (630 mT/m and 6300 T/m/s), provided the MRS data. A closed cycle, 14K quadrature cryocoil allowed for a 2.8 signal to noise increase relative to standard coils. The mice were anesthetized with 1.3 % percent isoflurane using MRI compatible CWE Inc. equipment. Anesthetized mice were placed on a Bruker scanning bed with tape. Tooth bar and ear bars were used to hold the mice. The body temperature and respiration rate of mice were monitored by the equipment from SA Instruments Inc. The mice were maintained at 37 °C with a water heating system built into the scanning bed. T2 weighted turbo spin echo sequences (TE 40ms, TR 2890ms, Turbo 7, FOV 20mm, 0.156 x 0.156 x 5.0 mm3) were acquired and used for the placement of the spectroscopy voxel. The scanning procedure took 40 min. A 2x5.5x3mm3 PRESS spectroscopic voxels (TE 135ms, TR 1500ms, 400avg, CHESS water suppression) was placed to cover both hippocampi. Spectrum analysis was performed using jMRUI (Naressi et al., 2001) to quantify the area under each peak in the spectrum. The area of the creatine (Cr) peak was used to normalize the peak areas of other metabolites.

3.3.4 Cognitive function testing: novel object recognition and open field test

Cognitive performance was evaluated using a NOR paradigm (Ennaceur and Delacour, 1988; Schoch et al., 2012). One day before treatment, each mouse was acclimated for 1 h to an empty, Plexiglas@ cage, which was dedicated to this mouse for all trials. Several hours after acclimation, the mouse was returned to the cage containing two identical objects (object A) placed at opposite corners, and the time spent exploring each object was recorded. A mouse was considered to be exploring when it pointed its nose toward the object at a distance of 2 cm or less. Throughout the protocol, the trial duration was 5 min unless the total exploration time was less than 10 s. In this case, the trial was extended to ensure a minimum of 10 s of exploration. On the day of treatment, mice were re-introduced to the two "familiar" objects (object A) in the morning. Four hours later, baseline memory function was evaluated by replacing one of the familiar objects with a novel object (object B). Immediately following the baseline memory trial, mice received an injection. One day after injection, the mice were exposed to the original two (familiar) objects (object A) and, after a 4 h interval, one of the familiar objects was replaced with a novel object (object C). At 3 days after treatment, memory was tested again (novel object D paired with familiar object A). Data are reported as a recognition index, which was calculated time spent exploring the novel object as the percentage of total exploration time. All trials were performed by an investigator blinded to treatment conditions. NOR test was performed by the K. E. Saatman laboratory, Spinal Cord and Brain Injury Research Center, University of Kentucky.

At 1 and 3 days after treatment, motor activity was tested using an Open Field test (Leibrock et al., 2013). Mice were placed in a 48 x 33cm empty Plexiglas@ box and videotaped from above for a 5-minute trial (EZVideoDV version 5.51). Trials were

performed by an investigator blinded to treatment conditions. Open field test was performed by the K. E. Saatman laboratory, Spinal Cord and Brain Injury Research Center, University of Kentucky.

3.3.5 Sample collection

Blood of mice was extracted cardiac puncture by cardiac puncture right after mice were being sacrificed. Blood was transferred into EDTA tube immediately. Inverted the tube approximately ten times to completely mix the blood with the anticoagulant in the tube. The tube containing blood was then centrifuged at 3000 rpm at 4 °C, 10 min. After centrifuging, plasma was separated from other blood components and then transferred into a microcentrifuge tube, instantly put into liquid nitrogen. Immediately after blood extraction, the mouse brain was extracted, placed in a microcentrifuge tube, and immediately frozen in liquid nitrogen. All plasma and brain samples were stored at -80 °C and ready for future experimental use.

3.3.6 Sample preparation

The individual frozen mouse brain was thawed slightly on ice and put in a Wheaton glass homogenizer. Use the glass rod to homogenize the brain tissues for approximately 40-45 passes in the cold isolation buffer [0.32 M sucrose, 20mM HEPES, 2 mM EDTA, 2mM EGTA, 10 μg/ml phosphatase inhibitor cocktail 2, and protease inhibitor 5 μg/ml aprotinin, 4 μg/ml leupeptin, 4 μg/ml pepstatin A, and 0.2 mM PMSF]. All brain homogenate was transferred to a microcentrifuge tube and vortexed. Next, Fisher 550 Sonic Dismembrator (Pittsburgh, PA, USA) was used to sonicate brain homogenate on ice for 10s at 20% power, two times with an interval of 20s rest. After estimation of protein

concentration with BCA assay, brain samples were ready for use.

Plasma samples were thawed on ice, diluted with cold isolation buffer, and estimated protein concentration by BCA assay.

3.3.7 Slot blot assay

Biomarkers of oxidative damage, including protein carbonyls (PC) and protein-bound 4-hydroxynonenal (HNE), were measured by slot blot assay. Brain or plasma samples were derivatized with 2,4-dinitrophenylhydrazine (DNPH) for measuring the level of PC or solubilized in Laemmli buffer for measuring the level of HNE. 250 ng of proteins from each sample were loaded onto a nitrocellulose membrane in respective wells of the slot-blot apparatus (Bio-Rad) under vacuum. Membranes were blocked in 3% bovine serum albumin (BSA) in TBS with 0.2% (v/v) Tween-20 (TBS-T) for 1.5 h, then incubated TBS-T with primary antibody (1:500 anti-dinitrophenylhydrazone or 1:5000 anti-protein-bound HNE, respectively) for 2 h, followed with three times of washing in TBS-T, 5 minutes for each washing. Next, the membrane was incubated for 1 h with secondary antibody (secondary linked to alkaline phosphatase, 1:10000), washed in TBS-T three times, 5, 10, and 10 minutes, respectively for each washing. Then, the membrane was develope in alkaline phosphatase activity (ALP) buffer containing 1:300 5-bromo-4-chloro-3-indolyl phosphate (BCIP), and 1:150 Nitro blue tetrazolium (NBT). The developed membrane was dried overnight and then scanned for analysis on the second day. Imaging analysis was performed using Scion Image (Scion Corporation, Frederick, MD).

3.3.8 Measuring the activity of Phospholipase C and phospholipase D

EnzChek® Direct Phospholipase C Assay Kit was used to measure the activity of phosphatidylcholine-specific phospholipase C (PC-PLC), while Amplex® Red Phospholipase D Assay Kit was used to measure the activity of phospholipase D, followed the manufactural instructions. The intensity of fluorescence was measured in the SPECTRAFluor Plus instrument and quantified using associated MagellanTM software by TECAN throughout 24 h incubation at 37 ℃, avoided light. The fluorescence is collected at the time of maximal fluorescence peak showed during the 24 h incubation corresponding to the positive control.

PC-PLC activity data was collected after 22.5h of incubation of assay reagents and samples. The PtdCho in the substrate is cleaved by PC-PLC, generates dye-labeled diacylglycerol (DAG), and phosphocholine. The excitation wavelength is 509 nm, and the emission wavelength is 516 nm for PC-PLC. PLD activity data was collected at 1h of incubation of assay reagents and samples. The PtdCho in the substrate is cleaved by PLD, generates the alcohol component of the head group of PtdCho, releasing choline. The excitation wavelength is 571 nm, and the emission wavelength is 585 nm for PLD.

3.4 Results

3.4.1 Dox administration results in increases in oxidative damage markers in both brain and plasma

Increased levels of TNF-α and oxidative damage in brain were found after Dox administration in the periphery despite that Dox is not able to cross the BBB (Aluise et al., 2011; Joshi et al., 2010; Joshi et al., 2007; Joshi et al., 2005; Tangpong et al., 2006). In the

current chapter, wild-type mice were separated into four groups, treated with saline, MESNA, Dox, and Dox plus MESNA, respectively. Brain and blood samples were collected 72 h post-Dox treatment. Protein carbonyl and protein-bound HNE levels were measured as indications of oxidative damage to proteins and lipids, respectively. In Fig. 3.1a and 3.1c, Dox led to significantly higher levels of protein carbonyls and protein-bound HNE in brain compared to saline-treated controls and MESNA protected brain from these oxidative damages. In Fig. 3.1b and Fig. 3.1d, increased protein carbonyl and protein-bound HNE levels in plasma were presented in Dox-treated group compared to saline-treated group and both of the elevated protein carbonyl and protein-bound HNE in plasma were ameliorated in co-administration of MESNA to Dox group. These results in both brain and plasma are consistent with our previous findings in plasma (Aluise et al., 2011) and brain (Joshi et al., 2010; Joshi et al., 2007) and consistent with the notion that co-treatment MESNA with ROS-generating anti-cancer drugs may reduce or prevent these consequences in brain.

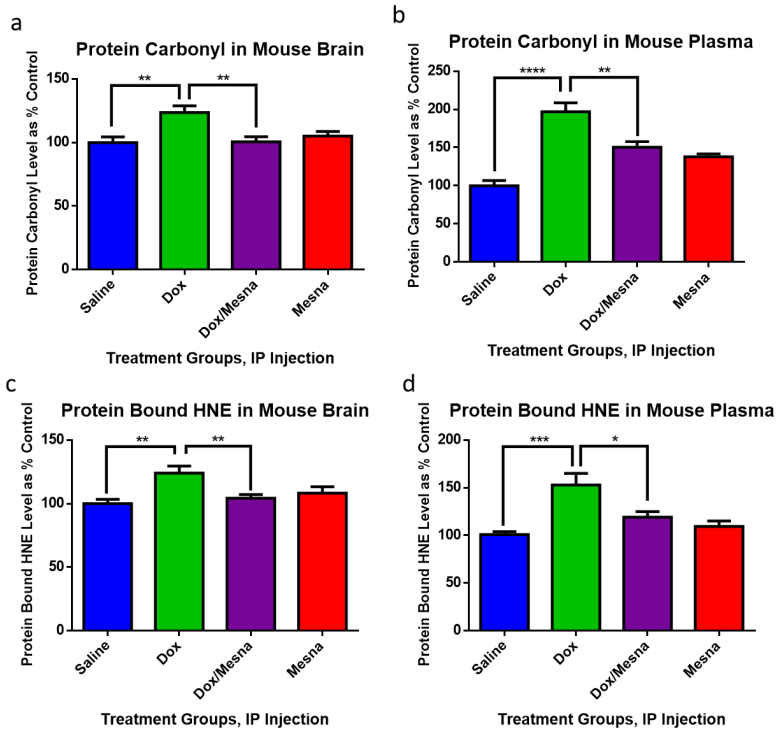

Figure 3.1 The effects of Dox and MESNA on the levels of PC and protein-bound HNE in brain and plasma.

Fig.3.1a-d showed the levels of protein carbonyl and protein-bound HNE in the brain and plasma of 2-3 month-old, male wild-type mice. The mice were treated with saline, MESNA, Dox, or Dox plus MESNA. Brian and plasma samples were collected 72 h post-treatment. Dox caused dramatical increases in the level of PC in both brain (a) (**$p<0.01$) and plasma (b) (****$p<0.0001$) of mice. Co-administration of MESNA with Dox mitigated these Dox-induced increases of protein carbonyl in both brain and plasma (**$p<0.01$, respectively). In (c) and (d), protein-bound HNE levels were significantly increased in brain (**$p<0.01$) and plasma (***$p<0.001$) of mice treated with Dox. Co-administration of MESNA with Dox significantly ameliorated Dox-induced elevation in protein-bound HNE in both brain (**$p<0.01$) and plasma (*$p<0.05$). (N=10-13 per treatment group). Slot blot assays were performed by Dr. Jeriel Keeney, Butterfield Lab, University of Kentucky. (Keeney et al., 2018)

3.4.2 Dox administration results in cognitive impairment and decreased locomotor activity

NOR was performed to measure the cognitive function of mice in all four treatment groups (Fig. 3.2a). This test involved brain regions of hippocampus and frontal cortex, which both are important to CICI.

Before Dox treatment, mice from each of the groups spent an average of 65-70% of total exploration time to explore the novel object.

At 24 h post-treatment, the mice were exposed to two familiar objects, followed with exposure to one novel, and one familiar object. The recognition index values were not significantly different in any group comparison.

At 72 h post-treatment, the RI value presented by Dox-treated mice decreased to an average of 40 and was significantly lower than all three other groups, whereas the saline and MESNA treatment groups still performed similarly as it before Dox treatment. The result indicated that Dox caused delayed memory decline, which could be rescued by co-administration with MESNA.

Open field testing was employed as a measurement of locomotor activity among treatment groups (Fig. 3.2b). At 24 h post-treatment, Dox led to decreased locomotor activity compared to MESNA control group. A progressive decline in locomotor activity was showed in Dox treatment group, which reached statistical significance by 72 h post-treatment in Fig. 3.2b. The similar decrease of the locomotor activity in Dox+MESNA groups at 72 h post-treatment (Fig. 3.2b), indicating MESNA selectively attenuates Dox-induced memory impairment.

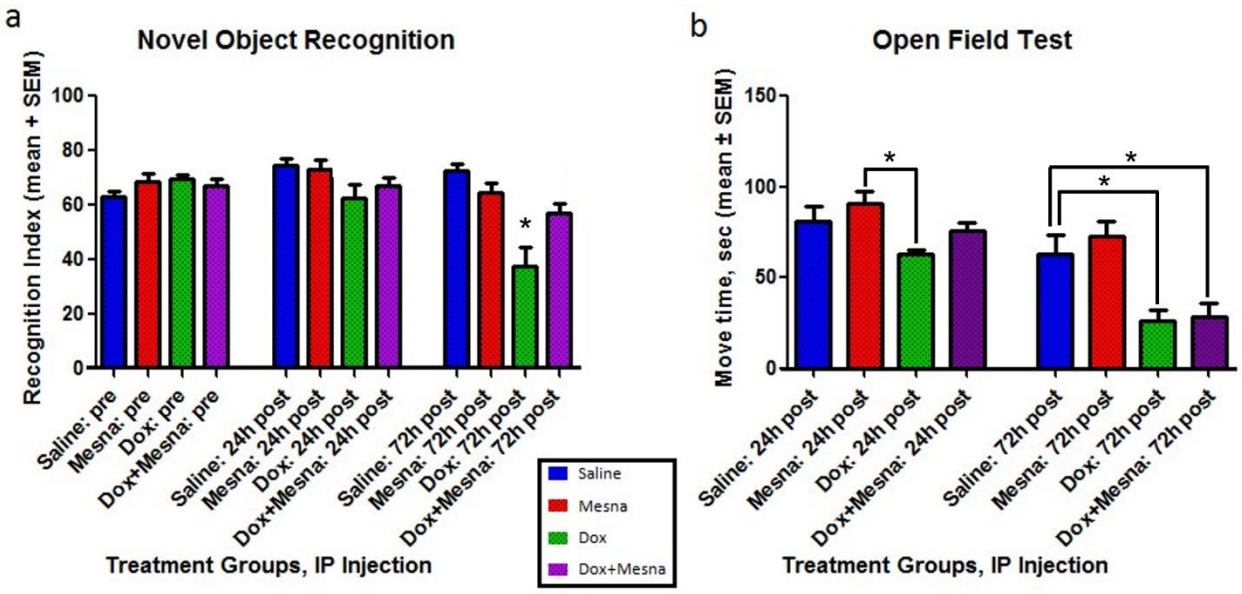

Figure 3.2 The effects of Dox and MESNA in behavioral NOR and open field tests.
(a) Through recognition memory, cognitive function was measured in Novel Object Recognition (NOR) testing. At 72 h post-treatment, the RI value of Dox group was significantly lower RI than Saline, MESNA and Dox plus MESNA (*$p<0.05$, respectively). Co-administration of MESNA rescued the deficits in memory function caused by Dox. (b) Locomotor activity was measured in open field test by acquiring the average of total movement time. At 24 h post-treatment, a significantly decreased locomotor activity was shown in Dox group compared to MESNA control group (*$p<0.05$). At 72 h post-treatment, the locomotor activity presented in either Dox treatment group or Dox+MESNA treatment group was both dramatically decreased compared to saline treatment group and MESNA treatment group, respectively (*$p<0.05$, comparisons to MESNA group were not labeled in this figure). The result showed that MESNA cannot relieve the decreased motor activity in an open field caused by Dox. NOR and open field tests were performed by the collaborator, Dr. Kathy Saatman, Physiology, University of Kentucky. (Keeney et al., 2018)

3.4.3 Dox administration results in a decreased level of choline-containing compounds in the hippocampus

Hippocampus involves learning and memory (Antunes and Biala, 2012; Clarke et al., 2010; Goulart et al., 2010; Meck et al., 2013; Sarkisyan and Hedlund, 2009). H^1-MRS can measure neurochemical metabolites of the living brain non-invasively. The peaks shown in this spectrum (Fig. 3.3a) allow quantification of these peaks in the living brain, including of N-acetylaspartate (NAA), Choline-containing compounds (Cho), creatine (Cr), myo-inositol, glutamate and glutamine, lipids, and lactate among others (Jansen et al., 2006). The area of the Cr peak was normally used to normalize other metabolites. The Cho peak is contributed principally by PCho and glycerophosphorylcholine.

NAA/Cr ratio was slightly but significantly decreased in the Dox-treated hippocampus compared to the saline group, indicating decreased neuronal integrity. Dox caused a much larger six standard-deviation decrease in Cho/Cr compared to the saline group. A slight increase in Cho/Cr can be observed from Dox-treated group to Dox plus MESNA treated group, although this elevation is not statistically significant (Fig. 3.3d). The result indicated that the protection of MESNA from Dox may involve in other mechanisms in addition to partial restoration of the Cho/Cr ratio.

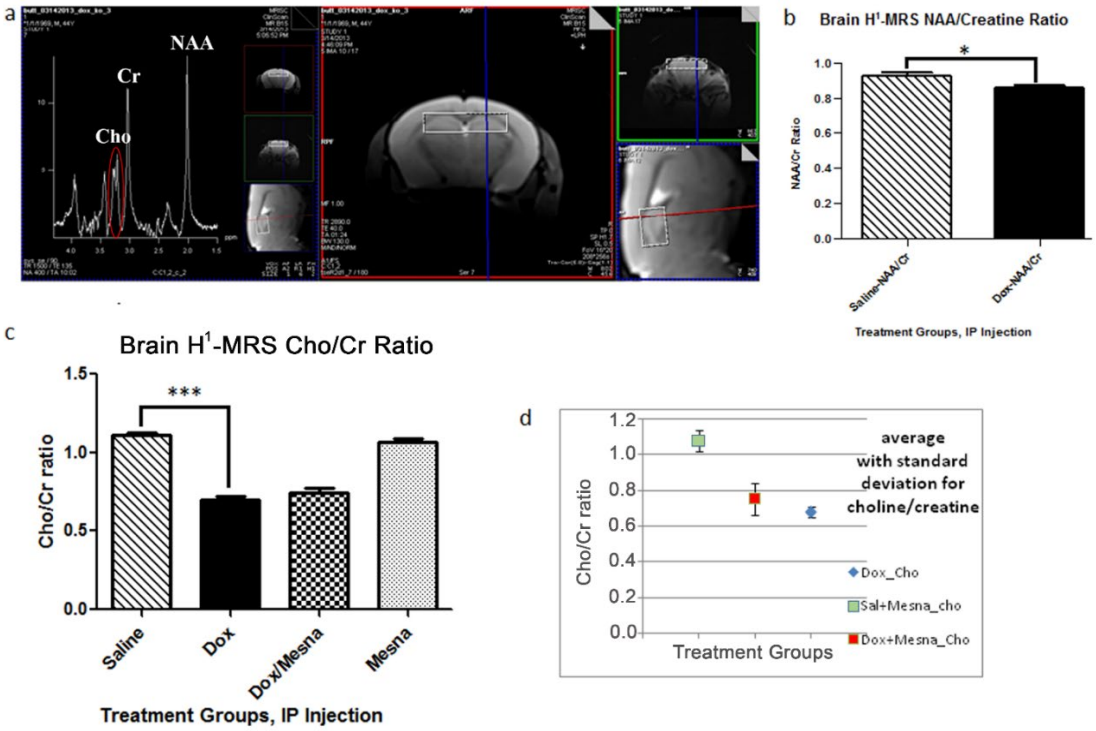

Figure 3.3 H^1-MRS results of mouse hippocampus.

(a) After 72 h post-treatment, H^1-MRS was employed to measure the hippocampus of living mice. H^1-MRS uses proton signatures from hydrogen to create two-dimensional images of the tissue on the right of Fig. 3.3a, and a neurochemical profile indexed by a spectrum of peaks including NAA, Cho, Cr, and others (on the left of Fig. 3.3a). (b) The NAA/Cr ratio in hippocampus of mice was slightly but statistically decreased in Dox group compared to Saline group (*$p<0.05$). (c) Dox led to a dramatic decrease (with six standard deviations) in the Cho/Cr ratio in the Dox-treated group compared to saline group (***$p<0.001$). (d) A trend toward rebound in Cho/Cr in the group of Dox plus MESNA compared to Dox alone was observed. MRS study was performed by the collaborator, Dr. David Powell, Magnetic Resonance Imaging and Spectroscopy Center, University of Kentucky. Data was collected by Dr. Keeney and Xiaojia. Figure was made by Dr. Keeney and amended by Xiaojia. (Keeney et al., 2018)

3.4.4 Dox administration results in decreased PC-PLC and PLD activity

PtdCho is a major source of Cho and phosphocholine (PCho). To further investigate the results of MRS studies, the activities of phospholipase enzymes were measured. PC-PLC cleaves the glycerol-phosphate bond of PtdCho, producing PCho, and diacylglycerol (DAG), which is a second messenger. Plasma protein phospholipase D (PLD) cleaves the headgroup from phospholipids of PtdCho, releasing soluble choline into cytosol. At 72 post-treatment, both activities of PC-PLC and PLD in brain were dramatically decreased in Fig 3.4a and Fig 3.4b. This result is consistent with our results in MRS studies in this chapter, explaining the reason for Dox-caused Cho/Cr ratio decreases. The decreased PC-PLC activity in Dox-treated group was fully restored compared to the saline-treated group by co-administration of MESNA. However, MESNA did not show any protection of PLC activity from Dox.

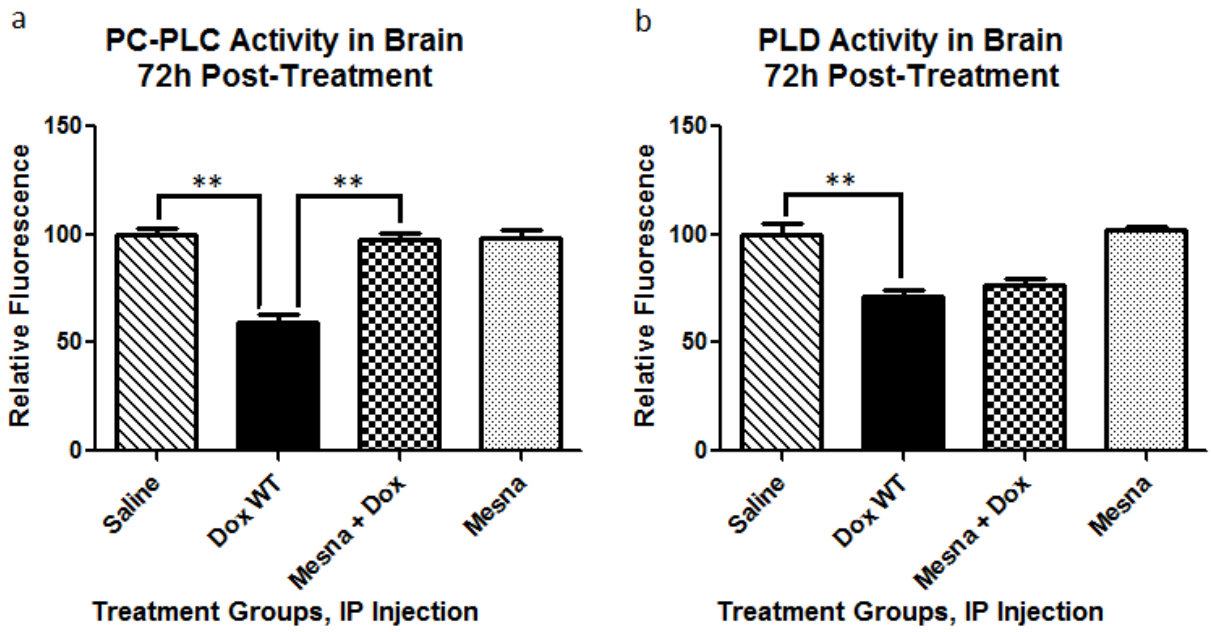

Figure 3.4 Phosphatidylcholine-specific phospholipase C (PC-PLC) and Phospholipase D (PLD) activity in brain 72 h post-treatment.

Each group is presented as percent saline control. (a) Dox treatment resulted in a significant loss in PC-PLC activity compared to saline-treated mice (**$p<0.01$), which can be rescued by co-administration of MESNA (**$p<0.01$). (b) Dox administration caused a significant decrease in PLD activity compared to saline-treated controls (**$p<0.01$). MESNA did not show protective effects on PLC activity from Dox treatment. Assays were performed by Dr. Keeney and Xiaojia. Figure was made by Dr. Keeney. (Keeney et al., 2018)

3.5 Discussion

Nearly half of FDA approved anti-cancer drugs can produce excessive ROS and induce oxidative damage (Chen et al., 2007), which is considered as one of the major candidates of mechanisms of CICI. The studies in this chapter provided more evidence to gain insights into mechanisms, and potential prevention of CICI, eventually to achieve successful management of CIC, improving the quality of life of cancer survivors. Fig. 3.5 summarizes major changes in brain following treatments of mice with non-BBB permeable Dox and modulation or amelioration of these changes by MESNA.

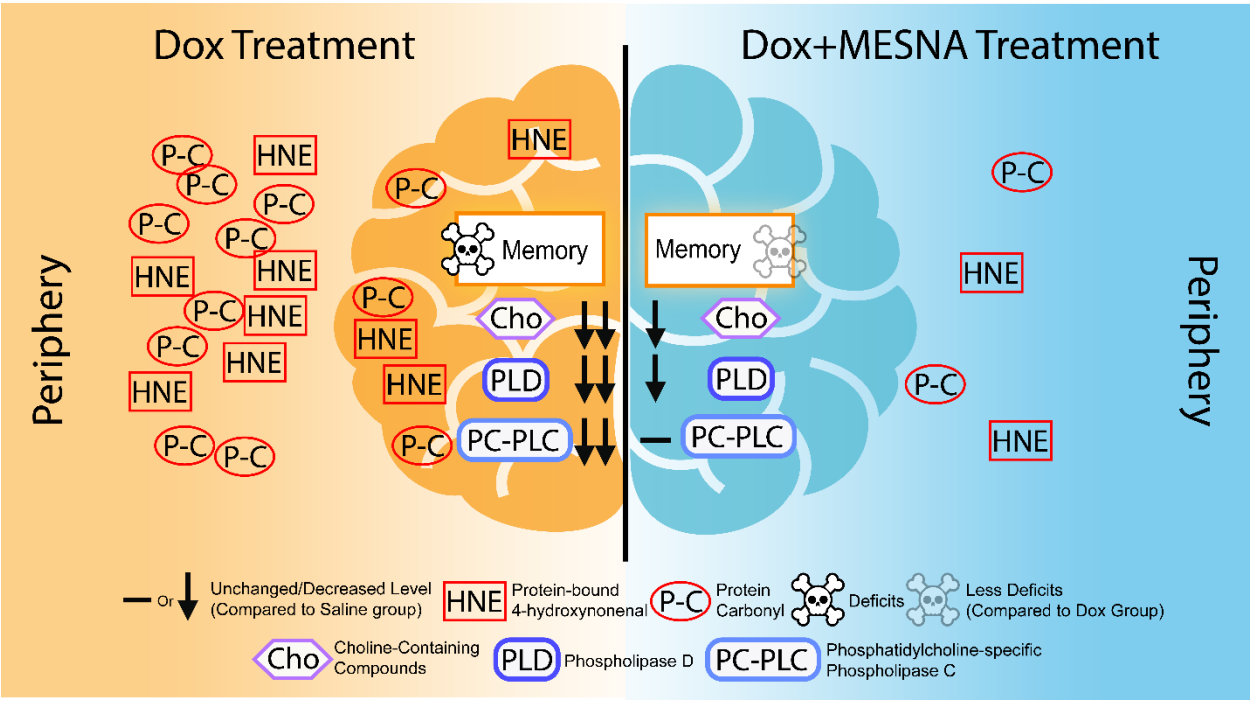

Figure 3.5 A pictorial summary of the effects of Dox and MESNA in plasma and brain of mice in the current chapter.

Dox-induced elevated oxidative damage and neurochemical alterations in the periphery and brain as well as cognitive decline (left) and MESNA-mediated protection against these Dox-facilitated effects in both plasma and brain (right). (Keeney et al., 2018)

ROS-generating chemotherapeutic drugs lead to oxidative damage of proteins, lipids, lipoproteins, and genetic molecules (Aluise et al., 2011; Bagchi et al., 1995; Chen et al., 2007; Joshi et al., 2010; Nithipongvanitch et al., 2007; Sterrenberg et al., 1984) by the non-targeted detrimental effects on both cancer cells and normal cells, leading to tissue damage (Butterfield, 2014; Chen et al., 2007). Brain is particularly vulnerable to oxidative damage because it has relatively high oxygen consumption and low antioxidant defenses, with enrichment of polyunsaturated fatty acids.

Dox is a prototype of ROS-generating anti-cancer drugs. Dox-induced cardiac dysfunction, in part, is due to mitochondrial damage, is well established and used as dose-limiting criteria in treatment protocols (Chen et al., 2006; DeAtley et al., 1999; Jungsuwadee et al., 2006; Jungsuwadee et al., 2012). The Dox-induced, oxidative damage-mediated elevation of TNF-α in the plasma leads to the elevation of local TNF-α in the brain, subsequently leading to neuronal death (Aluise et al., 2011; Tangpong et al., 2006), as a result, cognition is impaired by losing neurons. TNF-α is a pro-inflammatory cytokine, produced by activation of macrophages. TNF-α plays several roles in inflammation, catabolism in fat and muscle, triggering the synthesis of acute-phase proteins, neutrophil activation, and apoptosis. Acute responses of TNF-α are beneficial but are quite harmful if the responses of TNF-α are chronic or sustained.

Oxidative damage, in particular, protein-bound HNE, can alter the structure and function of proteins by covalently binding proteins via Michael addition (Butterfield and Lauderback, 2002; Di Domenico et al., 2017; Halliwell and Gutteridge, 1984; Sultana et al., 2013). The oxidative status of ApoA1 is crucial to its role in TNF-α suppression (Hyka et al., 2001; Yin et al., 2011). Dox-induced Protein-bound HNE-oxidized ApoA1 lost its

ability to suppress TNF-α release in plasma (Aluise et al., 2011; Keeney et al., 2013b). However, the co-administration of MESNA with Dox treatment can protect ApoA1 from oxidative damage, and suppress the Dox-induced oxidative damage-mediated TNF-α elevation. (Aluise et al., 2011). MESNA is rapidly oxidized, scavenging reactive species in circulation with a short time, thereby reducing the chance for potential unwanted side effects from oxidative stress (Mashiach et al., 2001).

In this chapter, the data of oxidative damage supported the results of our previous studies (Fig. 3.1). Dox can induce the increased level of both PC and protein-bound HNE in plasma and subsequently in the brain; the co-administration of MESNA with Dox prevented the elevated oxidative damage in both plasma and brain. The treatment groups receiving Dox displayed less total movement than those groups without Dox treatment. This finding is consistent with previous studies of others (Lira et al., 2016; Wu et al., 2016).

Memory and cognitive performance were measured by NOR (Fig. 3.2a). MESNA showed its ability for the prevention of the memory decline resulted from Dox at 72 h post-treatment. MESNA rescued much of this Dox-induced cognitive deficit, which we speculate is due to the prevention of oxidative damage in brain following Dox treatment. Dox-induced motor dysfunction is not ameliorated by MESNA treatment (Fig. 3.2b). The result of locomotor activity is consistent with other studies that Dox can cause the impairment of locomotor activity in non-tumor bearing mice (Lira et al., 2016; Wu et al., 2016), which conceivably could be due to protein oxidation of muscles and/or the effects of elevated levels of the pro-inflammatory cytokine TNF-α (Merzoug et al., 2014; Mohamed et al., 2011). However, the aspect of similar total movements displayed in Dox and Dox+MESNA group decreased potential confounds for the NOR test. The total object

exploration time decreased with repeated exposure to the environment. Dox-treated group had been already exhibiting the decreased trend of the preference for the novel object compared to the other treatment groups at 24h post-treatment. By day three (72h post-treatment), mice in Dox group had no preference for the novel object over the familiar one. The behavioral studies in this chapter are compelling evidence that the application of MESNA could potentially ameliorate CICI from the ROS-generating anti-cancer drugs.

The NAA/Cr ratio shown in the hippocampus of Dox-treated group is slightly but significantly decreased compared to the saline group, suggesting Dox led to neuronal damage (Fig. 3.3b). Along with the decreased NAA/Cr ratio in Dox group, the Cho/Cr ratio in hippocampus showed a significant decline of six standard deviations of the Dox-treated group compared to the saline-treated group. The decreased level of choline-containing compounds in the MRS studies potentially is associated with membrane turnover involving phospholipid synthesis and degradation (Bertholdo et al., 2013; Soares and Law, 2009). Decreased choline uptake was found in older adults, as well as decreased Cho peak in the aging brain (Cohen et al., 1995; Dezortova and Hajek, 2008; Soares and Law, 2009), which also could be considered as a potential indication of decreased cell density and necrosis (Gupta et al., 2000; Soares and Law, 2009).

The results presented in this chapter are consistent with another study that a time-related decrease in the Cho/Cr ratio followed chemotherapy treatment and was attributed to potential myelin damage (Ciszkowska-Lyson et al., 2003). Years after systemic chemotherapy treatment, defective alterations of gray matter, and lipid-rich myelin covered white matter still were found in some cases, associated with functional deficits (Briones and Woods, 2014; de Ruiter et al., 2012; Simo et al., 2013). Decreased myelination and

cognitive impairment were shown correlated to the chemotherapy-induced elevation of TNF-α (Briones and Woods, 2014). Supporting the hypothesis of this dissertation research, TNF-α is considered playing a central role in the mechanisms of CICI.

Elevated TNF-α may lead to PtdCho being less synthesized (Church et al., 2005; Mallampalli et al., 2000). PtdCho is one of the most common components forming membranes, normally located in the outer bilayer leaflet. The choline head group of PtdCho is on the cytosol side, mediating membrane-associated cell signaling. PtdCho also is the main component of high-density lipoprotein (HDL), collaborating with ApoA1 in cholesterol transport. PtdCho can be catalyzed by PC-PLC and PLD, generating phosphocholine plus second messenger DAG and choline, respectively. Choline is involved in the synthesis of ACh, a neurotransmitter with widespread functions, including motor and somatic divisions of the autonomic nervous system. ACh also is associated with memory, intelligence, and mood, partially mediated by ACh metabolism and the levels of choline in brain (Poly et al., 2011). In this chapter, activities of both PC-PLC and PLC in brain of Dox-treated mice were impaired (Fig. 3.4), supporting our observation that Dox led to the decreased level of Cho/ratio in hippocampus of mice (Fig . 3.3). The result that co-administration with MESNA protected the activity of PC-PLC from Dox, whereas MESNA did not show protection on PLC from Dox, may explain why MESNA showed a trend to recover the Dox-decreased level of Cho, but not significantly. Here, a Dox-induced, TNF-α mediated pathway of apoptosis is shown in Fig. 3.6.

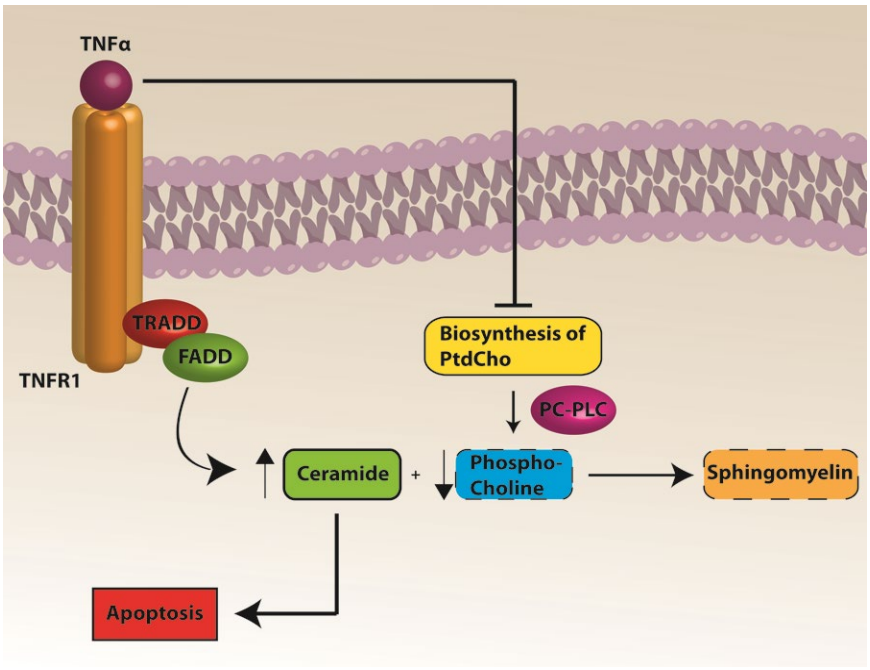

Figure 3.6 A putative pathway to apoptosis following Dox-induced TNF-α elevation. Dox results in the elevation of TNF-α. TNF-α triggers ceramide increase and subsequent extrinsic apoptosis via TNF receptor. Meanwhile, TNF-α inhibits the biosynthesis of PtdCho, coupled to decreased activity of PC-PLC caused by Dox, leading to a decreased level of PCho. As a result of decreased PCho, ceramide relatively increases due to the decreased conversion to sphingomyelin from ceramide plus PCho, leads to apoptosis. Figure was designed by Dr. Aaron Swomley, Butterfield Lab, University of Kentucky. (Keeney et al., 2018)

Decreased level of PCho could be due to inhibiting synthesis of PtdCho by Dox-induced elevation of TNF-α, or decreased activity of PC-PLC. Sphingomyelin can be synthesized by coupling of ceramide with PCho (Siegel, 2006). Thus, a decreased level of Pcho would possibly result in elevated ceramide, inducing apoptosis (Car et al., 2012; Geilen et al., 1997; Qin et al., 1998; Wang et al., 2012), and elevated apoptosis has been found after Dox treatment in brain of mice (Tangpong et al., 2007). Dox-induced decreased PC-PLC and PLD activities presented in this chapter may result in dysregulation of cell survival and apoptosis pathways that involve PC-PLC. More studies are required to elucidate the involvement of choline, PC-PLC, and PLD in mechanisms of CICI.

Based on previous work by our group (Aluise et al., 2011; Aluise et al., 2010; Butterfield, 2014; Joshi et al., 2005; Ren et al., 2017; Tangpong et al., 2006; Tangpong et al., 2008) and the results of the current and next chapters in this dissertation research, we propose the following model for the mechanisms of CICI and the protective effects of MESNA from Dox in Fig. 3.7.

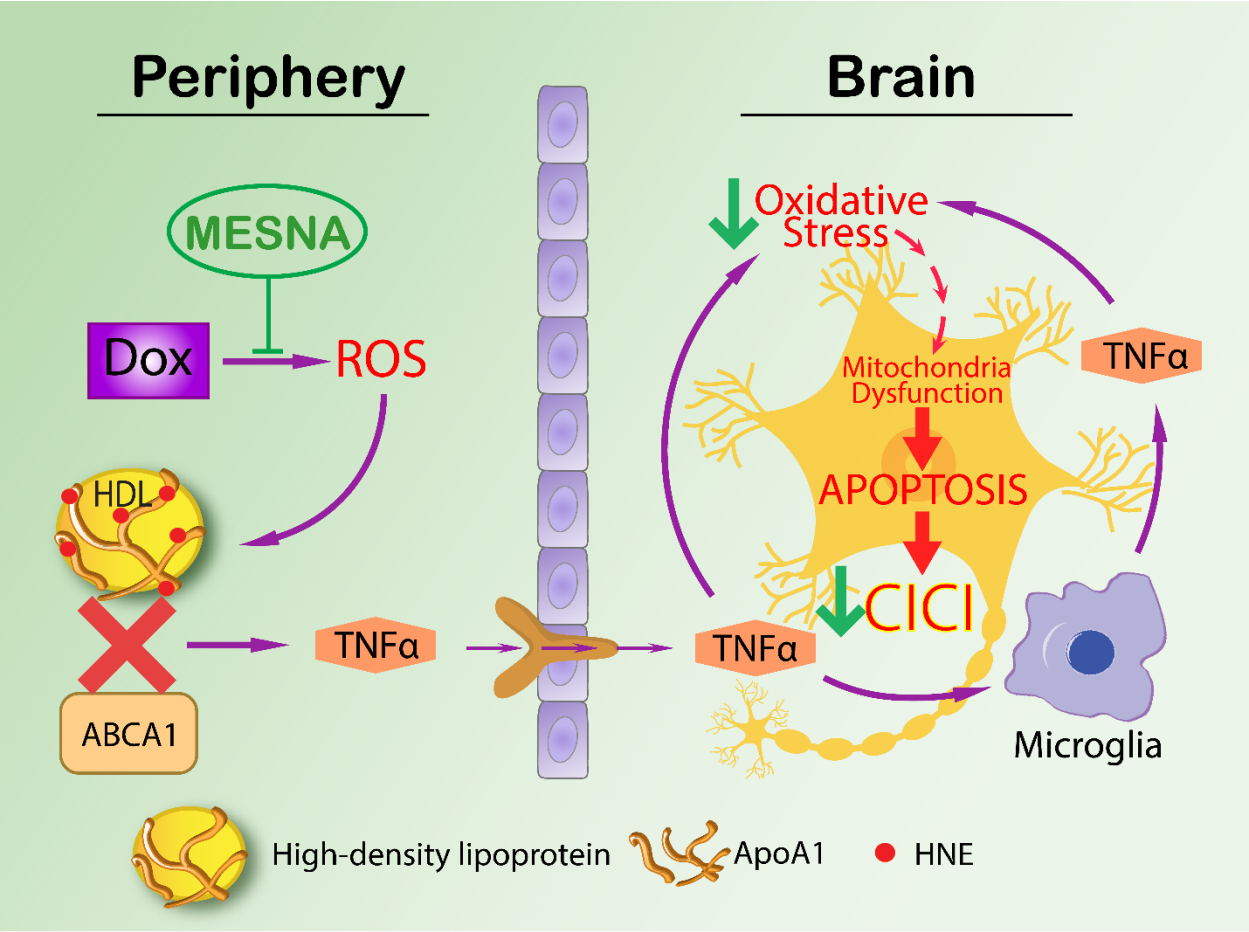

Figure 3.7 A proposed model of the mechanism of CICI and protective effect of MESNA. ROS-associated chemotherapeutic agent Dox causes elevation of oxidative stress, including protein-bound HNE. ApoA1 is oxidized by protein-bound HNE with conformational and further functional changes. ApoA1 thus loses its ability to interact with ABCA1, increasing TNF-α in the periphery as a consequence. TNF-α can then cross the blood-brain barrier by endocytosis of TNFR1, activate microglia in brain to make more local TNF-α, leading to neuronal mitochondrial dysfunction, apoptosis, and subsequent cognitive decline. MESNA can block the ROS in the periphery (plasma) and ameliorate oxidative stress and cognitive impairment in brain (labeled with green arrows in Fig. 3.7). (Keeney et al., 2018)

Peripheral Dox administration generates ROS, leading to oxidative damage to plasma proteins (Aluise et al., 2011; Tangpong et al., 2006). One plasma protein, ApoA1, has altered interaction involved in cholesterol transport with the ATP-binding membrane cassette transporter A1 (ABCA1) (Weber and Noels, 2011; Yin et al., 2011) due to its structure and function changed by oxidative damage (Subramaniam et al., 1997). The normal interaction of ApoA1 and ABCA1 could inhibit the production of TNF-α. Hence, oxidized ApoA1 would elevate the TNF-α in plasma, which can cross the BBB, leading to microglial activation, increased ROS and further TNF-α production in brain. Consequently, mitochondria are dysfunctional, along with subsequent cognitive decline (Aluise et al., 2010; Joshi et al., 2010). MESNA can protect both plasma and brain from oxidative damage including protein carbonyl and protein-bound HNE. MESNA also can save memory function and PC-PLC activity in brain following Dox administration.

The current chapter in this dissertation research presents strong evidence that MESNA potentially could protect both plasma and brain from oxidative damage, and subsequent cognitive impairment caused by the chemotherapeutic drug, Dox. The study provides a potential treatment method to CICI and strengthens the basis of investigations to gain insights into CICI.

CHAPTER 4. THE TRIANGLE OF DEATH OF NEURONS: OXIDATIVE DAMAGE, MITOCHONDRIAL DYSFUNCTION, AND LOSS OF CHOLINE-CONTAINING BIOMOLECULES IN BRAINS OF MICE TREATED WITH DOXORUBICIN: ADVANCED INSIGHTS INTO MECHANISMS OF CHEMOTHERAPY-INDUCED COGNITIVE IMPAIRMENT ("CHEMOBRAIN") INVOLVING TNF-A

4.1 Overview

Cancer treatments are developing fast and the number of cancer survivors could arise to 20 million in the United State by 2025. However, a large fraction of cancer survivors demonstrate cognitive dysfunction and associated decreased quality of life both acutely, and often long-term, after chemotherapy treatment. The etiologies of chemotherapy-induced cognitive impairment (CICI) are complicated, made more so by the fact that many anti-cancer drugs cannot cross the blood-brain barrier (BBB). Multiple related factors and confounders lead to difficulties in determining the underlying mechanisms. Chemotherapy-induced, oxidative damage-mediated tumor necrosis factor-alpha (TNF-α) elevation was considered as one of the main candidate mechanisms underlying CICI. As described early in this dissertation, the chemotherapeutic drug, doxorubicin (Dox), can generate reactive oxygen species (ROS). Peripheral Dox-administration results in oxidative damage of plasma protein elevation of TNF-α in both plasma and brain of mice (Tangpong et al., 2006). In the current chapter, TNF-α null (TNFKO) mice were employed to investigate the role of TNF-α in Dox-induced, oxidative damage-mediated alterations in brain. Both Dox-induced oxidative damage and mitochondrial dysfunction in brain were ameliorated in TNFKO brain. The slot blot technique was used to measure the oxidative damage, while the mitochondrial function was assessed by the oxygen consumption rate (OCR) acquired in Seahorse. Further, Dox-decreased levels of hippocampal choline-containing compounds and brain phospholipases activity are partially protected in the TNFKO group using MRS

study. The results provide strong evidence that Dox-targeted mitochondrial damage and levels of brain choline-containing metabolites, as well as phospholipases changes decreased in the CNS are associated with oxidative damage mediated by TNF-α. These results are consistent with the notion that oxidative damage and elevated TNF-α in brain underlie the damage to mitochondria and other pathological changes that lead to CICI. The results are discussed with reference to identifying a potential therapeutic target to protect against cognitive problems after chemotherapy.

4.2 Introduction

Cancer survivors often lose, at least in part, cognitive abilities of concentration, attention, learning and memory, and executive functions. Such patients often describe feelings of "chemofog" and feel it difficult to remember details, as well as slowness in problem-solving and multitasking. These symptoms are characteristic of chemotherapy-induced cognitive impairment (CICI). CICI could acutely or chronically happen to cancer survivors who had chemotherapy history and negatively affect their quality of life. However, many chemotherapeutic drugs are not able to cross the blood-brain barrier (BBB), but still can result in the injury to the CNS and lead to cognitive deficits. The mechanisms of CICI remain unclear. Although it is challenging to clarify the precise mechanisms of CICI, many candidates have been put forward, one of which is oxidative damage mediated elevation of pro-inflammatory cytokines (Butterfield, 2014; Ren et al., 2017).

Over half of FDA-approved chemotherapeutic drugs can generate reactive oxygen species which result in oxidative damage. (Chen et al., 2007). As noted above, Doxorubicin (Dox), an anthracycline antineoplastic drug, normally used as part of multi-drug chemotherapy regimens to treat solid tumors and lymphomas. In the presence of oxygen,

the conversion between the quinone and semi-quinone moiety of the structure of Dox undergo the redox cycling, producing superoxide radical anion ($O_2^{-\bullet}$) (Bachur et al., 1977; Cummings et al., 1991; Handa and Sato, 1975). Dox-induced oxidation of plasma-resident ApoA1 and resulting elevation of plasma levels of TNF-α that is transported to the brain are considered independently with the anti-tumor ability of Dox (Aluise et al., 2011; Bernacki et al., 1987; Hayslip et al., 2015). Oxidative and nitrosative damage in the brain occurs despite the fact that Dox cannot cross the BBB (Joshi et al., 2010; Joshi et al., 2007; Tangpong et al., 2007; Tangpong et al., 2006; Tangpong et al., 2008).

Toxic side effects of Dox-induced mitochondrial dysfunction are well known, especially in the cardiotoxicity of Dox (Chen et al., 2006; DeAtley et al., 1999; Jungsuwadee et al., 2006), which is an important factor for dose-limiting Dox treatment (Tangpong et al., 2007). Previous studies by the Butterfield and St. Clair lab presented the existence of Dox-induced brain mitochondrial dysfunction result from the nitration of manganese superoxide dismutase (MnSOD), a mitochondrial $O_2^{-\bullet}$ scavenger (Tangpong et al., 2007). Mitochondrial ROS involves activation of the nuclear factor κ-light-chain enhancer of activated B-cells (NF-κB) pathway (Chandel et al., 2000). Both inducible nitric oxide synthase (iNOS) and TNF-α are at the downstream of the NF-κB pathway (Griscavage et al., 1996; Keeney et al., 2013a).

Meanwhile, the volume of the hippocampus, essential to learning and memory, and neurogenesis are affected by TNF-α (Kesler et al., 2013; Kitamura et al., 2015), leading to behavioral deficits (Kwatra et al., 2016) such as anxiety and depressive-like behaviors, considered as chemotherapy-induced symptoms as well. The elevation of TNF-α in the periphery can cross the BBB by receptor-mediated endocytosis, after which elicit

microglial activation resulting in further local TNF-α release in brain (Ren et al., 2017). Hence, Dox-induced mitochondrial dysfunction likely is associated with TNF-α resulting in apoptosis (Chen et al., 2007) and, ultimately, in the cognitive decline of cancer survivors.

In the current chapter, the hypothesis was tested that TNF-α underlies alterations in brain measures of oxidative damage, hippocampal neurochemical profiles, phospholipase C and D activities, and loss of mitochondrial function in wild type (WT), but not TNF-α null (TNFKO) mice following *in vivo* Dox administration.

4.3 Methods and Materials

4.3.1 Chemicals

General chemicals, antibodies, and protease inhibitors were purchased from Sigma-Aldrich (St. Louis, MO). Pierce™ BCA Protein Assay Kit was purchased from ThermoFisher Scientific (Rockford, IL). The nitrocellulose membrane was purchased from Bio-Rad (Hercules, CA). EnzChek® Direct Phospholipase C Assay Kit and Amplex® Red Phospholipase D Assay Kit were purchased from Invitrogen/Life Technologies (Carlsbad, CA). Doxorubicin HCl was purchased from Bedford Laboratories™.

4.3.2 Animals

According to the U.S. National Institutes of Health Guide for the Care and Use of Laboratory Animals, all procedures were approved by the Institutional Animal Care and Use Committee of the University of Kentucky. The mice were housed in the University of Kentucky Animal Care Facility, following the standard conditions in an air-conditioned environment (22.1°C, 50.5% relative humidity, 12 h light-dark cycle), with free access to food and water. Male wild-type mice, B6C3F1/J (B6C3) mice, and TNF-α knockout

(TNFKO) B6.129S6-*Tnf*^{tm1Gkl}/J were purchased from the Jackson Laboratory. Each mouse was 2-3 months old and weighing approximately 25-30 grams. Dox was administrated to mice by a single intraperitoneal (i.p.) dose of 25mg/kg Dox or the same volume of saline as a control. MRS was performed on both wild-type and TNFKO mice 72 h post-treatment using methods described below. Following MRS studies, all mice were euthanized, immediately followed with plasma and brain tissue collection for molecular or biochemical experiments.

4.3.3 Hydrogen magnetic resonance spectroscopy (H^1-MRS)

H^1-MRS was used to measure the relative quantities of neurochemical changes in the mouse hippocampus in this chapter. MRS data was collected on a 7T BrukerClinscan horizontal bore system (7.0T, 30cm, 300Hz) equipped with a triple-axis gradient system (630 mT/m and 6300 T/m/s). A closed cycle, 14K quadrature cryocoil allowed for a 2.8 signal to noise increase relative to standard coils. Isoflurane (1.3%) was used to anesthetize mice before scanning in MRI compatible CWE Inc. equipment. Mice were placed on a Bruker scanning bed with tape. Tooth bar and ear bars were used to hold the mice on the bed. The equipment from SA Instruments Inc monitored the body temperature and respiration rate of the scanning mouse. The water heating system for the scanning bed maintained body temperature at 37°C. T2 weighted turbo spin echo sequences (TE 40ms, TR 2890ms, Turbo 7, FOV 20mm, 0.156 x 0.156 x 5.0 mm^3) were acquired and used for the placement of the spectroscopy voxel. The scanning procedure took 40 min. A 2x5.5x3mm^3 PRESS spectroscopic voxels (TE 135ms, TR 1500ms, 400avg, CHESS water suppression) was placed to cover both hippocampi. Spectrum analysis was performed using jMRUI (Naressi et al., 2001) to quantify the areas under each peak in the spectrum. The

area of the creatine (Cr) peak was used to normalize the peak areas of peaks of other metabolites.

4.3.4 Sample collection

Blood of mice was extracted cardiac puncture by cardiac puncture right after mice being sacrificed. Blood was transferred into EDTA tube immediately. Inverted the tube approximately ten times to completely mix the blood with the anticoagulant in the tube. The tube containing blood was then centrifuged at 3000 rpm at 4 °C, 10 min. After centrifuging, plasma was separated from other blood components and then transferred into a microcentrifuge tube, instantly put into liquid nitrogen. Mouse brain was extracted immediately following blood extraction, placed in a microcentrifuge tube, and immediately frozen in liquid nitrogen. All plasma and brain samples were stored at -80 °C and ready for future experimental use.

4.3.5 Sample preparation

The individual frozen mouse brain was thawed slightly on ice and put in a Wheaton glass homogenizer. Use the glass rod to homogenize the brain tissues for approximately 40-45 passes in the cold isolation buffer [0.32 M sucrose, 20mM HEPES, 2 mM EDTA, 2mM EGTA, 10 μg/ml phosphatase inhibitor cocktail 2, and protease inhibitor 5 μg/ml aprotinin, 4 μg/ml leupeptin, 4 μg/ml pepstatin A, and 0.2 mM PMSF]. All brain homogenate was transferred to a microcentrifuge tube and vortexed. Next, Fisher 550 Sonic Dismembrator (Pittsburgh, PA, USA) was used to sonicate brain homogenate on ice for 10s at 20% power, two times with an interval of 20s rest. After estimation of protein concentration with BCA assay, brain samples were ready for use.

Plasma samples were thawed on ice, diluted with cold isolation buffer described above, and estimated protein concentration by BCA assay.

4.3.6 Slot blot assay

Biomarkers of oxidative damage, including protein carbonyls (PC) and protein-bound 4-hydroxynonenal (HNE), were measured by slot blot assay. Brain or plasma samples were derivatized with 2,4-dinitrophenylhydrazine (DNPH) for measuring level of PC or solubilized in Laemmli buffer for measuring the level of HNE. 250 ng of proteins from each sample were loaded onto a nitrocellulose membrane in respective wells of the slot-blot apparatus (Bio-Rad) under vacuum. Membranes were blocked in 3% bovine serum albumin (BSA) in TBS with 0.2% (v/v) Tween-20 (TBS-T) for 1.5 h, then incubated TBS-T with primary antibody (1:500 anti-dinitrophenylhydrazone or 1:5000 anti-protein-bound HNE, respectively) for 2 h, followed with three times of washing in TBS-T, 5 minutes for each washing. Next, the membrane was incubated for 1 h with secondary antibody (secondary linked to alkaline phosphatase, 1:10000), washed in TBS-T three times, 5, 10, and 10 minutes, respectively for each washing. Then, the membrane was develope in alkaline phosphatase activity (ALP) buffer containing 1:300 5-bromo-4-chloro-3-indolyl phosphate (BCIP), and 1:150 Nitro blue tetrazolium (NBT). The developed membrane was dried overnight and then scanned for analysis on the second day. Imaging analysis was performed using Scion Image (Scion Corporation, Frederick, MD).

4.3.7 Brain mitochondria isolation and bioenergetic analysis

Cardiac puncture with cold mitochondrial isolation buffer [0.07 M sucrose, 0.22 M mannitol, 20 mM HEPES, 1 mM EGTA, and 1% bovine serum albumin, pH 7.2] was used

to perform brain perfusion of mice. Instantly, the brain was extracted. The method of mitochondrial isolation used in this chapter followed a published procedure (Mattiazzi et al., 2002) with modifications. Brain tissue was homogenized in cold mitochondrial isolation buffer with a Dounce homogenizer and centrifuged at 1500 × g at 4°C for 5 min. The supernatants were transferred to a clean microcentrifuge, while the pellets were resuspended with cold mitochondrial isolation buffer and centrifuged at 1500 × g at 4°C for 5 min. The supernatants collected after the second centrifugation was combined with the supernatants from the first centrifugation. The combined supernatants were recentrifuged at 1500 × g at 4°C for 5 min. The supernatants collected after the third centrifugation were centrifuged at 13,500 × g at 4°C for 10 min. The 4% Ficoll solution was used to purify the mitochondrial pellets collected after the fourth centrifugation, which were then resuspended in 50 µL cold mitochondrial isolation buffer. The Bradford Assay (Bradford, 1976) was then used to determine the protein concentration of the isolated brain mitochondria. The mitochondria isolation process was performed by Dr. Jeriel Keeney, Butterfield Lab, University of Kentucky.

The bioenergetics function of the freshly isolated mice brain mitochondria followed the procedure above was measured in the XF96 Analyzer (Agilent, Santa Clara, CA), which can measure the oxygen consumption rate (OCR) of mitochondria in real-time. 5µg mitochondria from each sample was added into one well of a XF96 culture plate. The respiration in each well was sequentially measured with substrate present (basal respiration) following the conversion of ADP to ATP, induced with the addition of oligomycin by the equipment. Next, the uncoupling agent FCCO was administrated by the analyzer to acquire the maximal uncoupler-stimulated respiration. At the end of the experiment, the

mitochondria respiration in each well was completely inhibited by the applied antimycin A, which is a complex III inhibitor. ORC was measured at four time-points with three replicates and plotted as a function of cells, showing the relative contribution of oxygen consumption, ATP-linked oxygen consumption, the maximal OCR after the addition of FCCP, and the reserve capacity of the cells. Seahorse analysis was performed by the D.K. St. Clair laboratory, Graduate Center for Toxicology, Department of Radiation Medicine, Markey Cancer Center, University of Kentucky.

4.3.8 Phospholipase C and phospholipase D activity assays

EnzChek® Direct Phospholipase C Assay Kit was used to measure the activity of phosphatidylcholine-specific phospholipase C (PC-PLC), while Amplex® Red Phospholipase D Assay Kit was used to measure the activity of phospholipase D, followed the manufactural instructions. The intensity of fluorescence was measured in SPECTRAFluor Plus instrument and quantified using associated MagellanTM software by TECAN throughout 24 h incubation at 37 ℃, avoided light. The fluorescence is collected at the time of maximal fluorescence peak showed during the 24 h incubation corresponding to the positive control.

PC-PLC activity data was collected after 22.5h of incubation of assay reagents and samples. The PtdCho in the substrate is cleaved by PC-PLC, generates dye-labeled diacylglycerol (DAG), and phosphocholine. The excitation wavelength is 509 nm, and the emission wavelength is 516 nm for PC-PLC. PLD activity data was collected at 1h of incubation of assay reagents and samples. The PtdCho in the substrate is cleaved by PLD, generates the alcohol component of the head group of PtdCho, releasing choline. The

excitation wavelength is 571 nm, and the emission wavelength is 585 nm for PLD.

4.4 Results

4.4.1 Dox administration results in increased oxidative damage markers in brain and plasma of WT mice that is absent in brain of TNFKO mice

Dox administration causes increased global oxidative damage in plasma and brain (Aluise et al., 2011; Joshi et al., 2007; Keeney et al., 2018). As one of the results, the plasma protein ApoA1 was oxidized that leads to elevation of TNF-α in plasma (Aluise et al., 2011; Joshi et al., 2010; Joshi et al., 2007; Joshi et al., 2005; Tangpong et al., 2006). Afterward, the peripheral TNF-α crosses the blood-brain barrier leading to oxidative damage in brain and apoptotic brain cell death (Aluise et al., 2011; Joshi et al., 2010; Joshi et al., 2007; Joshi et al., 2005; Tangpong et al., 2006). Consequently, to test the hypothesis that TNF-α is the principal cytokine elevated in plasma following Dox treatment that leads to brain oxidative and mitochondrial damage and resulting apoptotic cell death, the effects of Dox administration on oxidative damage in plasma and brain in TNF-α knockout (TNFKO) mice were investigated. Dox or saline was administrated to wild-type or TNFKO mice. Brain and plasma samples were collected 72 h post-Dox treatment, immediately following MRS studies. PC levels were used as a gauge of protein oxidation, while the lipid peroxidation product, protein-bound HNE, was used as an index of lipid damage.

Dox administration resulted in the elevation of oxidative damage markers, including both PC and protein-bound HNE, in both plasma and brain of WT mice (Fig. 4.1a-d). Due to its redox cycling properties associated with the quinone moiety in this anthracycline drug, TNFKO mice still had elevated PC levels and protein-bound HNE in plasma in Dox

group compared to saline-treated TNFKO mice; meantime, PC and protein-bound HNE levels following Dox treatment in brain of TNFKO mice both were found not to be significantly different from levels observed in saline-treated TNFKO mice (Fig. 4.1b and Fig. 4.1d). This result strongly supports our hypothesis that TNF-α plays a central role in Dox-induced oxidative damage in brain.

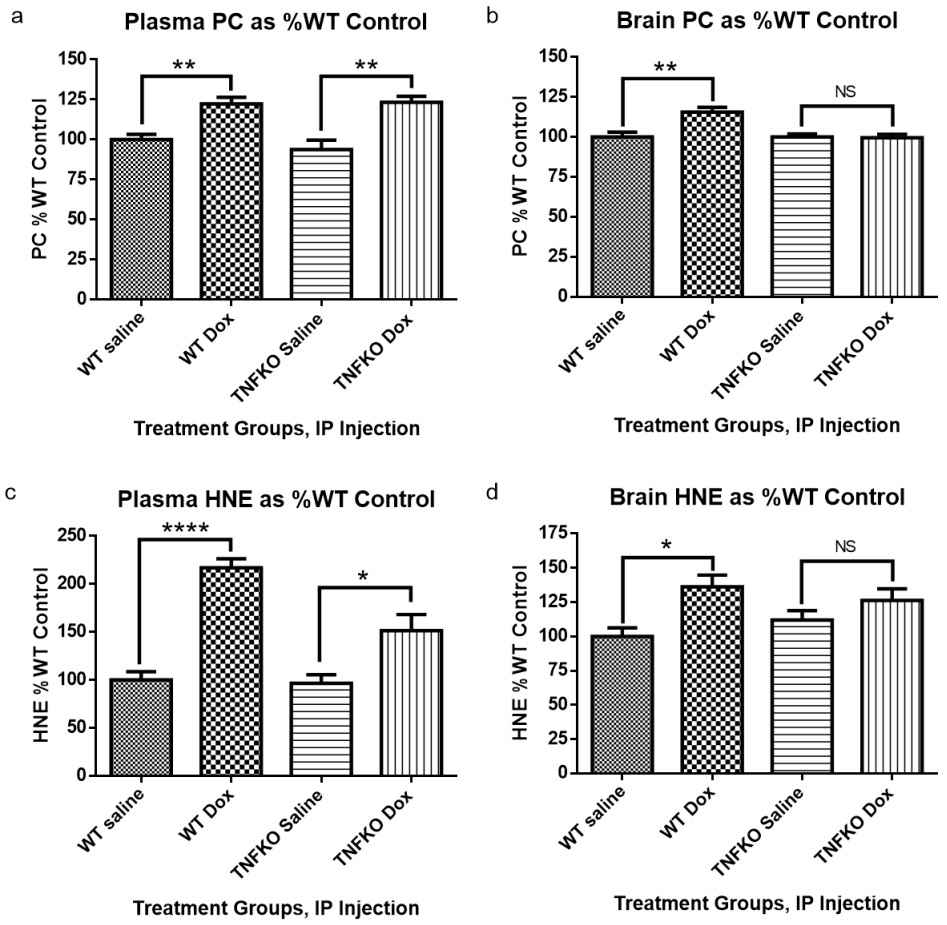

Figure 4.1 The levels of protein oxidation and lipid peroxidation were presented by the levels of PC and protein-bound HNE.

The levels of protein oxidation and lipid peroxidation were presented by the levels of PC and protein-bound HNE, respectively, in Fig. 4.1. Plasma and brain samples were collected 72 h post-treatment. (a) Dox administration resulted in significantly elevated PC levels in plasma of both wild-type and TNFKO mice compared to saline-treated wild-type and TNFKO mice, respectively. (b) The PC levels were significantly elevated following Dox treatment in brain of wild-type mice compared to saline-treated wild-type; however, the PC levels did not show significant differences in the brains between saline-treated and Dox-treated TNFKO mice. (c) Dox administration resulted in significantly elevated protein-bound HNE levels in plasma of both wild-type and TNFKO mice compared to saline-treated wild-type and TNFKO mice, respectively. (d) The protein-bound HNE levels were significantly elevated following Dox treatment in brain of wild-type mice compared to saline-treated wild-type; however, the protein-bound HNE levels did not show significant differences in the brains between saline-treated and Dox-treated TNFKO mice. (*$p<0.05$, **$p<0.01$, ***$p<0.001$, ****$p<0.0001$, NS = not significant). Assays and figure were performed by Dr. Jeriel Keeney, Butterfield lab, University of Kentucky. (Ren et al., 2018)

4.4.2 Dox administration leads to altered oxygen consumption rate in WT mice brain mitochondria that is prevented in TNFKO mice

Prior studies using a Clarke-type electrode demonstrated TNF-α-mediated mitochondrial dysfunction as assessed by oxygen utilization in brain as a consequence of peripheral Dox administration (Tangpong et al., 2007; Tangpong et al., 2006; Tangpong et al., 2008). In the current chapter shown in Fig. 4.2, the OCR of isolated brain mitochondria of mice was collected by the Seahorse analyzer. The OCR changes in mice brain mitochondria of saline-treated wild-type group, Dox-treated wild-type group, saline-treated TNFKO group, and Dox-treated TNFKO group were presented in blue circles, red squares, purple x, and green triangles, respectively in Fig. 4.2a. Basal, ATP-linked, maximal capacity, and reserve capacity OCR (related to ATP production) were ascertained in fresh brain mitochondria of each treatment group (Fig. 4.2b).

A significant decline in mitochondrial respiration in brain of Dox-treated WT mice as indexed by mitochondrial OCR was observed. Dox-treated WT mice significantly exhibited decreased mitochondrial OCR at every phase measured compared to wild-type mice (Fig. 4.2b). Compellingly, the mitochondrial OCR in brain of Dox-treated TNFKO mice was similar to that observed in saline-treated wild-type and saline-treated TNFKO group at every phase of mitochondrial OCR measured (Fig. 4.2b). This result supports our hypothesis that TNF-α is a key player in the observed mitochondrial dysfunction in brain from WT mice following Dox administration.

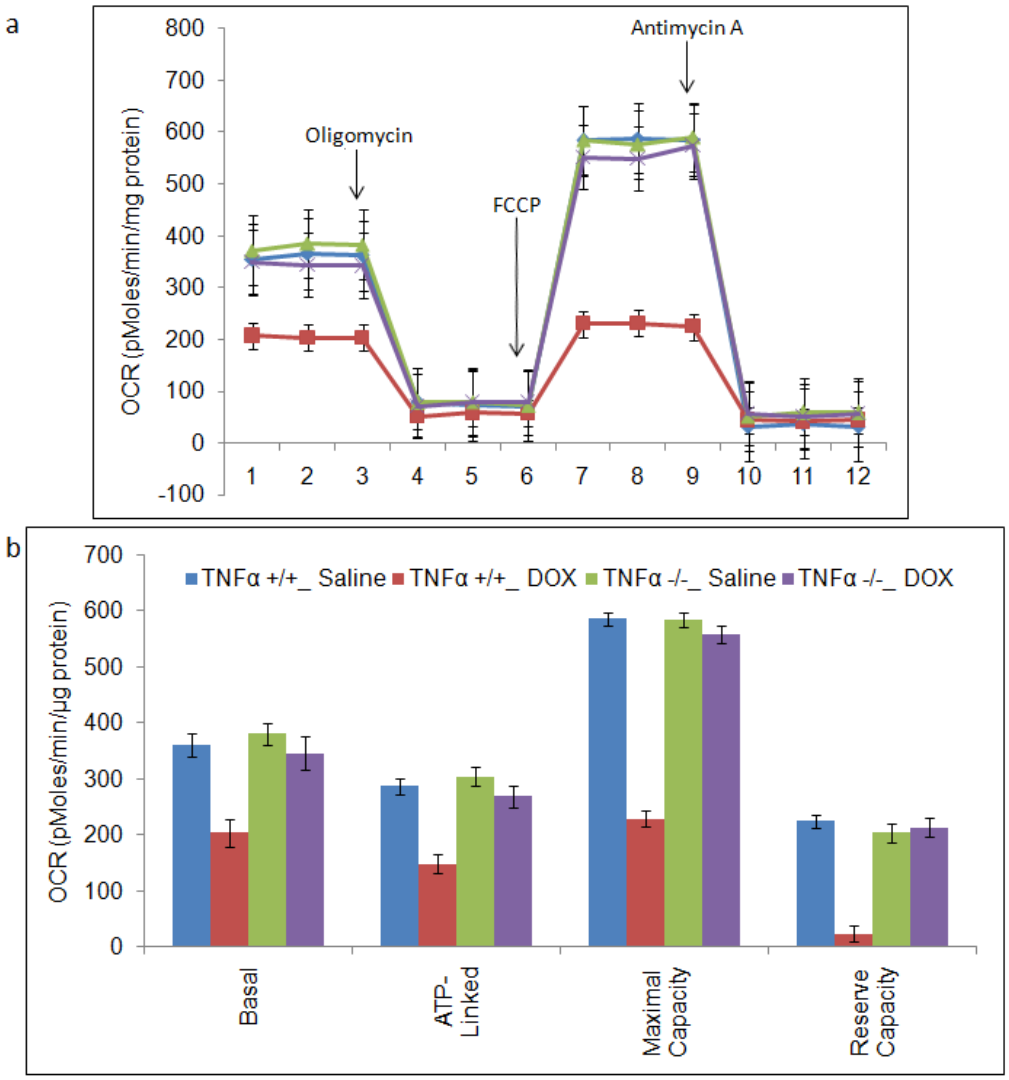

Figure 4.2 Mitochondrial function in brain of mice treated with Dox and Saline.

Mitochondrial protein (5 µg) were plated into wells of Seahorse Bioscience tissue culture plates and centrifuged before the measurement of total ORC. ORC of brain mitochondria indicates the mitochondrial function in brain, exhibited in blue for saline-treated wild-type mice; red for Dox-treated wild-type mice; purple for saline-treated TNFKO mice; and green for Dox-treated TNFKO mic. (a) For each sample, OCR was measured at four time-points in real-time and plotted as a function of cells under the basal condition followed by the sequential addition in different wells of Oligomycin (1µg/ml), FCCP (3µM) and Antimycin (2µM). (b) Quantification showing the relative contribution of oxygen consumption, ATP-linked oxygen consumption, the maximal OCR after the addition of FCCP, and the reserve capacity of the mitochondria.All data are shown as the Mean±SEM of triplicate samples and are representative of 3 independent experiments. Seahorse analysis was performed by D.K. St. Clair laboratory, Graduate Center for Toxicology, Department of Radiation Medicine, Markey Cancer Center, University of Kentucky. (Ren et al., 2018)

4.4.3 Changes to the neurochemical profile in hippocampus following Dox administration

Bilateral H^1-MRS scans of hippocampus revealed a dramatic decrease in the ratio of peak area of Choline-containing compounds (Cho) to that of Cr in Dox-treated WT mice compared to that in saline-treated control WT mice (Figure 3) confirming our earlier studies with WT mice (Keeney et al., 2018). The Cho/Cr ratio in Dox-treated TNFKO mice brain was still lower than that observed in saline-treated TNFKO mice, but profoundly higher than that (the Cho/Cr in brain) of Dox-treated WT mice, showing significant protection in the Cho/Cr ratio in mice hippocampus if TNF-α were absent. This result also provides strong evidence of TNF-α involvement in the Dox-induced decreased Cho/Cr ratio in brain.

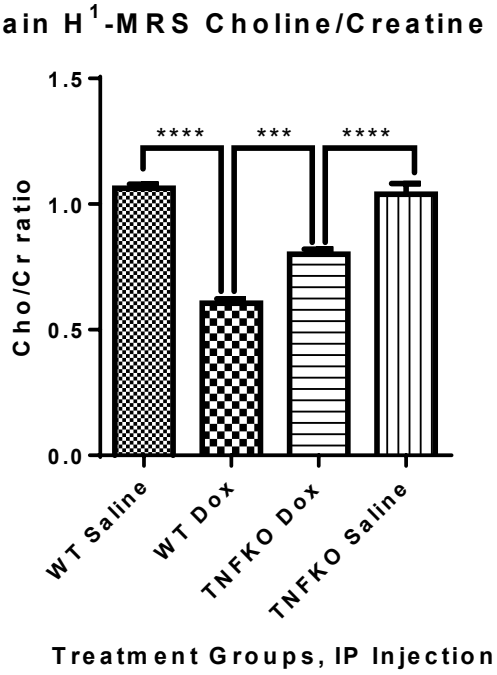

Figure 4.3 Dox-resulted Cho/Cr ratio decreases in hippocampus could be partially protected by the absence of TNF-α.

Bilateral H1-MRS scans of hippocampus revealed a large decrease in the Cho/Cr ratio in the Dox-treated WT group compared to saline control mice (****$p<0.0001$). Dox administration to TNFKO mice resulted in a rebound of the hippocampal Cho/Cr ratio over that of Dox-treated WT mice (***$p=0.0002$), although there also was a significant difference in the Cho/Cr ratio in mice hippocampus of TNFKO mice between saline and Dox treatment groups (****$p<0.0001$). MRS was performed by Dr. David Powell, Magnetic Resonance Imaging and Spectroscopy Center, University of Kentucky.

4.4.4 Dox administration to TNFKO mice results in partial preservation of PLD activity

Dox administration to WT mice resulted in significantly decreased activities of both PC-PLC and PLD in mouse hippocampus that likely contribute to the loss of Cho/Cr as determined by MRS (Keeney et al., 2018). The protection of the Cho/Cr ratio in the hippocampus of TNFKO mice observed by MRS (Fig. 4.3) led to the examination of the effect of TNF-α on activities on phospholipases responsible for the cleavage of choline and phosphocholine from PtdCho. Dox administration resulted in decreased activity of PC-PLC (Fig. 4.4a) in brain of WT mice compared to saline-treated WT mice. Dox also led to a decreased activity of PC-PLC in TNFKO mice compared to saline-treated TNFKO mice, the results did not show any protection on PC-PLC activity in TNFKO mice following Dox treatment. As shown in Fig. 4.4b, Dox administration resulted in significantly decreased activity of PLD in brain of mice in both WT and TNFKO groups, compared to saline-treated WT and TNFKO mice, respectively. However, a significant difference in PLD activity in mice brain also existed between the Dox-treated WT group and the Dox-treated TNFKO group, which indicated that brain PLD activity in TNFKO mice was protected from loss following Dox administration, but not completely. The results are consistent with the notion that TNF-α plays an important role in diminution of PLD activity following Dox treatment.

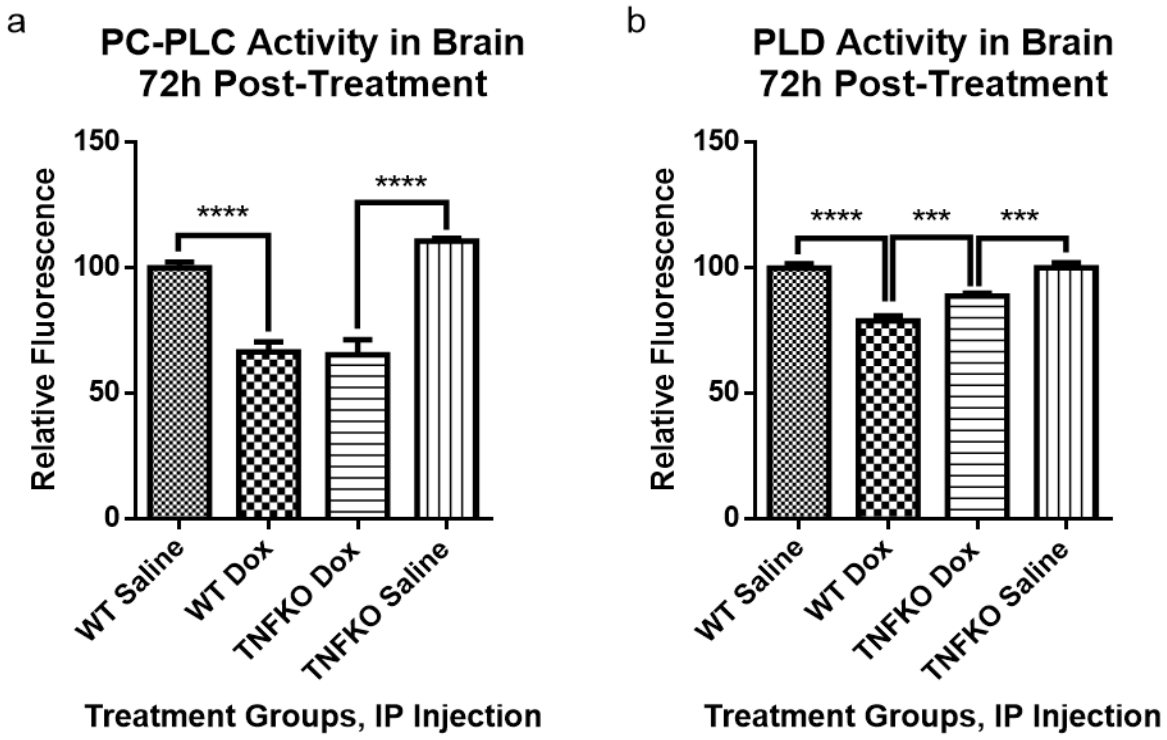

Figure 4.4 PC-PLC and PLD activities in brain of wild-type and TNFKO mice after Dox or saline treatment.

PC-PLC and PLD activity assays were performed at room temperature in the dark according to the manufacturers' instructions. The data are presented as percent saline control. (a) PC-PLC activity was measured after 22.5h of incubation of assay reagents and samples, the time at which the fluorescence of the corresponding positive control was maximum. Dox administration to WT mice caused a significant decrease in PC-PLC activity compared to saline-treated WT mice (****$p<0.0001$). Dox treatment of TNFKO mice resulted in a similar decrease in PC-PLC activity compared to saline-treated TNFKO mice (****$p<0.0001$). (b) Brain PLD activity at 1h of incubation of assay reagents and samples, the time of maximal fluorescence of the corresponding positive control in these trials, was performed according to manufacturer's instructions at 37oC protected from light. Dox treatment resulted in significantly decreased PLD activity in WT mice brain compared to that of saline-treated WT mice (****$p<0.0001$). Dox treatment also resulted in significantly decreased PLD activity in TNFKO mice brain compared to that of saline-treated TNFKO mice (***$P=0.0005$). However, PLD activity was preserved in Dox-treated TNFKO mice, significantly higher than PLD activity in brain of Dox-treated WT mice (***$p=0.0008$). The assays were performed by Dr. Keeney and Xiaojia.

4.5 Discussion

Many chemotherapy patients experience cognitive deficits following chemotherapy (Raffa and Tallarida, 2010), and as the number of cancer survivors increases with improved treatment, CICI should be taken into account so the quality of life after cancer treatment is not materially affected. Understanding the mechanisms of etiology and pathogenesis of CICI is necessary for prevention strategies for this condition. We propose that TNF-α, one of the chemotherapy-induced, oxidative damage associated, pro-inflammatory cytokines, plays a crucial role in CICI. Accordingly, the TNF-α knock-out animal model is an important and useful tool to investigate the hypothesized central role of TNF-α in CICI.

Dox is used in our laboratory as a prototypical ROS-generating chemotherapeutic agent that does not cross the BBB to investigate CICI. Dox administration led to damage with significantly increased oxidative damage and TNF-α elevation in both plasma and brain (Aluise et al., 2011; Keeney et al., 2018; Tangpong et al., 2007; Tangpong et al., 2006; Tangpong et al., 2008). The subsequent CNS injury included dysfunction of antioxidant enzymes, damaged brain mitochondria, neuronal death, and resultant cognitive dysfunction (Joshi et al., 2010; Keeney et al., 2018; Tangpong et al., 2007; Tangpong et al., 2006). Poor performance on the novel objective recognition tests of mice presented in chapter 3 of this dissertation research, and passive avoidance tests of rats (Konat et al., 2008) following Dox administration demonstrated that this ROS-generating chemotherapeutic agent leads to learning and memory deficits in rodents that mimics cognitive changes in CICI.

In Fig. 4.5, the results investigated in the current study provide compelling evidence for the central role TNF-α in chemotherapy-induced mitochondrial and neuronal damage and likely in the mechanisms of CICI. Every result will be discussed below, respectively.

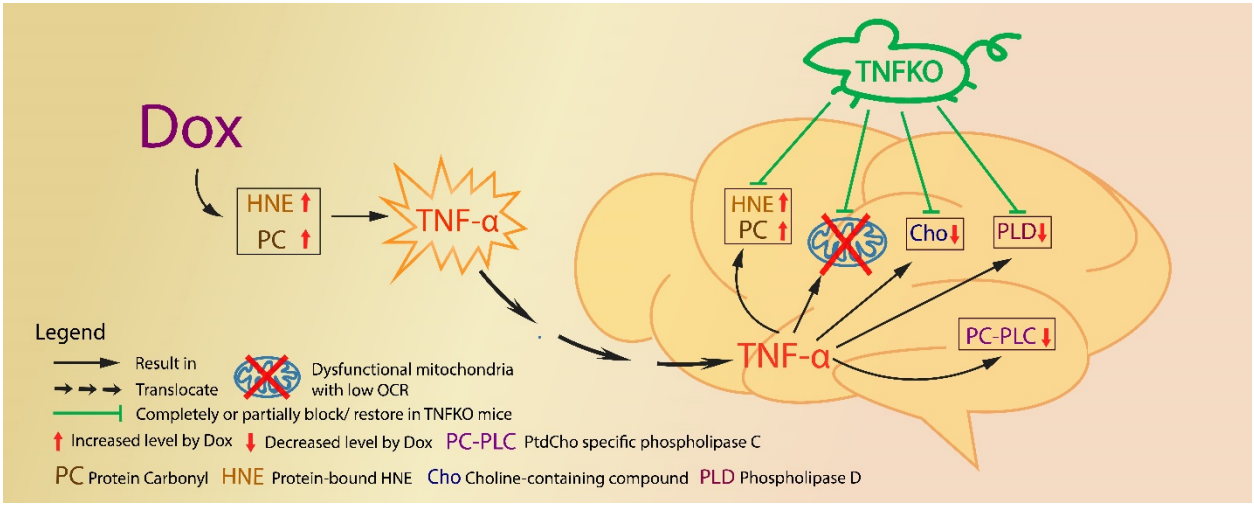

Figure 4.5 Schematic illustration of the sequelae of events in brain following Dox treatment of mice and their prevention or modulation in mice lacking the gene for TNF-α.

The red arrows represent the changes following Dox administration in mice observed in the present study and the green lines represent that most of these changes are completely or partially prevented in TNFKO mice.

Protein oxidation and lipid peroxidation in plasma and brain of Dox-treated WT mice were also shown in plasma of Dox-treated TNFKO mice (Fig. 1a, 1c), but no different than control in brain of the latter was observed (Fig. 4.1b, 4.1d). That oxidative damage still can occur in the periphery with absence of TNF-α is consistent with the characteristics of Dox, generating superoxide free radicals via redox cycling of its quinone moiety in the presence of oxygen. The absence of oxidative damage in TNFKO mice brain following Dox treatment provides stronger evidence that TNF-α is a critical player in elevation of Dox-induced oxidative damage in brain of WT mice.

One of the most detrimental consequences in brain following chemotherapy is mitochondria dysfunction (Joshi et al., 2010; Tangpong et al., 2007; Tangpong et al., 2006; Tangpong et al., 2008). Mitochondrial dysfunction is considered as a potential causal factor in a variety of neurodegenerative disorders, including Alzheimer disease, Parkinson disease, amyotrophic lateral sclerosis, and Huntington disease among others (Butterfield, 2014; Butterfield et al., 2012; Chaturvedi and Flint Beal, 2013). The brain has a high and constant energy requirement coupled with low energy stores. Mitochondria are responsible for meeting much of this energy demand (Siegel, 2006). Impairment of mitochondrial function in brain indexed by a decrease in Complex I activity of the electron transport chain following systemic Dox administration has been observed (Tangpong et al., 2006). Here, using Seahorse technology, the effect of Dox administration on mitochondrial respiration indexed by OCR was presented (Fig. 4.2). Peripheral Dox-treatment resulted in decreased mitochondrial basal, ATP-linked OCR as well as reduced OCR maximal and reserve capacities in brain of WT mice (red, Fig. 4.2b). Strikingly, mitochondrial OCR in brain of Dox treated TNFKO mice (purple, Fig. 4.2) was preserved, equivalent to the level of that

observed in saline-treated WT and TNFKO mice (blue and green, Fig. 4.2), indicating a central role of TNF-α in the decreased mitochondrial function in brain present following Dox administration. Once Dox-induced, TNF-mediated dysfunction of brain mitochondria happens, opening of the mitochondrial permeability transition pore associated with the observed loss of cytochrome c and elevated apoptotic brain cell death (Tangpong et al., 2006) likely underlies the loss of cognitive ability in mice following Dox administration (Keeney et al., 2018).

H^1-MRS allows non-invasive measurement of neurochemical changes in living brain (Jansen et al., 2006). As shown in chapter 3, changes in the neurochemical profile indexed by MRS in brain of WT mice following Dox administration was observed (Keeney et al., 2018). Dox-treatment resulted in dramatic decreased ratio of Cho/Cr in the hippocampus, a brain region critically involved in learning and memory (Clarke et al., 2010; Goulart et al., 2010; Meck et al., 2013; Sarkisyan and Hedlund, 2009), and whose volume could be affected by Dox-induced TNF-α (Kwatra et al., 2016). In H^1-MRS, choline, phosphocholine (PCho), and glycerophosphorylcholine (GPC) contribute to a cluster of peaks representing Cho (Keeney et al., 2018). Elevated TNF-α reportedly inhibits the synthesis of PtdCho, a major source of Cho, PCho, and GPC in the brain (Church et al., 2005; Mallampalli et al., 2000). In the current study, bilateral hippocampal H^1-MRS showed a profound decreased Cho/Cr ratio at 72 h following Dox treatment of WT mice (Fig. 4.3), while similar MRS measurements in brain of TNFKO mice showed a significant rebound of the Cho/Cr ratio from levels observed in Dox-treated WT mice (Fig. 4.3). Changes in choline-containing compounds on MRS are thought to be associated with membrane turnover (phospholipid synthesis and degradation) (Bertholdo et al., 2013;

Soares and Law, 2009) and have been attributed to myelin damage following chemotherapy (Ciszkowska-Lyson et al., 2003). The absence of TNF-α afforded significant protection of the Cho/Cr ratio in brain suggesting involvement of TNF-α in neuronal membrane damage.

In order to gain further insight into the involvement of TNF-α in the decreased Dox-mediated Cho/Cr ratio indexed in brain by MRS and a potential contributor to mechanisms of CICI, in the current study the activities of phospholipases responsible for the cleavage of choline and phosphocholine from PtdCho in the brain in TNFKO mice were investigated. Activities of both PC-PLC and PLD were found to be significantly diminished in brain of Dox-treated WT mice at 72 h post-treatment (Fig. 4.4), confirming prior studies (Keeney et al., 2018). PC-PLC activity remained lowered in brain of Dox-treated TNFKO mice, while PLD activity was significantly higher in brain of TNFKO mice following Dox treatment, providing evidence of TNF-α involvement in Dox-induced inhibition of PLD activity. Although Dox does not cross the BBB, Dox-induced ROS in the periphery possibly leads to the oxidative impairment of the BBB, allowing a small amount of Dox go into brain with local TNF-α elevation (Banks, 2016; Tabaczar et al., 2017), as well as brain oxidative damage (Fig. 4.1).

Reportedly, *PLCδ1* is a target gene for TNF receptor-mediated protection against cardiac injury by Dox (Lien et al., 2006). Expression of PLCδ1 was decreased in TNF receptor knockout mice with Dox treatment (Jang et al., 2008a) result that conceivably could contribute to the observation of the current study that PC-PLC still shows a lower level in brain of the Dox-treated TNFKO group. In recent research, leptin-induced TNF-α elevation reportedly occurs through activation of PLD (Lee et al., 2014), suggesting that PLD is possibly affected more than PLC by TNF-α deficiency, consistent with our present

findings using TNFKO mice. Moreover, phosphatidic acid, an intermediate of the PLD pathway, stimulated Ca^{2+}-mobilization and displayed growth factor-like activity (De Valck et al., 1993), which could help decrease Dox-induced mitochondrial dysfunction in TNFKO mice brain. This observation conceivably might contribute to the partial rescue of PLD in TNFKO mice. On the other hand, as noted, PLD also affects the level of TNF-α, consistent with the notion that PLD inhibition could lead to less cytokine production, including that of TNF-α (Friday and Fox, 2016; Urbahn et al., 2018; Zhang et al., 2001). Consonant with this idea, PLD was recently shown to be involved in TNF-α regulation by improving survival and decreasing TNF-α following LPS treatment in PLD knockout mice (Urbahn et al., 2018). Further supporting this concept, LPS induced TNF-α elevation in mouse macrophage-like cells could be partially decreased by inhibition of PC-PLC or PC-PLD and completely blocked by inhibition of both phospholipases (Zhang et al., 2001).

In addition to TNF-α-related inhibition of PtdCho biosynthesis (Mallampalli et al., 2000), TNF-α has been linked to a decline in phosphatidic acid levels (Oprins et al., 2002). PLD activity as well as the mRNA message for *PLD* have been shown to be increased during cellular differentiation and decreased during apoptosis (Jang et al., 2008a; Nakashima and Nozawa, 1999). Enzymatic activity of PLD was seen as essential to cell survival, and structural damage to PLD and decreased PLD activity is thought to promote apoptotic events (Jang et al., 2008b; Nozawa, 2002). There could be a cross-talk between the phospholipases and TNF-α expression due to their mutual dependence. Consequently, our results are consistent with the notion that ROS-generating chemotherapy agents' involvement in PLD inhibition potentially makes a significant contribution to CICI.

CHAPTER 5. PROFILES OF BRAIN OXIDATIVE DAMAGE, VENTRICULAR ALTERATIONS, NEUROCHEMICAL METABOLITES IN THE STRIATUM, AND BRIAN PROTEOME OF *PINK1* KNOCKOUT RATS AS FUNCTIONS OF AGE AND GENDER: RELEVANCE TO PARKINSON DISEASE

5.1 Overview

Parkinson disease (PD) is the second most common neurodegenerative disease associated with aging. Dopaminergic neuronal degeneration and α-synuclein aggregation are commonly found in the PD brain. Oxidative damage and inflammation often are considered as etiological factors of PD, although the detailed mechanisms still remain unknown. Gender and aging are two important risk factors to PD, and gene mutations and certain environmental factors have been implicated in this disease. The current study employed *PTEN-induced putative kinase -1* (*PINK1*) knockout (KO) rats, since mutations in *PINK-1* lead to familial PD. We evaluated the oxidative damage in the brain of *PINK1* KO rats, and MRI and MRS were used to measure the ventricle sizes and neurochemical metabolite profiles in these rats as a function of age and gender. We also investigated the brain proteome of *PINK1* KO rats with age and different genders. Distinct gender- and age-related alterations were found in *PINK1* KO brain. The results are discussed with respect to the suitability of this unique rat as a faithful model of known characteristics of PD.

5.2 Introduction

The second most common age-related neurodegenerative disease is Parkinson disease (PD), with about 10 million people in the world diagnosed with this disorder (Pinares-Garcia et al., 2018). Clinically, PD is characterized by motor dysfunction, including unstable postures, rigidity, bradykinesia, and resting tremors, and non-motor symptoms, including hallucination and anosmia, among others, and, in late-stage of PD, cognitive

deficits are observed (Poewe et al., 2017). Anosmia often happens many years prior to the appearance of motor symptoms appear. Pathologically, degeneration of dopaminergic neurons (DA) in the *substantia nigra pars compacta* and aggregation of phosphorylated α-synuclein in Lewy bodies are observed in PD brain that eventually lead to less dopamine in the striatum. The mechanisms of the pathology of PD still are not fully defined. However, gene mutation, exposure to halocarbons and/or some metal ions and metalloids in the environment are suspected to play a role in the development of PD. Oxidative damage, inflammation, dysfunction of brain mitochondria, and altered proteostasis also are thought to be associated with the pathophysiology and progression of PD (Triplett et al., 2015).

Mitochondrial dysfunction and DNA abnormalities have been complicatedly associated with PD (Greenamyre, 2018; Grünewald et al., 2018). Mutations of *PTEN-induced putative kinase-1* (*PINK1*) has been identified as a common genetic cause of familial PD. The protein PINK1 is a kinase maintaining the dynamics and integrity of mitochondria and providing neuroprotection to the brain. In addition, PINK1 is important for long term survival of human dopaminergic neurons (Wood-Kaczmar et al., 2008). Abnormal and dysfunctional mitochondria accumulate when PINK1 is absent, although in the mouse model of PD with knock-out of the *PINK1* gene, deposition of α-synuclein and degeneration of DA neurons were not found (Akundi et al., 2011; Jiang and Dickson, 2018; Pickrell and Youle, 2015).

Aside from aging, men have a higher risk, earlier onset, and faster progression of PD than women (Pinares-Garcia et al., 2018). The *PINK1* and *α-synuclein* genes were reported to be upregulated in males compared to females (Cantuti-Castelvetri et al., 2007). Dopaminergic neurons may have different metabolic properties in the substantia nigra of

human males and females, leading the male gender to be a high risk to develop PD (Cantuti-Castelvetri et al., 2007).

Up to now, the consensus is that a good mouse model to mimic all human PD characteristics does not exist (Dawson et al., 2010). A genetic rat model could have some advantages as a rodent model of PD, a bigger brain size compared to a knockout mouse model. In this current study, brain oxidative damage was measured by the slot-blot technique and the levels of metabolites in the striatum by MRS, and the ventricular size in brain of rats were measured by MRI, all to characterize whether the *PINK1* KO rat model we used is a suitable animal model that fulfills the criteria and manifests the characteristics of PD. We used wild-type (WT) 2 months-old rats as the control group and studied the *PINK1* knockout rat groups (hereafter, *PINK1* knockout is represented by KO in Chapter 5 of this dissertation) at 2, 4, 6, and 8 months of age separated into male and female groups. To our knowledge, the current research is the first study to show combined oxidative damage and striatum neurochemical profiles, as well as ventricular size, with the *PINK1* KO rats as a function of age and gender variables that provide insights into mechanisms of the pathobiology of familial PD.

5.3 Materials and methods

5.3.1 Chemicals

All chemicals used in this study were purchased from Sigma-Aldrich (St. Louis, MO, USA) unless otherwise noted. Pierce BCA protein assay was purchased from Thermo Scientific (Waltham, MA, USA). Criterion precast polyacrylamide gels, TGS electrophoresis running buffers, Precision Plus Protein All Blue and unstained Standards,

and nitrocellulose membranes were purchased from Bio-Rad (Hercules, CA, USA). Amersham ECL IgG horseradish peroxidase-linked secondary antibodies and ECL Plus Western blotting detection reagents were procured from GE Healthcare (Pittsburgh, PA, USA). Protein carbonyl detection kits were purchased from Millipore (Billerica, MA, USA). Anti-HNE and anti-nitrotyrosine primary antibodies were purchased from Alpha Diagnostic International Inc (San Antonio, TX, USA) and Sigma-Aldrich, respectively.

5.3.2 Animals

All animal studies were approved by the University of Kentucky Institutional Animal Care and Use Committee and followed NIH Guidelines for the Care and Use of Laboratory Animals. Both male and female, WT and KO rats were purchased from the Sage Research Labs (Horizon, Inc.) at 2 months old. All rats were kept under standard conditions housed in the University of Kentucky Animal Facility. Rats were sacrificed at 2 months, 4 months, 6 months and 8 months, respectively, after MRS was performed following methods described below. Rats were anesthetized using CO_2 before sacrificing. All methods provide a surgical plan of anesthesia prior to tissue harvest or exsanguination. The whole brain was excised immediately and frozen in liquid nitrogen for molecular and biochemical studies.

5.3.3 Hydrogen magnetic resonance spectroscopy

H^1-MRS (hydrogen magnetic resonance spectroscopy) was used to quantify neurochemical changes in the rat striatum. MRS data were acquired on a 7T BrukerClinscan horizontal bore system (7.0T, 30cm, 300Hz) equipped with a triple-axis gradient system (630 mT/m and 6300 T/m/s). A standard 2x2 array surface coil was used. Isoflurane (1.3%) was used to anesthetize rats before scanning in MRI compatible

equipment (CWE Inc.). Rats were placed on a Bruker scanning bed with a tooth bar, ear bars, and tape. Body temperature and respiration rate were monitored using equipment from SA Instruments Inc. The water heating system for the scanning bed maintained rat body temperature at 37°C. T2 weighted turbo spin echo sequences (TE 40ms, TR 2890ms, Turbo 7, FOV 20mm, 0.156 x 0.156 x 5.0 mm^3) were acquired and used for the placement of the spectroscopy voxel. The scanning procedure took 40 min. A 2x5.5x3mm^3 PRESS spectroscopic voxels (TE 135ms, TR 1500ms, 400avg, CHESS water suppression) was placed to cover both striatum. ^{1}H-MRS spectra were processed and the concentrations of the metabolites were derived using LCModel on a Linux operating system. LCModel uses a linear combination of model spectra of metabolite solutions in vitro to analyze the major resonances of *in vivo* spectra (Provencher, 1993). The area of the creatine peaks (Cr+PCr) was used to normalize the area of peaks of all other metabolites. MRI and H^1-MRS scans were performed by Dr. David Powell, Magnetic Resonance Imaging and Spectroscopy Center, University of Kentucky Medical Center.

5.3.4 Measuring Ventricle sizes of rat's brain on the MRI imaging

The ventricle size of these rats were analyzed using the FSL software, including two lateral ventricles, 3rd ventricle and 4th ventricle. Ventricle size was accessed using a T2 MRI scan, which resulted in the CSF within the ventricles showing up as a light gray to white color in the images. Imaging dimensions of voxels was increased by a factor of ten to compensate for the difference between human and rat brain size because of FSL is designed for human brains. BET was run to remove everything including skull and neck on the MRS images except for the brain (Smith, 2002). After running BET, the program FAST was run (Zhang et al., 2001). The restore output gave a bias field corrected brain to view. Waxholm

Rat was then used to scalable brain atlas and determine the ventricular system and entire brain by measuring the areas in voxels on each slice of the MRI imaging and then add the values of each slice together, for the ventricular system and entire brain, respectively. Normalization of the dimension of the ventricular system was acquired by the ratio of the voxels of all ventricles divided by the voxels of the entire brain consisting of the parenchyma and the ventricular system. MRI was performed by Dr. David Powell, Magnetic Resonance Imaging and Spectroscopy Center, University of Kentucky Medical Center.

5.3.5 Sample preparation

Wheaton glass homogenizer with ice-cold isolation buffer [0.32 M sucrose, 2 mM EDTA, 2 mM EGTA, 20 mM HEPES, 0.2 μg/mL PMSF, 5 μg/mL aprotinin, 4 μg/mL leupeptin, 4 μg/mL pepstatin, and 10 μg/mL phosphatase inhibitor cocktail 2] were used to homogenize the brains of rats. The homogenates were then sonicated on ice for 10 seconds, two times with 10 seconds rest in between. Protein concentrations of homogenates were determined by the Pierce BCA method (Rockford, IL, USA) after sonication.

5.3.6 Slot blot assay

Protein carbonyls (PC) and protein-bound 4-hydroxy-2-trans-nonenal (HNE) were detected by slot blot assay (Castegna et al., 2003; Sultana and Butterfield, 2008). For determination of PC, samples were derivatized with 2,4-dinitrophenylhydrazine (DNPH) in advance. For determination of HNE and 3-NT, brain homogenates were prepared with Laemmli buffer. Protein (250 ng) from each sample were loaded onto a nitrocellulose membrane in separate wells in a slot-blot apparatus (Bio-Rad, Hercules, CA, USA) under

vacuum formed by a water suction system. Membranes were blocked in 5% bovine serum albumin (BSA) in TBS-Tween20 (0.2% v/v) for 1.5 h and followed with incubation in primary antibody (anti-dinitrophenylhydrazone primary, anti-protein-bound HNE or anti 3-NT, respectively, each produced in rabbit, Sigma-Aldrich) for 2 h, washed three times in TBS-T and then incubated for 1 h with secondary antibody (goat anti-rabbit secondary linked to alkaline phosphatase). Membranes were developed for alkaline phosphatase activity (ALP) buffer containing 5-bromo-4-chloro-3-indolyl-phosphate (BCIP, 1:300) dipotassium and nitro blue tetrazolium (NBT, 1:150) chloride, and then dried overnight, followed with image scanning for analysis performed using Scion Image (Scion Corporation, Frederick, MD).

5.3.7 Isoelectric focusing (IEF)

To separate the proteins at the 1st dimension by their isoelectric point, 150 µg brain samples were added with freshly prepared IEF rehydration buffer [8 M urea, 2 M thiourea, 2.0% (w/v) CHAPS, 50 mM dithiothreitol (DTT), 0.2% Biolytes, 0.01% Bromophenol Blue] to reach the total volume to 200 µl, then shaken on a vortex at 22 °C for 2 h. After the 2h shaking, samples were sonicated for 10 s on ice at 20% power and then transferred to the focusing tray. Each sample in the focusing tray was covered with one 11 cm ReadyStrip IPG strips, pH 3-10 (Bio-Rad, Hercules, CA, USA), immediately followed with the rehydration process on the Protean IEF cell (Bio-rad, Hercules, CA)). The IPG strips were actively rehydrated at 20 °C for 18 h at 50 V. Each strip was covered with 2 ml mineral oil after the rehydration started 45 minutes. Then, the strips were isoelectrically focused at a constant temperature of 20 °C beginning at 300 V for 2 h linearly, 500 V for 2 h linearly, 1000 V for 2 h linearly, 8000 V for 8 h linearly, and finishing at 8000 V for 10 h rapidly.

The IPG strips were then instantly transferred into a i12 Rehydration/Equilibration tray (Bio-Rad, Hercules, CA, USA) and stored at the -80 °C freezer.

5.3.8 Two-dimensional polyacrylamide gel electrophoresis (2D-PAGE)

After the IEF separation, 2D-PAGE was used to separate proteins at the 2nd dimension based on their migration rate, which depends on molecular weight and protein shape. The i12 Rehydration/Equilibration tray containing the IPG strips was thawed at room temperature for 5 min. The 4 ml equilibration buffer A [6 M urea, 1% (w/v) SDS, 30% (v/v) glycerol, 50 mM Tris– HCl (pH 8.8), 0.5% DTT] was added to each strip in the tray for 10 min and then the equilibration buffer A was poured out of the tray, immediately followed adding the equilibration buffer B [6 M urea, 1% (w/v) SDS, 30% (v/v) glycerol, 50 mM Tris–HCl, pH 8.8, 4.5% iodoacetamide (IA)] for 10 min. IPG strips were next placed into Linear Gradient (8-16%) Precast Criterion Tris–HCl polyacrylamide gels, 11 cm. Precision Plus Protein All Blue molecular weight standards were run with samples at a constant voltage of 200 V for approximately 45 min in Tris-Glycine SDS running buffer.

5.3.9 Sypro Ruby staining

Sypro Ruby gel protein stain allows for the detection and quantification of total protein content. After scanning the 2D gels, the gels were fixed in 50 mL fixing solution [7% (v/v) acetic acid, 10% (v/v) methanol] for 45 min. After removing the fixing solution, 50 mL of Sypro Ruby stain was added for overnight staining (16-18hr) at 22˚C with gentle rocking. Gels were rinsed off the background by putting the gel in another round of 50 ml fixing solution, gently rocking for 45-60min. The gels are then rinsed and transferred to 50 mL DI water and scanned at 450 nm using the afore-mentioned scanners. Gels were stored in

DI water at 4 °C until protein spot excision.

5.3.10 PDQuest image analyses

Spot intensities from Sypro Ruby-stained 2D-gel images were quantified densitometrically according to the total spot density using PDQuest 2D analysis software (Bio-Rad). Differential protein expression Spot intensities from Sypro Ruby-stained 2D-gel images were quantified by densitometry. The intensities of gel spots were normalized to the total gel density. Protein spots of gels from a particular study were first manually matched together and then matched by the PDQuest program using powerful auto-matching algorithms for accurate spot-matching. Resultant data of normalized intensity of each protein spot were compared between groups using the appropriate statistical analysis.

5.3.11 In-gel trypsin digestion

Significant protein spots were excised from 2D-gels with a clean, sterilized razor blade or pipette tip and individually transferred to Eppendorf microcentrifuge tubes. Gel plugs were incubated with 20 µL of 0.1 M ammonium bicarbonate (NH4HCO3) for 15 min, and with 30 µL of ACN for 15 min. Gel plugs were dried under a flow hood at RT for 30 min. Next, 30 µL of 20 mM DTT in 0.1 M NH4HCO3 was added at 56°C for 45 min. The DTT/NH4HCO3 solution was then removed and replaced with 30 µL of 0.05 M IA in 0.1 M NH4HCO3 and 28 incubated at 22˚C for 15 min. Next, the IA solution was removed and plugs incubated for 15 min with 150 µL of 0.05 M NH4HCO3. Then, 200 µL ACN was added to this solution and incubated for 15 min. The solvent was removed and gel plugs were allowed to dry for 30 min under a flow hood. Plugs were rehydrated with 10 µL modified trypsin solution (Promega, Madison, WI, USA) in 0.05 M NH4HCO3 (enough

to completely cover the gel plugs) and incubated with shaking overnight at 37 °C.

5.3.12 Gel-peptide extraction and desalting

The next day, the digest solution was transferred into a new Eppendorf microcentrifuge tube. Next, approximately 20 µL of a 5% ACN, 0.1% formic acid (FA) solution was added to the old tube containing the gel plug (twice the volume necessary to submerge the gel) and sonicated in a bath for 15 min. To this, 30 µL of a solution containing 95% ACN, 0.1% FA and 0.001 M NH4CO3 was added and sonicated for 15 min. This resulting solution was combined with the supernatant digest solution in the new Eppendorf tube. Using a Speed Vac, the samples were concentrated to a volume of 10 µl. Using C18 ZipTips (SigmaAldrich, St. Louis, MO, USA), salts and contaminants were removed from the tryptic peptide solutions. To prepare the column in the ZipTip, 10 µL of 100% ACN was aspirated into the tip and then expelled 5 times. Next, 10 µL of a 50% ACN solution containing 0.1% FA was aspirated and expelled 5 times for column equilibration. The trypsin digested solution was then slowly drawn up and pushed gently out of the column 10 times for peptide adherence. Unwanted contaminants 29 were removed from the peptides in the ZipTip by washing with 10 µL of a 5% ACN and 0.1% FA solution 3 times. To elute the peptides from the column, 10 µL of a 50% ACN and 0.1% FA solution was drawn up and then expelled into a new Eppendorf tube. The eluant was drawn up and expelled 5 times to ensure complete peptide removal from the column. Samples were stored at -80˚C until MS/MS analysis.

5.3.13 LC-MS analysis, data interrogation and protein identification

In-gel digested samples were desalted with C18 ZipTips, dried by speedvac, reconstituted in 10 µL 5% ACN/0.1% FA, and analyzed by an Easy nLC 1000-Orbitrap Elite system (Thermo Scientific, San Jose, CA) in data dependent scan mode. An in-house packed capillary column (0.1 x 130 mm column packed with 3.6 µm, 200Å XB-C18) and a gradient with 2% ACN/0.1% FA and 80% ACN/0.1% FA at 200 nL/min was used for separation. The MS spectra were acquired by the Orbitrap at 60,000 mass resolution and MS/MS spectra of the five most intense peaks in MS scan were obtained by the Orbitrap at 30,000 mass resolution.

Data files from all samples in this dissertation research were searched against the most current version of the Swiss-Prot database by SEQUEST and Mascot (Proteome Discoverer v1.4, Thermo Scientific). At least two high-confidence peptide matches were required for protein identification with false discovery rate (FDR) at 1% and proteins matched with the same peptides are reported as one protein group.

5.4 Results

5.4.1 Age and gender both affect the oxidative damage in the rat brains.

The rats were sacrificed at different ages (2 months, 4 months, 6 months and 8 months). Homogenates of rats brains were analyzed by the slot blot assay to measure the level of oxidative damage, including PC, HNE and 3-NT in the whole brain of WT and *PINK1* KO rats, male and female, by reading the intensity of bands for each sample. All intensities were normalized to the average of all samples of 2-mos WT group for each oxidative damage biomarker, respectively. The data were shown in the percentage of 2 mos-old WT

rats (including both male and female). PC, HNE and 3-NT levels are presented in Fig. 5.1-a, 5.1-b, and 5.1-c, respectively. The columns represent oxidative damage levels in the brains of all rats, including both males and females at each genotype and age group. The blue triangle and red circle symbols represent only males and females at different ages, respectively. In Fig. 5.1-a, 2 mos-old *PINK1* KO rats showed a trend of higher but not significantly increased PC levels in the whole brain compared to WT rats at the same age (2 mos). Then, as the age increased, the PC level increased at 4 mos in *PINK1* KO rats, significantly different from 2 mos-old WT rats. However, PC levels were reduced at the age of 6 mos in *PINK1* KO rat brain, and then significantly increased at 8 mos. PC levels of 8 mos-old KO rats also are significantly higher than both WT rats and *PINK1* KO rats both at 2 mos-old age. Similar trends were observed after separation by gender. No significant differences were observed between males and females of each genotype at the same age.

Fig. 5.1-b showed the HNE levels in the brains of rats. The trends as age increased show that HNE levels in the brain of *PINK1* KO rats at 4 mos were significantly higher than all other groups when analyzing all rats with both genders and also in analyzing only females. The 4 mos-old *PINK1* KO male rats show significant increased HNE levels compared to 2 mos-old WT, 2 mos-old *PINK1* KO and 6 mos-old *PINK1* KO rats, respectively). The decreased HNE levels at 6 mos of *PINK1* KO male rats were significantly elevated at 8 mos, which is similar to the trend of PC levels of 6 mos-old *PINK1* KO rats in Fig. 5.1-a. At the age of 4 mos-old, male *PINK1* KO rats have less HNE levels in the brains than the *PINK1* KO females.

Fig. 5.1-c shows the 3-NT levels in the brains of rats. The *PINK1* KO rats group at 6

mos of age showed a significant decreased 3-NT level in the brain compared to 4 and 8 mos-old *PINK1* KO rats in Fig. 5.1-c. Male KO rats have more significant changes than female KO rats as age increased. The 3-NT levels were significantly higher at 4 mos and 8 mos of age for *PINK1* KO male rats brain compared to 2 mos-old WT rats. A significant decrease in the level of 3-NT in the brain from 4 mos-old *PINK1* KO male rats also was observed at the age of 6 mos, which increased again at the age of 8 mos. At the age of 8 mos-old, male KO rats have more 3-NT levels in the brains compared to female KO rats.

a) Oxidative damages:
Protein Carbonyl

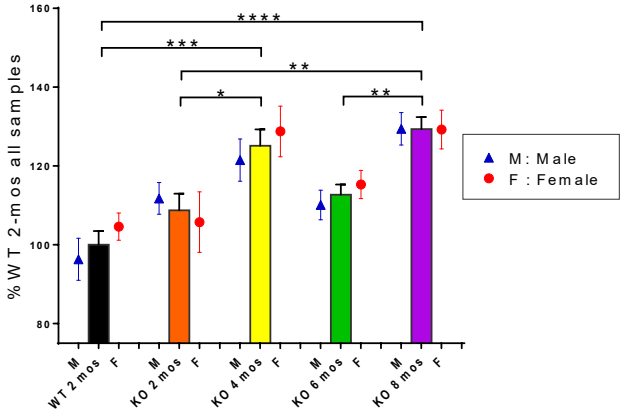

b) Oxidative damages:
Protein-bound HNE

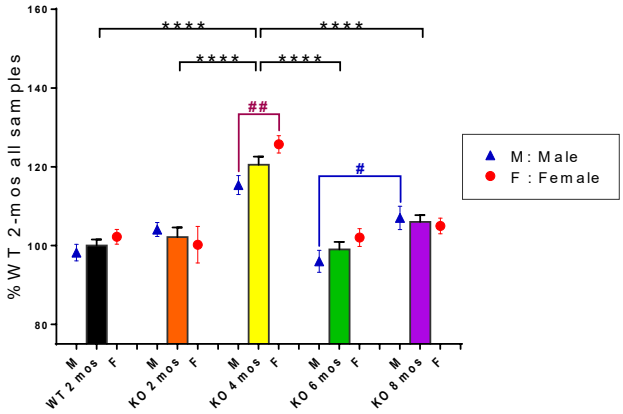

c) Oxidative damages:
3-NT

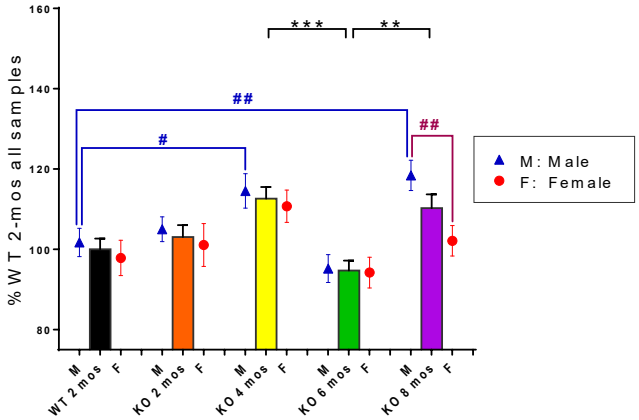

Figure 5.1 The levels of the biomarker of oxidative damage: protein carbonyl, protein-bound HNE, and 3-NT in the brain of WT and *PINK1* KO rats at different ages and genders. The oxidative damage levels were revealed by the intensity on the slot blot of each brain sample and normalized the *PINK1* KO groups to the percentage of 2 mos-old WT level for each biomarker. Black stars (*) and significant lines marked the significant changes between different age and genotype groups, consisting of both male and female. Purple # and purple significant lines (in 5.1-b and 5.1-c) marked the significant changes between male and female at same age and genotype group. The levels of oxidative damage were affected more in the *PINK1* KO rats. Blue # and blue significant lines (in 5.1-b and 5.1-c) were used to show significant changes among different age groups for only male rats when the male rats have additional significant changes compared to total sample groups. (a) The protein carbonyl (PC) levels change as age increased with all samples, including both male and female. Both genders follow a similar trend: *PINK1* KO rats reaching a high level at 4 mos of age, decreased at 6 mos, and increased again at 8 mos. WT 2-mos vs. KO 4-mos (***, $p<0.001$); WT 2-mos vs. *PINK1* KO 8-mos (****, $p<0.0001$); *PINK1* KO 2-mos vs. *PINK1* KO 4-mos (*, $p<0.05$); *PINK1* KO 2-mos vs. *PINK1* KO 8-mos (**, $p<0.01$); *PINK1* KO 6-mos vs. *PINK1* KO 8-mos (**, $p<0.01$). No significant differences between male and female at each age were found at each age group. (b) The protein-bound HNE (shorted to HNE) levels changed as age increased with all samples, including both male and female. *PINK1* KO 4-mos rats showed a significantly higher level compared to all other groups. *PINK1* KO 4-mos vs. WT 2-mos (****, $p<0.0001$); *PINK1* KO 4-mos vs. *PINK1* KO 2-mos (****, $p<0.0001$); *PINK1* KO 4-mos vs. *PINK1* KO 6-mos (****, $p<0.0001$); *PINK1* KO 4-mos vs. *PINK1* KO 8-mos (****, $p<0.0001$). All female rat groups followed a similar pattern as the total sample groups with all four significant differences (significant lines were not shown; $p<0.0001$). However, significant increased HNE levels in *PINK1* KO male brain were observed from the 6 mos-old group to 8 mos-old group (blue #, $p<0.05$), instead of a significant difference between *PINK1* KO 4-mos group and *PINK1* KO 8-mos group of only males. At the age of 4 mos, a significant gender difference also was observed (purple ##, $p<0.01$). At this age, female *PINK1* KO rats are more affected by HNE damage than were male rats. (c) The 3-NT levels change as age increased with all samples, including both male and female. Both *PINK1* KO 4-mos group and *PINK1* KO 8-mos group showed significantly higher levels of 3-NT than the *PINK1* KO 6-mos group. *PINK1* KO 4-mos vs. *PINK1* KO 6-mos (***, $p<0.001$); *PINK1* KO 8-mos vs. *PINK1* KO 6-mos (**, $p<0.01$). Female rats groups followed a similar pattern as the total sample groups as age increased, but only one significant decreased level of 3-NT was observed in only female rats with increasing age, which is *PINK1* KO 4-mos female vs. *PINK1* KO 6-mos female (the significant line was not shown, $p<0.05$). *PINK1* KO male rats demonstrated more changes in brain 3-NT levels compared to female rats. In addition to *PINK1* KO 6-mos male vs. *PINK1* KO 4-mos male (the significant line was not shown, $p<0.01$) and *PINK1* KO 6-mos male vs. *PINK1* KO 8-mos male (the significant line was not shown, $p<0.01$), significantly increased 3-NT levels also were observed when WT 2-mos male vs. *PINK1* KO 4-mos male (blue ##, $p<0.01$), and WT 2-mos male vs. *PINK1* *PINK1* KO 8-mos male (blue #, $p<0.05$). At age of 8 mos, a significant gender difference also was observed (purple ##, $p<0.01$). At this age, male *PINK1* KO rats were more affected by 3-NT damages than were female rats. (Ren et al., 2019b)

5.4.2 *PINK1* KO male rats have larger ventricle size than female *PINK1* KO rats at the same age, suggesting more edema occurs in male PINK1 KO rats.

Ventricle sizes were normalized to the entire brain size and then were assessed for significance using multiple t-tests (Fig. 5.2-a). Male *PINK1* KO rats always showed significantly increased ventricle size compared to female *PINK1* KO rats at each age ($p<0.05$, $p<0.01$, $p<0.001$, $p<0.01$, respectively), consistent with the notion that more edema occurred in the brains of male *PINK1* KO rats. Fig. 5.2-b is presenting representative brain images with on MRI at the levels of both hippocampus and striatum. The brain images on the first row are from one male *PINK1* KO rat at 8 mos-old, in which the ventricles are marked with blue color. While the brain images on the second row are from one female *PINK1* KO rat at 8 mos-old, in which the ventricles are marked in red. The *PINK1* KO rats at 2, 4, and 6 mos old show the same pattern: ventricle sizes of male *PINK1* KO rats are larger than the ventricle sizes of female *PINK1* KO rats at the same age (images are not shown for all age groups). WT rats do not show this pattern.

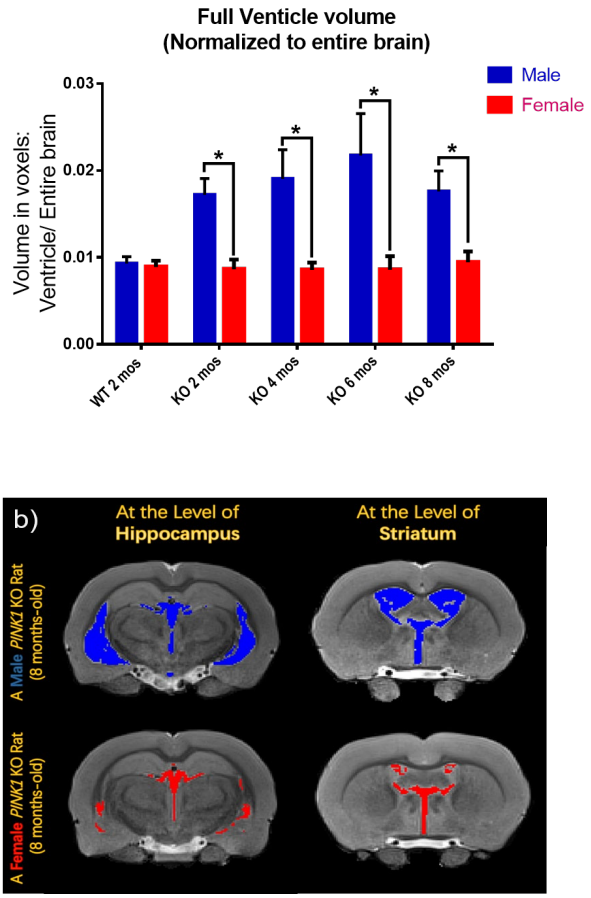

Figure 5.2 The ventricle sizes were measured from MRI images.

The dimensions of the entire brain and all ventricles including two lateral ventricles, 3rd ventricle, and 4th ventricle were measured using the Waxholm Rat program after adjusting all the factors. The dimensions were acquired in voxels for each individual slice image of each brain. The values of each slice were added together to obtain the size of ventricles or the entire brain. The size of the ventricular system was normalized to the size of the entire brain. a) In the *PINK1* KO rats, the male rats showed significantly larger sizes of ventricles in brain compared to those of females at the same ages. No differences were observed between males and females in the WT group. b) Representative images of brains from one male and one femalre from group of *PINK1* KO rats at 8 mos-old. Brain images are presented at levels of both hippocampus and striatum. Ventricles of the male *PINK1* KO rat is marked in blue, while the female *PINK1* KO rat is marked in red. The images support the data showing in Fig. 5.2-a that male *PINK1* KO rats have larger ventricles than female *PINK1* KO rats. *$p<0.05$, significantly different.

(Ren et al., 2019b)

5.4.3 Changes in neurochemical metabolites in striatum of rats were observed as age or gender varies.

Bilateral H^1-MRS scans of striatum revealed changes of metabolites, including glutamine (Gln), glutathione (GSH), taurine, inositol (Ins) and N-acetylaspartate (NAA) as functions of age and/or gender (Fig. 5.3-5). The peak area of metabolites was divided by the total peak areas of Cr and PCr together. One-way ANOVA was used to analyze the results for the function of age, while multiple t-tests were applied to analyze the metabolites in the striatum at the same age with different genders. All of the *PINK1* KO rats showed a significantly higher level of Gln in the striatum compared to the WT control group (Fig. 5.3-a). A trend of decreased taurine was observed in the striatum as age increased (Fig. 5.4-a). The 6 mos-old *PINK1* KO group showed significantly decreased levels compared to both 2 mos-old WT and 2 mos-old *PINK1* KO group, respectively. The 8 mos-old *PINK1* KO group showed significantly decreased levels compared to 2 mos-old WT, 2 mos-old *PINK1* KO, and 4 mos-old *PINK1* KO group. In Fig. 5.5-a, the 2, 4, and 6 mos-old *PINK1* KO groups showed a decreased level of Ins in the striatum but not significantly compared to the WT group. The 8 mos-old *PINK1* KO rats showed a significantly increased level of Ins in the striatum compared to all other *PINK1* KO group of younger ages. Gender differences are shown in Fig. 5.3-b, 5.3-c, 5.4-b, and 5.5-b. At the age of 8 mos, the female *PINK1* KO rats have significantly higher levels than male *PINK1* KO rats for metabolites Gln, GSH, and NAA in the striatum (Fig. 5.3-b, 3-c, 5-b, respectively). The taurine levels in the striatum of *PINK1* KO male were always higher than *PINK1* KO female at all other ages (Fig. 5.4-b).

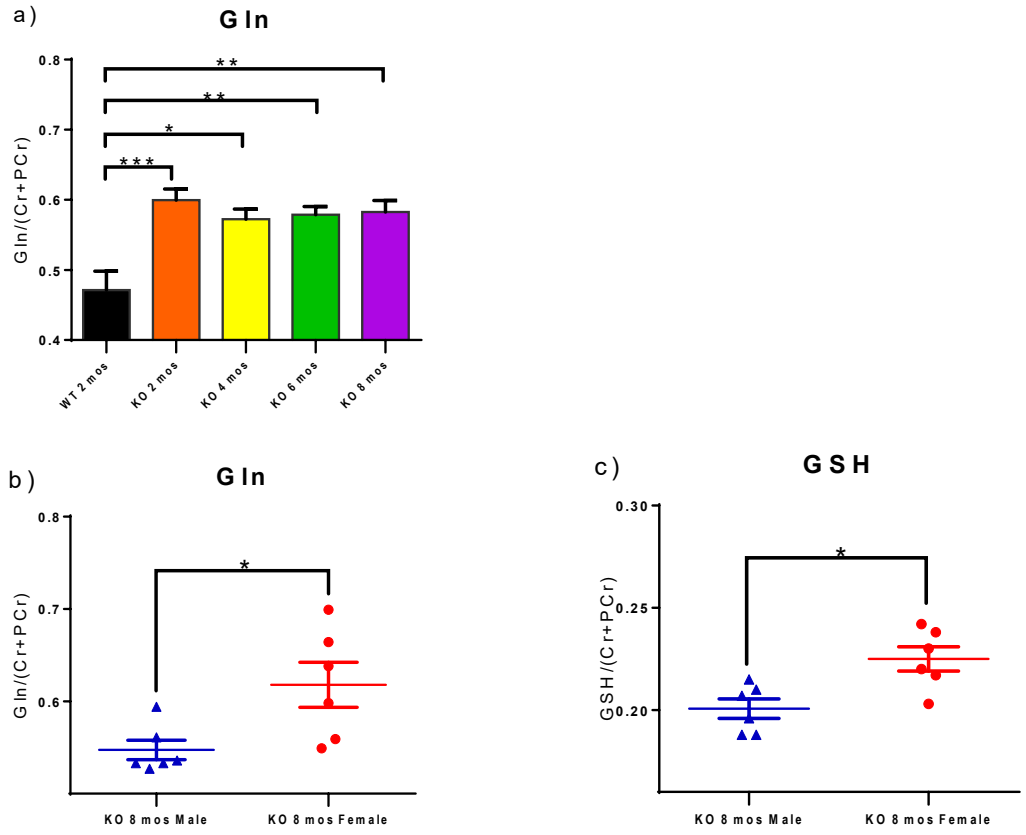

Figure 5.3 H^1-MRS was used to quantify the changes in levels of neurochemical metabolites in the rat striatum.

The peak area of each metabolite was divided by the total peak area of Cr and PCr together to normalize the levels of metabolites. (a) All *PINK1* KO groups at each age had significantly higher levels of Gln than the WT group. WT 2-mos vs. *PINK1* KO 2-mos (***, $p<0.001$). WT 2-mos vs. *PINK1* KO 4-mos (*, $p<0.05$). WT 2-mos vs. *PINK1* KO 6-mos (**, $p<0.01$). WT 2-mos vs. *PINK1* KO 8-mos (**, $p<0.01$). (b, c) In order to determine if brain levels of Gln or GSH were different in female and male *PINK1* KO rats at a given age, comparisons were made only among *PINK1* KO rats. At the age of 8 mos, female *PINK1* KO rats have higher levels of both Gln and GSH compared to male *PINK1* KO rats (*$p<0.05$). (Ren et al., 2019b)

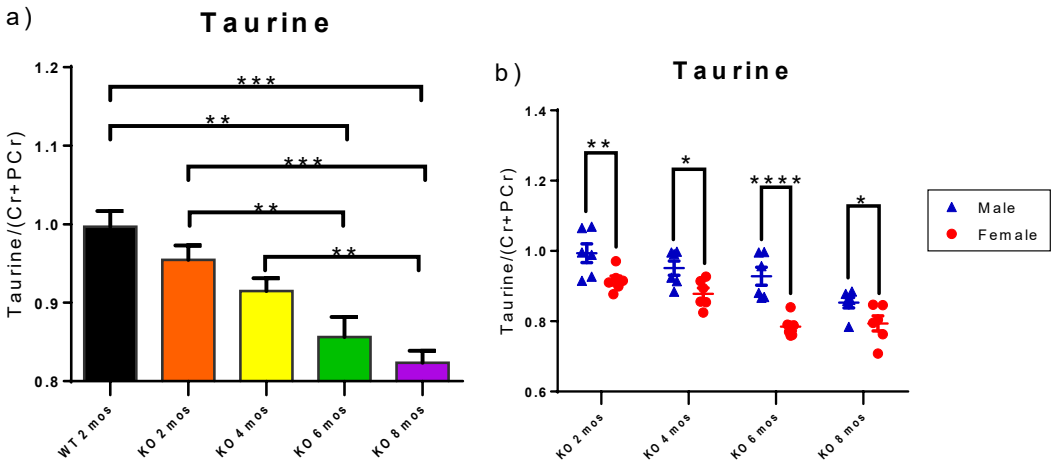

Figure 5.4 H^1-MRS was used to quantify the neurochemical metabolites changes in the rat striatum.

The peak area of each metabolite was divided by the total peak area of Cr and PCr together to normalize the levels of metabolites. (a) Taurine showed a decreased trend from 2 mos-old WT to 8 mos-old *PINK1* KO combined male and female animals. WT 2-mos vs. *PINK1* KO 6-mos (**, $p<0.01$). WT 2-mos vs. *PINK1* KO 8-mos (***, $p<0.001$). *PINK1* KO 2-mos vs. *PINK1* KO 6-mos (**, $p<0.01$). *PINK1* KO 2-mos vs. *PINK1* KO 8-mos (***, $p<0.001$). *PINK1* KO 4-mos vs. *PINK1* KO 8-mos (**, $p<0.01$). (b) In *PINK1* KO rat striatum, the male has a higher level of taurine than females at each same age group. *$p<0.05$, **$p<0.01$, ***$p<0.001$. (Ren et al., 2019b)

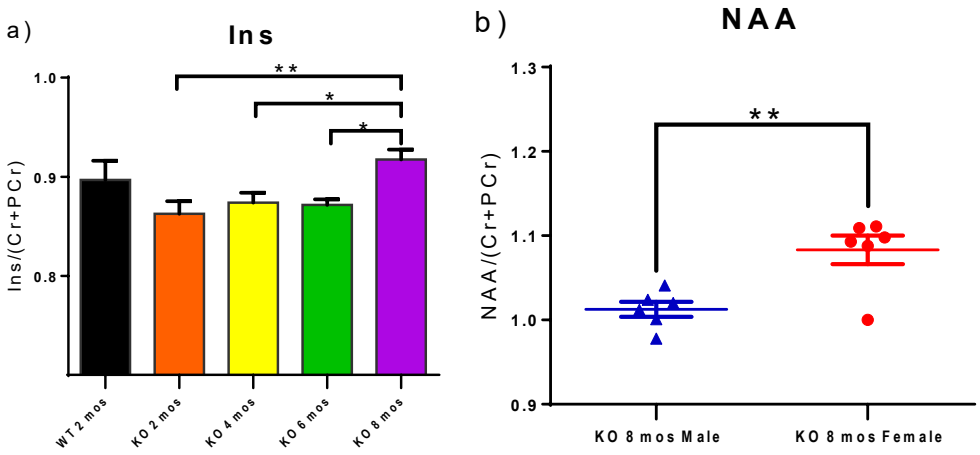

Figure 5.5 H^1-MRS was used to quantify the neurochemical metabolites changes in the rat striatum.

The peak area of each metabolite was divided by the total peak area of Cr and PCr together to normalize the levels of metabolites. (a) The 8 mos-old KO rats showed increased levels of Ins in the striatum compared to the other three younger KO groups. KO 2-mos vs. KO 8-mos (**, $p<0.01$). KO 4-mos vs. KO 8-mos (*, $p<0.05$). KO 6-mos vs. KO 8-mos (*, $p<0.05$). (b) NAA levels in the striatum of 8 mos-old female KO rats are higher than male at the same age. **$p<0.01$. (Ren et al., 2019b)

5.4.4 Changes in the brain proteome of *PINK1* KO rats associated with age

PDQuest analysis of all of the 2-D images found seven proteins that had intensities that were significantly changed with age. Four of these proteins are associated with energy metabolism. The intensities of the protein spots on the gels were normalized to the protein intensities of the 2 mos-old *PINK1* KO rat group. After in-gel trypsin digestion and peptide extraction, MS/MS analyses coupled to interrogation of protein databases were utilized to determine the identities of the proteins. All proteins were identified by more than one unique peptide sequence. Table 5.1 lists the relevant information from the MS/MS analyses that led to the identity of each protein from the brains of *PINK1* KO rats that showed significantly altered expression with age. A representative 2d-gel image is presented in Figure 5.6. The selected spots are labeled on the gel image. Table 5.2 shows the fold-changes for each identified protein.

Table 5.1 Proteins with altered expression in brain of *PINK1* KO rats.

PDQuest and MS/MS results of brain proteins with significantly altered expression with age changes in the *PINK1* KO rats. The LC-MS analysis, data interrogation, and protein identification analysis was performed by Dr. Jian Cai, School of medicine, University of Louisville.

Spot #	Abbreviation	Protein Identified	Accession #	Coverage (%)	# of Unique Peptides	MW (kDa)	calc. pI
0212	Enoph1	Enolase-phosphatase E1	Q5PPH0	13.41	4	28.9	4.97
4505	Fas	Fascin	P85845	17.24	8	54.5	6.74
5104	Tpi1	Triosephosphate isomerase	P48500	17.27	4	26.8	7.24
6306	Aldoc	Fructose-bisphosphate aldolase C	P09117	45.45	18	39.3	7.12
6407	Got1	Aspartate aminotransferase, cytoplasmic	P13221	33.90	14	46.4	7.21
7504	Pafah1b1	Platelet-activating factor acetylhydrolase IB subunit alpha	P63004	28.05	11	46.6	7.37
7702	Aco2	Aconitate hydratase, mitochondrial	Q9ER34	32.05	23	85.4	7.83

Table 5.2 Fold changes of the seven identified proteins as age increases in the brain of *PINK1* KO rats.

The fold changes were calculated by dividing the average of 2, 4, 6 and 8 mos *PINK1* KO protein spot intensities, respectively, by that of the 2 mos-old *PINK1* KO protein spot intensities.

Abbreviation	Protein Identified	Fold Changes (vs 2 mos)	
Tpi1	Triosephosphate isomerase	*2 mos*	1
		4 mos	1.33
		6 mos	1.41
		8 mos	1.69
Aldoc	Fructose-bisphosphate aldolase C	*2 mos*	1
		4 mos	0.89
		6 mos	0.69
		8 mos	0.98
Got1	Aspartate aminotransferase, cytoplasmic	*2 mos*	1
		4 mos	0.98
		6 mos	0.74
		8 mos	1.02
Aco2	Aconitate hydratase, mitochondrial	*2 mos*	1
		4 mos	0.95
		6 mos	0.64
		8 mos	1.09
Enoph1	Enolase-phosphatase E1	*2 mos*	1
		4 mos	0.67
		6 mos	0.57
		8 mos	0.16
Fas	Fascin	*2 mos*	1
		4 mos	0.37
		6 mos	1.69
		8 mos	0.94
Pafah1b1	Platelet-activating factor acetylhydrolase IB subunit alpha	*2 mos*	1
		4 mos	0.94
		6 mos	0.49
		8 mos	0.86

The identified proteins can be subdivided into two categories: the proteins related to energy metabolism and glutamate regulation; and the proteins related to cell migration, motility, and adhesion. As age increased, expression of Tpi1 in brain of *PINK1* KO rats was increased. Aldoc, Got1, and Aco2 showed decreased levels at 6 mos-old, compared to all other three age groups, respectively. These changes of proteins in the brain of KO rats at 6 mos-old may provide evidence that contributes to the decreased levels of oxidative damage in brains of 6 mos-old *PINK1* KO rats. The expression of Enoph1 significantly decreased as age increases. Fas and Pafah1b1 significantly increased and decreased at 6 mos of age, respectively.

5.5 Discussion

The current chapter focused on oxidative damage changes, and proteome in the whole brain, and the sizes and levels of neurochemical metabolites of the striatum of *PINK1* KO rats with increasing age and gender variation compared to 2 mos-old WT rats. Male and female *PINK1* KO rats at 2, 4, 6, 8 months of ages were selected (Ren et al., 2019b).

Biomarkers of oxidative damage, including protein carbonyls, protein-bound HNE, and 3-NT, all showed increased levels as age increased compared to the WT 2 months-aged rats. However, the levels of all types of oxidative damage had a similar trend, namely, a decreased at 6 months of age. The elevated markers of oxidative damage in this PD rat model are consistent with mitochondrial changes known in PD (Greenamyre, 2018). PINK1 is a monitor of mitochondrial structure and function (Deas et al., 2009), and mutations in *PINK1* are a known cause of familial PD (Jiang and Dickson, 2018). Mutations in *PINK1* likely result in excess superoxide leak from damaged mitochondria and could be related to our observed elevated oxidative damage in brain of *PINK1* KO rats,

since the ultimate mutation in *PINK1* is the absence of the gene.

In addition, ventricle size in the rat brain and neurochemical metabolites level in the striatum, including NAA, Gln, GSH and taurine, also exhibited greater changes in male KO rats, which are consonant with the known increased risk to develop PD among males. The energy metabolism and cell migration, and motility are disrupted in the brain of *PINK1* KO rats.

The possibly earliest PD biomarker that appears before symptoms, decreased glutathione (GSH) and elevated GSSG, the oxidized form of GSH in the parenchyma (Chinta et al., 2006; Mischley et al., 2016), could contribute to greater oxidative damage in KO rats at younger ages. Blood GSH decreased in the blood of PD patients with age (Mischley et al., 2016). The reason for the decreased levels of all types of oxidative damage at 6 mos age for KO rats is unknown; this could be speculatively posited as due to compensatory responses in the brain. *PINK1* KO mice started to show a PD phenotype when a decreased level of dopamine was observed (Akundi et al., 2011). The accumulation of oxidative damage conceivably triggered PD symptoms and compensation. However, as age increased with consequent more impaired mitochondria and neurons, the oxidative damage increased again as observed here at 8 mos in brains of *PINK1* KO rats (Fig. 1a, 1b, 1c).

The MRS studies in the current study were on the striatum, which involves both motor and rewards systems. Synaptic plasticity and decreased dopamine release were found in the striatum of *PINK1* KO mice (Kitada et al., 2007). The ventricular system in the brain parenchyma is filled with cerebrospinal fluid (CSF), and the choroid plexus is where CSF is produced. CSF circulates up and around the brain and is absorbed into the venous system

to protect the brain, to support cerebral blood flow, and to maintain brain homeostasis. Idiopathic normal pressure hydrocephalus was found in a patient with parkinsonism and initially consistent with PD symptoms (Cucca et al., 2018). The observed larger ventricle sizes of the male brain at all ages of *PINK1* KO rats (Fig. 4) conceivably could be due to hydrocephaluism. Our results provide a hypothesis to potentially explain why males have a higher risk to develop PD compared to females.

DA and Glu signaling are dysregulated in the PD striatum (Gardoni and Bellone, 2015). Gln is one source for making Glu then forming GSH, but extra Gln could lead to excitotoxicity. In the current study, the higher level of Gln in the striatum of *PINK1* KO groups at all ages compared to 2 mos-old WT group (Fig. 5-a) is consistent with the known decreased plasma GSH level, an early biomarker of PD (Chinta et al., 2006; Mischley et al., 2016). Here in striatum of 8 mos-old male *PINK1* KO rats, decreased levels of both Gln and GSH compared to those of females were observed (Fig. 5-b,c). The accumulation of Gln compared to WT rats is consistent with the observations that less GSH and Glu were found in PD (Buchanan et al., 2014). DA denervation may regulate glutamatergic signals and neural plasticity (Lange et al., 1997). A glutamate antagonist led to anti-akinetic effects in PD mice (Lange et al., 1997). γ-glutamyl cysteine ligase, a Nrf2-dependent enzyme, is the rate-limiting enzyme during the synthesis of GSH, under control of vitagenes network (Miquel et al., 2018). Vitagenes network is composed of several genes that can sense and respond to cellular stress to sustain the homeodynamics *in vivo* (Calabrese et al., 2018; Miquel et al., 2018). Vitagenes can produce antioxidants and anti-apoptotic molecules including GSH (Calabrese et al., 2014). In the brain, vitagenes mediate the redox homeostasis and integrated survival responses (Miquel et al., 2018), confirmed the notion

that male sex is a higher risk to PD than female, and confirmed our result in fig. 3-c that female *PINK1* KO rats have higher level of GSH, which means higher stress tolerance in brain of female *PINK1* KO rats than the stress tolerance in brain of male *PINK1* KO rats at 8 mos of age. This result conceivably could be contributed by the regulation of estrogen, a notion consistent with the finding that estradiol could upregulate the antioxidant expression in human erythrocytes during the menstrual cycle (Chang et al., 2015).

Taurine is an amino sulfonic acid that is important for neuroprotection and calcium homeostasis (Villeneuve et al., 2016). Taurine also is associated with mitochondrial function and oxidative damage (Hansen et al., 2010; Schaffer et al., 2009). We showed in this study that the taurine levels in the striatum had a decreasing trend (Fig. 5.4-a). The level of taurine of 6 mos-old *PINK1* KO group was significantly lower than the taurine levels of 2-mos WT and 2-mos *PINK1* KO groups. The taurine level in the *PINK1* KO group at 8 mos-old was significantly lower than the taurine levels in the WT control group, 2- and 4-mos old *PINK1* KO groups, respectively. The males always appeared to have higher levels than females in each *PINK1* KO age group (Fig. 5.4-b). Decreased levels of taurine were found in PD patients (Engelborghs et al., 2003), supporting our results that *PINK1* KO rats had a decreased level of taurine in the striatum. Another study on *PINK1* KO rats also showed that the taurine level is lower in the *PINK1* KO rats at 18 weeks (4.5 months) but became higher at 34 weeks (8.5 months) (Villeneuve et al., 2016).

NAA and Ins are commonly assessed by MRS for neurodegenerative diseases (Saeed et al., 2017). NAA is located in neurons and is involved in neuronal metabolism and integrity. About 5 percent decreased NAA levels were observed in the lentiform nucleus of PD patients (Firbank et al., 2002). We did not observe a decreasing trend of NAA

dependent on age. However, the higher level of NAA in female KO groups than male KO groups at age of 8 mos (Fig. 5.5b) indicated that females might have healthier neuronal conditions than male under stress from PINK1 deficiency and aging, consistent with the oxidative damage observed in current study (Fig. 5.1). The inositol level increased at 8 mos of age in *PINK1* KO rats (Fig. 5.5-a), suggesting glial activation could become highly mobilized, with more inflammatory cytokines as a consequence, in later stages of PD.

The proteomics study in this chapter focused on the changes in protein levels in brain of *PINK1* KO rats as a function of age. Seven proteins were revealed with significantly altered expression levels in the brain of *PINK1* KO rats as age increases. The depletion of ATP is involved in the apoptosis cascade. The four energy-related proteins were identified, including three proteins involved in glycolysis and the TCA cycle (Tpi1, Aco2, and Aldoc), and one protein (Got1) involved in the malate-aspartate shuttle, converting a TCA intermediate into glutamate (Glu), essential for learning and memory. The remaining three identified proteins are Enoph1, Fas, and Pafah1b1, involved in cell migration and motility.

Increasing glycolysis may slow the neurodegeneration in PD (Cai et al., 2019). Enhanced glycolysis was reported to be associated absence of PINK1 (Gandhi et al., 2009; Scheele et al., 2007). PINK1 also was reported as a growth suppressor. PINK1 deficiency sustains cell proliferation by reprogramming glucose metabolism via hypoxia-inducible factor-1α (HIF1α) (Requejo-Aguilar et al., 2014). The stabilization of HIF1α is mediated by the mitochondrial ROS, leading to up-regulated pyruvate dehydrogenase kinase-1, which inhibits the activity of the enzyme pyruvate dehydrogenase (Requejo-Aguilar et al., 2014). It was reported that familial PD patients with PINK1 mutation had increased astroglial proliferation (Prestel et al., 2008). The up-regulation of glycolytic enzyme Aldoc

enhances the overproduction of methylglyoxal (Liu et al., 2013), which is cytotoxic and formed by decomposition of the two triose phosphates in the glycolysis process. Meanwhile, accumulation of citrate is linked to the inhibition of Aco2 and results in the inhibition of phosphofructose kinase (PFK), associated with inhibition of glycolysis (Anandhan et al., 2017). The deceased expression level of Aldoc and Aco2 may contribute to the decreased level of oxidative damage of *PINK1* KO rats at 6-mos of age by decreasing the production of methylglyoxal. In addition, Aco2 is inactivated by the oxidative damage from the *PINK1* mutation. The inactivation of Aco2 can be compensated by α-ketoglutarate dehydrogenase which allows Glu to support the TCA cycle (Anandhan et al., 2017), which also could contribute to the decreased level of Aco2 at 6 mos-old with a consequently decreased level of oxidative damage, due to less glutamate and subsequent less excitotoxicity. The latter also could have resulted by the decreased Got1 level observed in this current chapter. ATP depletion was found in neurodegeneration of DA neurons in PD. Less Got1 also suggests that less NADH was transferred into the electron transport chain on the inner mitochondrial membrane, leading to the accumulation of insufficient energy level, which may result in the elevated oxidative damage again at 8 mos of age. Inactivation of Tpi1 could contribute to the generation of methylglyoxal (Gracy et al., 1998; Hipkiss, 2011). Increased level of Tpi1 could possibly decrease the methylglyoxal, contributing to the oxidative damage caused by the absence of PINK1 and aging, as well as compensate for the disrupted homeostasis and altered energy metabolism.

Enoph1 is a bifunctional enzyme that regulates the biosynthesis of methionine (Met) via ubiquitous methionine salvage pathway (Wang et al., 2005), which may be involved in modulating stress sensitivity. A recent study reported that Enoph1 was upregulated by

increasing metastatic potential, as a prognostic factor of hepatocellular carcinoma (HCC) patients (Zhuang et al., 2019). HCC cell migration and invasion were promoted by overexpression of Enoph1, whereas these characteristics were inhibited by downregulation of Enoph1 (Zhuang et al., 2019). Pafah1b1 is important to cell division and motility by binding to cytoplasmic dynein, a microtubule (MT) minus end-directed motor protein (Moon and Wynshaw-Boris, 2013), regulating MT function and dynein motor activity (Tanaka et al., 2004a). During neuronal migration, Pafah1b1 is necessary for nuclear movement (Tanaka et al., 2004b). Fas is an actin-bundling protein that maintains the cell adhesion, along with motility and invasion by regulating the cytoskeletal structures. Fas also is essential for suppressing immunological synaptic formation. Importantly, cytoskeletal remodeling, including actin dynamics, is essential for learning and memory, and in late stages of PD, dementia is often observed (Yang et al., 2016). In the brain of *PINK1* KO rats, the expression of Enoph1 decreased as age increases. Decreased expression of Pafah1b1 was observed at 6 mos of age with a dramatically increased expression of Fas. It was reported that cell growth and migration was suppressed by the absence of PINK1 in lung cancer cells (Liu et al., 2018). Overexpression of PINK1 upregulated the phosphorylation of Akt, leading to enhanced cell motility (Murata et al., 2011). The elevated expression of Fas at 6 mos-old may compensate the insufficient cell migration due to the decreased expression of Enoph1 and Patah1b1. The dramatically decreased expression of Fas at age of 4 mos may contribute to the early onset of PD. Although the interaction and relationship between these three proteins are not clear in *PINK1* KO rats, the cell migration, invasion, and motility are associated with aging and deficiency of PINK1.

CHAPTER 6. CONCLUSIONS AND FUTURE STUDIES

The results of experiments presented in this dissertation have mainly investigated oxidative damage, brain proteome, and neurochemical metabolites in cognitive and neurodegenerative disorders, including chemotherapy-induced cognitive impairment (CICI) and a potential model of familial Parkinson disease (PD), to gain insights into the pathological and etiological mechanisms and to take steps toward discerning protective and preventive strategies.

The research supports the overall hypothesis that oxidative damage is one of the critical factors underlying cognitive and neurodegenerative disorders, including CICI and PD, while together with biochemical changes and mitochondrial dysfunctions in brain contribute to the pathological mechanisms of CICI and PD.

6.1 Conclusions and future studies of project 1: CICI

6.1.1 Conclusions of CICI project

With the large and increasing number of cancer survivors in the world, such people are seeking a longer and better quality of life. CICI is subtle with loss of learning ability, memory, attention, executive function and processing speed, and these conditions can be long-lasting or short-term, affecting the quality of life of cancer survivors. Patients are eager to recover a normal life not only physically, but also mentally. That this condition is so debilitating necessitates that urgent investigations into the biochemical mechanisms of CICI, ranging from the effects of anti-cancer drugs, prevention and protection of patients from cognitive deficits, and other side effects be undertaken.

In the first project, attempts to build a fuller picture of mechanisms of CIC, and thereby

for future studies and clinical treatments designed to improve the quality of life of cancer survivors without the interference of chemotherapeutic efficacy, were investigated. This project investigated the mechanisms of CICI using mouse, and the prototype of ROS-generating chemotherapeutic drug, doxorubicin (Dox). The effects of 2-mercaptoethane sulfonate sodium (MESNA) in Chapter 3 and role of tumor necrosis factor-alpha (TNF-α) in CICI in Chapter 4 were studied on the etiological and pathological mechanisms of doxorubicin (Dox)-induced cognitive impairment and oxidative damage.

The first part of the CICI project showed that co-administration of MESNA with Dox protects not only plasma, but also brain of mice *in vivo* against Dox-induced oxidative stress. In addition to the known MESNA function that can prevent bladder bleeding, the results showed that Dox-mediated deficits of memory are prevented by MESNA. Concomitantly, the results demonstrated that metabolism of choline-related compounds was affected in Dox-treated mice. The diminished level of choline-containing compound in the mice hippocampus, likely are as the consequence of the decreased activities of PC-PLC and PLD. These studies are the first to demonstrate the protective effects of MESNA on Dox-induced cognitive impairment, choline-containing compounds level in hippocampus, and PC-PLC activity in brain, providing more evidence for MESNA as a potential treatment for CICI.

In the second part of CICI project, TNFKO mice were used to test the hypothesis that TNF-α plays a critical role in our laboratory's proposed mechanisms of CICI. Dox-induced oxidative damage in brain was absent in TNFKO mice. Assessed by oxygen consumption rate, mitochondria in brain from TNFKO mice are protected following Dox treatment compared to brain mitochondria from the saline-treated WT group. Choline levels in

hippocampus and phospholipase D activity of the whole brain also were elevated in Dox-treated TNFKO mice compared to Dox-treated WT mice. We confirmed the pivotal role of oxidative stress-mediated TNF-α in CICI, providing more evidence to support and expand our proposed CICI model and subsequent potential intervention. These data provided strong evidence that TNF-α is critically involved in the mechanisms of CICI for future studies.

Multiple pathogenic mechanisms most likely are involved in the mechanisms of CICI. The cross-talk and interaction among all possible candidates erect a complicated network of processes that lead to eventual neuronal apoptosis and cognitive deficits in many cancer survivors. Altered brain structures, decreased neural plasticity and telomere shortening could contribute to the observed long term cognitive dysfunction. DNA damage, hormone changes and polymorphism of genes involved in neural repair and neurotransmission also conceivably could contribute to CICI. Neural inflammation and oxidative damage to key proteins, lipids, DNA and membranes are considered to be fundamental phenomena underlying CICI mechanisms, potentially leading to other contributors to CICI. Oxidative damage is one of the most important candidate mechanisms supported by the studies in the Project 1 of this dissertation research. The key pro-inflammatory cytokines, including TNF-α, that are elevated in the periphery by ROS associated chemotherapeutic drugs, cross the BBB, to lead to subsequent neuronal death, particularly in the hippocampus and pre-frontal cortex. These changes are postulated to result in the clinical presentation of CICI, consistent with oxidative damage-mediated elevation of TNF-α, inflammatory cytokines and mitochondrial damage found in brain. Subsequent opening of the mitochondrial permeability transition pore leads to release Cyt c to activate apoptotic pathways.

Combining with the previous work, the data shown in Project 1 allow us to develop a more fully detailed model of the mechanisms of Dox-induced, oxidative damage and TNF-α-mediated CICI (Ren et al., 2019a). The expanded model is shown in Fig. 6.1.

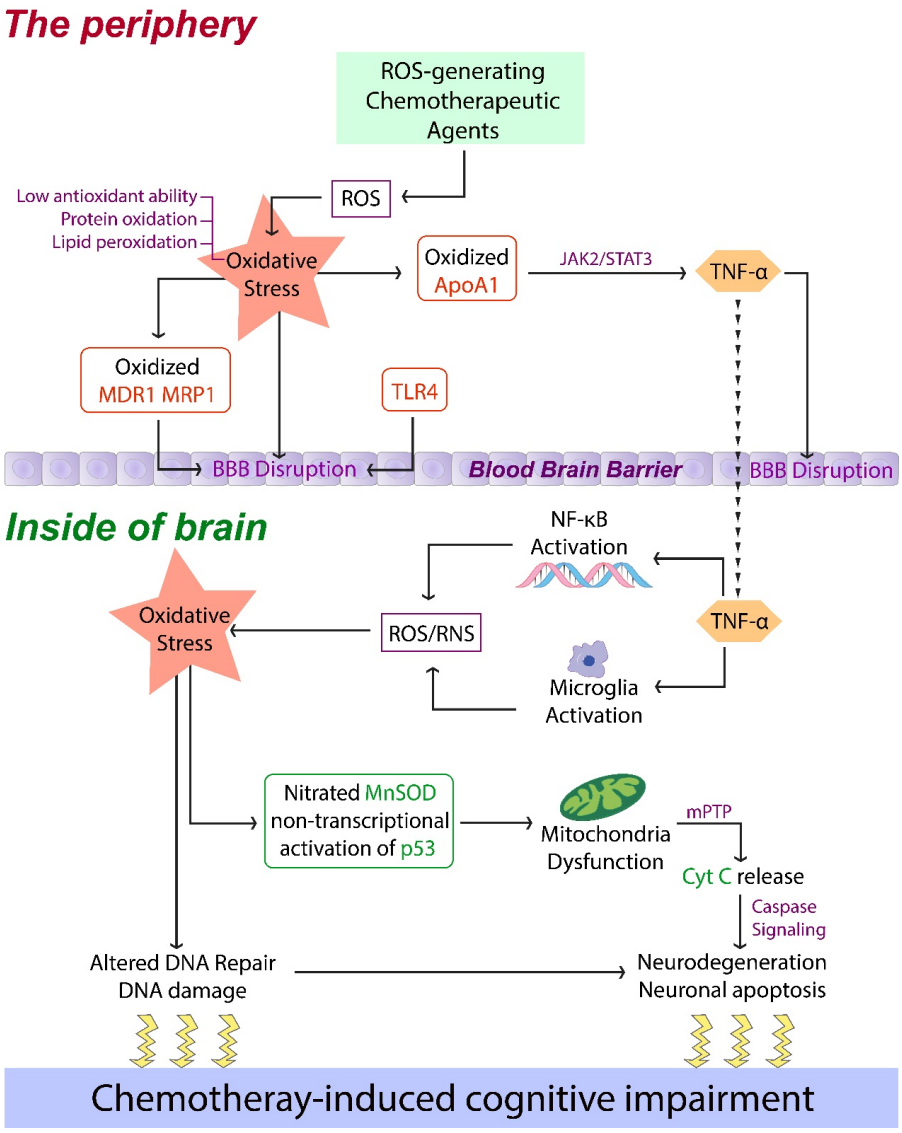

Figure 6.1 An expanded model of the mechanism of CICI. This proposed mechanism of CICI mediated by ROS-generating chemotherapeutic drugs and associated oxidative stress. Such anti-cancer drugs in the periphery trigger oxidative stress and result in protein oxidation and lipid peroxidation, producing elevated TNF-α that crosses the BBB by receptor-mediated endocytosis or by oxidative stress-mediated disruption of the BBB. According to previous studies, TLR4 activation may lead to BBB disruption and cytokines productions such as TNF-α. Once TNF-α goes into brain, the local immune response is triggered by microglia activation and NF-κB activation, triggering ROS/RNS leading to oxidative stress. DNA repair systems are affected by oxidative stress in brain and lead to neurodegeneration. Impaired mitochondria function follows the nitration of MnSOD and p53 non-transcriptional activation. As a result, the mitochondria permeability transition pore (mPTP) is opened. Cyt c released from the pore initiates caspase activation, leading to neural apoptosis. Once neurodegeneration and neuronal death happen, cognitive deficits of chemotherapy-treated cancer survivors appear.

6.1.2 Future studies of CICI

Due to the central role of TNF-α in the mechanism of CICI, it would be elaborated upon and extended if the further involvement of TNF-α is taken into account. Combining MESNA treatment and TNF-α absence or block together would be beneficial to further study the oxidative stress-mediated TNF-α elevation and subsequent changes in both plasma and brain, especially for the activities of PC-PLC and PLD. Since PC-PLC is protected by MESNA and PLC is protected by the absence of TNF-α, it would not be surprising that both PC-PLC and PLD are fully or partially protected against Dox treatment. Considering the cross-talk between TNF-α and PLC, and PLD, study the Dox effects on TNF-α and oxidative damage with inhibitor of PLC and/or PLD would be helpful to elucidate the relationship of the phospholipase and TNF-α, associated with cognitive impairment, to provide more potential markers for protecting cancer survivors against CICI. Moreover, the impacts of chemotherapy on the choline metabolism pathway would yield quite interesting information, including the alteration of important relative molecules acetylcholine, sphingomyelin, and ceramide following Dox.

6.2 Conclusions and future studies of project 2: PD

6.2.1 Conclusions of PD project

The studies in Project 2 examined the suitability of PINK1 KO rat for studying PD by investigations into the brain of this KO rat model. Oxidative damage and neurochemical metabolites were measured in the brain of PINK1 KO rats as a function of age and gender. Adding the female KO rats to the study is important for fully investigating PD. The risk factor of gender in PD pathology is supported and explained by employing the female rats

together with male rats, especially shown in this dissertation research by the different ventricle sizes between male and female rats. The presented elevation of oxidative damage, associated with neurochemical changes, reveals altered antioxidant ability, altered level of amino sulfonic acid, and altered neuron condition with the absence of PINK1, which is consistent with the changes in familial PD brain. Both gender and age contributed to the alterations in the brain.

In addition, the brain proteome of PINK1 KO rats with increasing age was measured. The majority of the significantly altered proteins by the absence of PINK1 studied in this project are involved in vital processes that can be subdivided into two main categories: energy metabolism and glutamate regulation, along with and the migration and motility of neurons in KO rat brain.

Taken together, Project 2 showed the biochemical and structural changes in brains of PINK1 KO rats as a function and/or age. The results build more full description of the features of the *PINK1* KO rat, providing the references for future studies of finding an ideal animal model for PD, and for studying of PINK1 in PD to take forward steps of investigation of mechanisms of PD.

6.2.2 Future studies of PD

It is too early to permit a definitive answer to whether *PINK1* KO rat is a good animal model for PD. While there are changes in oxidative damage in brain with age and, in the case of 3-NT, with gender, as well as changes in ventrical sizes and striatal metabolites with age and gender difference. Proteomics analyses provided insights that are worth further exploration into energy metabolism, glutamate regulation, and cell migration and motility. However, there was no α-synuclein deposition in brain, severely dampening the

notion that the *PINK1* KO rat is a model of PD with high fidelity. For further study of this *PINK1* KO rat model at older age may be helpful. Investigations into the key proteins and metabolites may conceivably provide potential additional insights into specific treatment or prevention of Parkinson diseases, eventually lead to extended and healthy human lifespan with a better quality of life.

APPENDIX

TABLE TO SUPPLEMENT TABLES OR FIGURES

Figure 3.3 b

	Saline	Dox
	0.916	0.908
	1.01	0.836
	0.897	0.761
	0.828	0.877
	0.888	0.844
	0.983	0.870
	1.01	0.879
	0.853	0.926
	0.858	0.860
	0.974	0.837
	0.966	0.857
N	11	11
Mean	0.926	0.860
Std	0.065731409	0.043103048
SEM	0.068317413	0.0464915

Figure 3.3 c

	Saline	Dox	Dox/Mesna	Mesna
	1.07	0.722	0.775	1.09
	1.01	0.769	0.693	1.05
	1.10	0.709	0.735	
	1.22	0.870	0.840	
	1.11	0.728	0.662	
	1.17	0.764		
	1.05	0.757		
	1.14	0.723		
	1.08	0.727		
	1.13	0.650		
		0.624		
		0.532		
		0.581		
		0.624		
N	9	13	4	1
Mean	1.112	0.697	0.733	1.050
Std	0.062805	0.091026694	0.07766	0.028284
SEM	0.059552	0.109049653	0.090738	0.027603

Figure 4.3

WT Saline	WT Dox	TNFKO Dox	TNFKO Saline
1.08	0.65	0.789	1.04
1.13	0.624	0.772	0.981
1.04	0.532	0.783	1.02
1.05	0.581	0.882	1.2
1.01	0.624	0.776	0.954
1.07	0.622		

N	6	6	5	5
Mean	1.063333	0.6055	0.8004	1.039
Std	0.045497	0.046403	0.046079	0.09601
SEM	0.018574	0.018944	0.020607	0.042937

Fig 4.4 a,b

WT Saline	WT Dox	TNFKO Dox	TNFKO Saline
98.23009	50.97345	58.40708	108.8153
96.63717	64.77876	54.69027	112.8414
105.1327	61.59292	46.19469	113.397
95.37947	73.06174	79.39569	110.8571
95.60287	80.13816	83.8658	112.2998
109.0177	68.66167	70.09187	111.4734
			105.5331
N	6	6	6	7
Mean	100	66.53445	65.4409	110.7453
Std	4.037514	11.1401	16.31988	1.841031
SEM	1.648308	4.547927	6.662564	0.695844

WT Saline	WT Dox	TNFKO Dox	TNFKO Saline
89.4845	73.93095	83.72857	97.75567
103.4013	66.00141	86.06037	99.13375
107.1142	74.92252	94.67936	101.9916
96.954	79.73763	86.05748	104.3349
100.8836	79.49543	86.13155	101.8802
102.1091	77.23817	94.46626	105.6355
97.13444	87.15967	89.9338	90.01151
101.0374	88.87319	85.04753	
101.8814	82.0748	87.30135	
	79.75942	89.42641	
		93.88762	
N	9	10	11	7
Mean	99.99999	78.91932	88.79275	100.1062
Std	6.743146	5.581468	4.232344	2.5926
SEM	2.247715	1.765015	1.2761	0.979911

Fig 5.1 a

	M	WT 2 mos	F		M	KO 2 mos	F		M	KO 4 mos	F
	106.9156	106.4359	106.4359		110.6896	110.6896	113.7463		109.4692	109.4692	135.9455
	110.9991	112.8093	112.8093		128.0578	128.0578	122.1465		129.5828	129.5828	134.6138
	91.85923	96.26248	96.26248		100.3649	100.3649	84.67331		105.364	105.364	113.4719
	84.4733	102.8765	102.8765		108.1402	108.1402	79.01053		121.1789	121.1789	115.2734
	87.36865	106.9156			105.4724	105.4724	117.3096		99.79194	99.79194	109.5391
		110.9991			117.8448	117.8448	117.5626		128.9895	128.9895	116.1444
		91.85923				113.7463			140.5999	140.5999	160.9503
		84.4733				122.1465			136.9134	136.9134	144.2356
		87.36865				84.67331				135.9455	
						79.01053				134.6138	
						117.3096				113.4719	
						117.5626				115.2734	
										109.5391	
										116.1444	
										160.9503	
										144.2356	
N	5	9	4		6	12	6		8	16	8
Mean	96.32318	100	104.596		111.7616	108.7515	105.7415		121.4862	125.129	128.7718
Std	11.91755	10.38899	6.910084		9.861785	14.64791	18.78922		15.11979	16.56983	18.14945
SEM	5.329691	3.462998	3.455042		4.026057	4.228487	7.670666		5.345652	4.142458	6.416799

	M	KO 6 mos	F		M	KO 8 mos	F
	119.558	119.558	114.914		136.9579	136.9579	140.0042
	112.6031	112.6031	116.58		139.528	139.528	136.194
	90.83826	90.83826	111.6142		114.7677	114.7677	118.2119
	115.8763	115.8763	94.36012		122.3837	122.3837	109.8961
	106.3091	106.3091	126.2803		125.7692	125.7692	119.4038
	99.39035	99.39035	112.3736		122.3302	122.3302	139.4795
	114.1828	114.1828	120.1636		144.244	144.244	141.5439
	122.0245	122.0245	126.0585			140.0042	
		114.914				136.194	
		116.58				118.2119	
		111.6142				109.8961	
		94.36012				119.4038	
		126.2803				139.4795	
		112.3736				141.5439	
		120.1636					
		126.0585					
N	8	16	8		7	14	7
Mean	110.0978	112.6954	115.293		129.4258	129.3367	129.2476
Std	10.61017	10.38709	10.15861		10.85154	11.50138	12.99369
SEM	3.751262	2.596772	3.591611		4.101496	3.073872	4.911152

Fig 5.1 b

	M	WT 2 mos	F		M	KO 2 mos	F		M	KO 4 mos	F
	98.8789	104.6823	104.6823	0	105.4453	105.4453	102.8702	0	118.7694	118.7694	129.3203
	99.42412	103.9507	103.9507		103.0602	103.0602	109.7833		116.5919	116.5919	116.5346
	90.10179	103.6053	103.6053		110.5361	110.5361	114.3942		119.3617	119.3617	122.9786
	101.9699	96.64338	96.64338		105.6537	105.6537	97.72884		115.1414	115.1414	127.5731
	100.7436	98.8789			102.218	102.218	83.21787		119.3121	119.3121	133.8613
		99.42412			97.48986	97.48986	93.2734		118.2757	118.2757	132.7073
		90.10179				102.8702			116.519	116.519	122.8654
		101.9699				109.7833			98.95969	98.95969	119.726
		100.7436				114.3942				129.3203	
						97.72884				116.5346	
						83.21787				122.9786	
						93.2734				127.5731	
										133.8613	
										132.7073	
										122.8654	
										119.726	
N	5	9	4		6	12	6		8	16	8
Mean	98.22366	100	102.2204		104.0672	102.1392	100.2113		115.3664	120.5311	125.6958
Std	4.696265	4.552383	3.745041		4.334923	8.428754	11.3395		6.799543	8.237661	6.181288
SEM	2.100234	1.517461	1.87252		1.769725	2.433172	4.629332		2.404002	2.059415	2.185415

	M	KO 6 mos	F		M	KO 8 mos	F
	104.6561	104.6561	100.3971	0	109.0645	109.0645	108.0446
	102.1251	102.1251	100.8044		110.6557	110.6557	97.87628
	101.7083	101.7083	110.6841		104.1143	104.1143	97.69983
	80.28591	80.28591	98.74709		100.378	100.378	111.219
	98.2735	98.2735	111.6196		122.1543	122.1543	107.2055
	95.05537	95.05537	103.9642		103.1616	103.1616	104.8361
	89.92893	89.92893	95.13411		99.67559	99.67559	107.8935
	95.86136	95.86136	94.84415			108.0446	
		100.3971				97.87628	
		100.8044				97.69983	
		110.6841				111.219	
		98.74709				107.2055	
		111.6196				104.8361	
		103.9642				107.8935	
		95.13411					
		94.84415					
N	8	16	8		7	14	7
Mean	95.98682	99.00558	102.0243		107.0291	105.9985	104.9678
Std	7.88216	7.595772	6.377756		7.829768	6.492272	5.247882
SEM	2.786764	1.898943	2.254877		2.959374	1.735133	1.983513

Fig 5.1 c

	M	WT 2 mos	F		M	KO 2 mos	F		M	KO 4 mos	F
	89.68431	97.51335	97.51335	0	113.2659	95.2887	95.2887	0	135.4538	111.564	111.564
	109.5689	98.13586	98.13586		96.55184	105.1529	105.1529		115.6369	134.9594	134.9594
	106.7277	87.10676	87.10676		100.0258	124.734	124.734		125.1377	110.4472	110.4472
	104.0292	108.6752	108.6752		114.3165	97.50757	97.50757		120.5083	115.7808	115.7808
	98.55875	89.68431			106.4491	86.18965	86.18965		111.1066	106.6983	106.6983
		109.5689			99.46337	97.67488	97.67488		102.1957	96.29762	96.29762
		106.7277				113.2659			99.82921	104.0446	104.0446
		104.0292				96.55184			106.4831	106.0648	106.0648
		98.55875				100.0258				135.4538	
						114.3165				115.6369	
						106.4491				125.1377	
						99.46337				120.5083	
										111.1066	
										102.1957	
										99.82921	
										106.4831	
N	5	9	4		6	12	6		8	16	8
Mean	101.7138	100	97.85779		105.0121	103.0517	101.0913		114.5439	112.638	110.7321
Std	7.855982	8.005499	8.809029		7.53644	10.38279	13.08219		12.14209	11.53109	11.36635
SEM	3.513302	2.6685	4.404514		3.076739	2.997254	5.340781		4.292878	2.882772	4.01861

	M	KO 6 mos	F		M	KO 8 mos	F
	111.4891	104.1084	104.1084	0	109.2907	116.0204	116.0204
	106.2988	105.1315	105.1315		129.1392	111.4152	111.4152
	98.08235	90.28207	90.28207		130.1861	104.5377	104.5377
	95.91336	95.53654	95.53654		115.805	99.64329	99.64329
	90.193	93.68998	93.68998		122.334	85.16485	85.16485
	90.93321	106.1284	106.1284		103.065	99.66792	99.66792
	84.43519	80.51105	80.51105		119.1603	98.43136	98.43136
	84.39599	78.23112	78.23112			109.2907	
		111.4891				129.1392	
		106.2988				130.1861	
		98.08235				115.805	
		95.91336				122.334	
		90.193				103.065	
		90.93321				119.1603	
		84.43519					
		84.39599					
N	8	16	8		7	14	7
Mean	95.21763	94.71	94.20238		118.4258	110.2758	102.1258
Std	9.806818	9.99029	10.8216		9.959651	12.78152	9.989135
SEM	3.467234	2.497573	3.826015		3.764394	3.416004	3.775538

Fig 5.2

	Male					
WT 2 mos	0.008012	0.010771	0.009051			
KO 2 mos	0.014837	0.012963	0.0213	0.013542	0.016041	0.024416
KO 4 mos	0.024492	0.012845	0.009123	0.031238	0.021476	0.015073
KO 6 mos	0.009455	0.032917	0.019473	0.038861	0.011437	0.018332
KO 8 mos	0.020223	0.012837	0.017765	0.027521	0.015562	0.011611
N	5	5	5	4	4	5
Mean	0.015404	0.016467	0.015342	0.027791	0.016129	0.015404
Std	0.007003	0.009241	0.005846	0.010607	0.00412	0.007003
SEM	0.003132	0.004133	0.002614	0.005304	0.00206	0.003132
	Female					
WT 2 mos	0.009341	0.009855	0.007422			
KO 2 mos	0.008832	0.013815	0.006094	0.007968	0.006603	0.00845
KO 4 mos	0.010697	0.007673	0.007242	0.006612	0.010464	
KO 6 mos	0.006497	0.004857	0.006923	0.011262	0.01324	
KO 8 mos	0.007276	0.014471	0.006574	0.007036	0.011396	0.009804
N	5	5	5	5	5	5
Mean	0.015404	0.015404	0.015404	0.015404	0.015404	0.015404
Std	0.007003	0.007003	0.007003	0.007003	0.007003	0.007003
SEM	0.003132	0.003132	0.003132	0.003132	0.003132	0.003132

Fig 5.3 a

WT 2 mos	KO 2 mos	KO 4 mos	KO 6 mos	KO 8 mos	KO 2 mos
0.544	0.526	0.593	0.557	0.664	105.4453
0.415	0.608	0.683	0.558	0.699	103.0602
0.455	0.66	0.565	0.607	0.549	110.5361
0.471	0.6	0.514	0.593	0.559	105.6537
	0.657	0.564	0.648	0.638	102.218
	0.622	0.536	0.643	0.598	97.48986
	0.535	0.617	0.594	0.561	102.8702
	0.628	0.564	0.534	0.533	109.7833
	0.485	0.526	0.534	0.594	114.3942
	0.639	0.533	0.568	0.527	97.72884
	0.62	0.633	0.585	0.533	83.21787
	0.616	0.539	0.525	0.536	93.2734

N	4	12	12	12	12	12
Mean	0.47125	0.599667	0.57225	0.5788	0.582583	102.1392
Std	0.053916	0.055006	0.050516	0.0406	0.057166	8.428754
SEM	0.026958	0.015879	0.014583	0.0117	0.016502	2.433172

Fig 5.3 b

KO 8 mos Male	KO 8 mos Female
0.561	0.664
0.533	0.699
0.594	0.549
0.527	0.559
0.533	0.638
0.536	0.598

N	6	6
Mean	0.547333	0.617833
Std	0.025758	0.05953
SEM	0.010516	0.024303

Fig 5.3 c

KO 8 mos Male	KO 8 mos Female
0.207	0.238
0.196	0.23
0.21	0.22
0.215	0.203
0.188	0.242
0.188	0.217

N	6	6
Mean	0.200667	0.225
Std	0.011622	0.014533
SEM	0.004745	0.005933

5.4 a

WT 2 mos	KO 2 mos	KO 4 mos	KO 6 mos	KO 8 mos
0.544	0.526	0.593	0.557	0.664
0.415	0.608	0.683	0.558	0.699
0.455	0.66	0.565	0.607	0.549
0.471	0.6	0.514	0.593	0.559
	0.657	0.564	0.648	0.638
	0.622	0.536	0.643	0.598
	0.535	0.617	0.594	0.561
	0.628	0.564	0.534	0.533
	0.485	0.526	0.534	0.594
	0.639	0.533	0.568	0.527
	0.62	0.633	0.585	0.533
	0.616	0.539	0.525	0.536
N	4	12	12	12	12
Mean	0.47125	0.599667	0.57225	0.5788	0.582583
Std	0.053916	0.055006	0.050516	0.0406	0.057166
SEM	0.026958	0.015879	0.014583	0.0117	0.016502

5.4 b

	Male					Female						
KO 2 mos	0.915	0.989	0.996	0.927	1.069	1.065	0.877	0.923	0.915	0.899	0.91	0.971
KO 4 mos	0.996	0.924	0.914	0.884	0.998	0.991	0.914	0.856	0.854	0.927	0.894	0.825
KO 6 mos	0.957	0.997	0.867	0.881	0.996	0.869	0.759	0.84	0.788	0.77	0.79	0.761
KO 8 mos	0.858	0.784	0.878	0.861	0.852	0.885	0.846	0.795	0.708	0.804	0.763	0.847
N	4	4	4	4	4	5	5	5	5	5	5	5
Mean	0.932	0.924	0.914	0.888	0.979	0.015	0.015	0.015	0.015	0.015	0.015	0.015
Std	0.059	0.099	0.058	0.028	0.091	0.007	0.007	0.007	0.007	0.007	0.007	0.007
SEM	0.030	0.049	0.029	0.014	0.046	0.003	0.003	0.003	0.003	0.003	0.003	0.003

5.5 a

WT 2 mos	KO 2 mos	KO 4 mos	KO 6 mos	KO 8 mos
0.951	0.834	0.88	0.857	0.897
0.862	0.87	0.863	0.842	0.938
0.895	0.861	0.828	0.891	0.883
0.879	0.855	0.873	0.855	0.909
	0.832	0.931	0.876	0.878
	0.881	0.861	0.9	0.942
	0.879	0.907	0.9	0.939
	0.775	0.803	0.862	0.882
	0.837	0.873	0.893	0.976
	0.858	0.897	0.86	0.874
	0.949	0.872	0.867	0.932
	0.919	0.899	0.855	0.958
N	4	12	12	12	12
Mean	0.89675	0.8625	0.873917	0.8715	0.917333
Std	0.038595	0.044182	0.034352	0.0199	0.034576
SEM	0.019298	0.012754	0.009917	0.0057	0.009981

5.5 b

KO 8 mos Male	KO 8 mos Female
1.001	1.098
1.012	1.111
1.041	1.109
1.02	1.088
0.978	1
1.024	1.093
N	6	6
Mean	1.012667	1.083167
Std	0.021556	0.041711
SEM	0.0088	0.017028

Table 5.2

Tpi

	KO 2 mos	KO 4 mos	KO 6 mos	KO 8 mos
	606.7	547.7	706.5	923.3
	338.1	462.3	385.4	427.1
	411	671.7	535.4	534.9
	474.3	466	566.1	925.9
	436.9	501	450.2	649.9
	241.8	354.2	1047.9	758.2
	496	743.2	1403.1	929.1
	485.9	833.4	463.6	391.3
	236	605.1	630.4	789.8
	394.8	404.3	348.4	1500.7
	557.3	442.7	544	544.7
	623.6	1035.9	368.9	607.9
N	12	12	12	12
Mean	441.8667	588.9583	620.825	748.57
Std	126.4232	200.365	311.1434	302.98
SEM	36.49524	57.84039	89.81937	87.464

Aldoc

	KO 2 mos	KO 4 mos	KO 6 mos	KO 8 mos
	1795.4	2208.6	1484.8	1902.7
	2479	1417.9	1022.9	2850
	2318.9	2095.2	1399.8	2940.9
	2053.4	1845.2	1637.9	1780.8
	2100.5	1569.3	1776.1	1756
	2176.1	1478.5	901.7	3276.6
	3171.8	3182.4	1998.6	3358.7
	3198.4	2643	2286.8	1173.1
	2866.5	1283.2	2188.1	2527.5
	1288.6	1284.6	1113.8	2669.9
	2914.1	3791.9	1303	1730.9
	1338	1785.5	1933.4	1260.3
N	12	12	12	12
Mean	2308.392	2048.775	1587.242	2269
Std	647.7731	794.2024	458.9222	760.56
SEM	186.996	229.2665	132.4794	219.55

Got1

KO 2 mos	KO 4 mos	KO 6 mos	KO 8 mos
4356.2	4344.8	2956.9	4499.6
4955.1	4519.6	1638.6	4589.1
4978.9	4911.9	2659.7	5835.2
4385.3	4976	3655.5	5820.8
5446.1	5167.2	4915.2	4481.4
3509.9	3762.8	3449.5	5186.9
6981.3	6808.5	4152.9	7430.3
8100.8	5954	5232.3	3693.6
5150.8	3980.4	3139.3	4860.6
3072.1	4779.9	4849.7	6859.2
5580	4963.8	2426.8	4789.9
2994.6	4016.9	5102.5	2767.4
N	12	12	12	12
Mean	4959.258	4848.817	3681.575	5067.8
Std	1502.494	862.837	1175.448	1284.8
SEM	433.7326	249.0796	339.3226	370.88

Aco2

KO 2 mos	KO 4 mos	KO 6 mos	KO 8 mos
1905.3	1074.8	1466.1	2814.1
1673.5	1092.9	309.6	2173.7
1552	3667.3	1882.4	1818.1
1440.2	1882.7	631.7	2953.8
3469.6	2583.8	1215.8	1487.1
942.8	825.9	531.5	2389.5
1921.6	1017.8	1457.4	1564.2
2448.5	1669.5	2185.2	1851.6
1394.7	853.9	1360.9	1661
1625.8	2387.5	1564.6	2618.7
2608.6	1966.6	1083.2	2307.7
1746.8	2607.2	903.1	1160.7
N	12	12	12	12
Mean	1894.117	1802.492	1215.958	2066.7
Std	668.834	885.8047	555.4547	564.55
SEM	193.0757	255.7098	160.346	162.97

Enoph1

KO 2 mos	KO 4 mos	KO 6 mos	KO 8 mos
242.5	110.6	2.5	228.3
134.1	180.5	3.5	2.9
245.1	174.5	300.5	4.5
161.3	140.1	154	6.8
315.5	373.6	244.8	10.4
242.3	5.7	8.7	2.1
8.8	10	4.6	5.7
272.4	165.6	3.7	8.3
256.3	5.5	85.3	5.8
234.9	238	87.5	12.1
6.5	3.7	144.1	2.6
5.2	5.7	169.8	55.7
N	12	12	12	12
Mean	177.075	117.7917	100.75	28.767
Std	112.8474	117.6457	103.0423	64.504
SEM	32.57623	33.96139	29.74574	18.621

Fas

KO 2 mos	KO 4 mos	KO 6 mos	KO 8 mos
369	131.5	2.5	1230
625.3	617.6	596.2	2.9
3.5	9.9	893.5	4.5
1142.6	13	970.9	6.8
477.1	11.7	4.4	154.5
9.8	5.7	788.5	2.1
8.8	10	1104.2	5.7
662.1	458.4	757.5	207.5
396.8	5.5	645.7	5.8
744.4	370.8	11.2	734.8
6.5	3.7	822.5	672.3
5.2	5.7	915.9	1174.6
N	12	12	12	12
Mean	370.925	136.9583	626.0833	350.13
Std	376.5283	217.8129	397.7133	474.87
SEM	108.6944	62.87717	114.8099	137.08

Pafah1b1

	KO 2 mos	KO 4 mos	KO 6 mos	KO 8 mos
	438.1	154.8	174.2	501.2
	672.1	581.4	212.5	630.8
	531.8	588.2	359.7	331.2
	453.7	295.2	222.1	523
	809.7	789.3	258.3	355.6
	437.7	188.3	246.3	401.4
	471.5	724.1	465.4	689.3
	924.9	695.1	402.4	770.3
	560	315.9	340.1	208.8
	369.4	812.7	470	913
	1026.4	965.7	195	341.3
	473	637.5	178.5	531.4
N	12	12	12	12
Mean	597.3583	562.35	293.7083	516.44
Std	213.7312	263.793	109.2953	205.36
SEM	61.69888	76.15047	31.55084	59.282

REFERENCES

Ahles, T.A., and Saykin, A.J. (2007). Candidate mechanisms for chemotherapy-induced cognitive changes. Nat Rev Cancer 7, 192–201.

Ahles, T.A., Saykin, A.J., McDonald, B.C., Furstenberg, C.T., Cole, B.F., Hanscom, B.S., Mulrooney, T.J., Schwartz, G.N., and Kaufman, P.A. (2008). Cognitive function in breast cancer patients prior to adjuvant treatment. Breast Cancer Res. Treat. 110, 143–152.

Aksenov, M.Y., Aksenova, M.V., Butterfield, D.A., Geddes, J.W., and Markesbery, W.R. (2001). Protein oxidation in the brain in Alzheimer's disease. Neuroscience 103, 373–383.

Akundi, R.S., Huang, Z., Eason, J., Pandya, J.D., Zhi, L., Cass, W.A., Sullivan, P.G., and Büeler, H. (2011a). Increased mitochondrial calcium sensitivity and abnormal expression of innate immunity genes precede dopaminergic defects in Pink1-deficient mice. PLoS ONE 6, e16038.

Aluise, C.D., Miriyala, S., Noel, T., Sultana, R., Jungsuwadee, P., Taylor, T.J., Cai, J., Pierce, W.M., Vore, M., Moscow, J.A., et al. (2011). 2-Mercaptoethane sulfonate prevents doxorubicin-induced plasma protein oxidation and TNF-alpha release: implications for the reactive oxygen species-mediated mechanisms of chemobrain. Free Radic Biol Med 50, 1630-1638.

Aluise, C.D., Sultana, R., Tangpong, J., Vore, M., St Clair, D., Moscow, J.A., and Butterfield, D.A. (2010). Chemo brain (chemo fog) as a potential side effect of doxorubicin administration: role of cytokine-induced, oxidative/nitrosative stress in cognitive dysfunction. Advances in experimental medicine and biology 678, 147-156.

An, J.M., Kim, S.S., Rhie, J.H., Shin, D.M., Seo, S.R., and Seo, J.T. (2011). Carmustine induces ERK- and JNK-dependent cell death of neuronally-differentiated PC12 cells via generation of reactive oxygen species. Toxicology in Vitro 25, 1359–1365.

Anandhan, A., Jacome, M.S., Lei, S., Hernandez-Franco, P., Pappa, A., Panayiotidis, M.I., Powers, R., and Franco, R. (2017). Metabolic Dysfunction in Parkinson's Disease: Bioenergetics, Redox Homeostasis and Central Carbon Metabolism. Brain Res. Bull. 133, 12–30.

Antunes, M., and Biala, G. (2012). The novel object recognition memory: neurobiology, test procedure, and its modifications. Cognitive processing 13, 93-110.

Avila, J., Llorens-Martín, M., Pallas-Bazarra, N., Bolós, M., Perea, J.R., Rodríguez-Matellán, A., and Hernández, F. (2017). Cognitive Decline in Neuronal Aging and Alzheimer's Disease: Role of NMDA Receptors and Associated Proteins. Front Neurosci 11, 626.

Bachur, N.R., Gordon, S.L., and Gee, M.V. (1977). Anthracycline antibiotic augmentation of microsomal electron transport and free radical formation. Mol. Pharmacol. 13, 901–910.

Bagchi, D., Bagchi, M., Hassoun, E.A., Kelly, J., and Stohs, S.J. (1995). Adriamycin-induced hepatic and myocardial lipid peroxidation and DNA damage, and enhanced excretion of urinary lipid metabolites in rats. Toxicology 95, 1-9.

Banks, W.A. (2016). From blood-brain barrier to blood-brain interface: new opportunities for CNS drug delivery. Nat Rev Drug Discov 15, 275-292.

Bansal, N., Amdani, S.M., Hutchins, K.K., and Lipshultz, S.E. (2018). Cardiovascular disease in survivors of childhood cancer. Current Opinion in Pediatrics 30, 628–638.

Barry, R.L., Byun, N.E., Tantawy, M.N., Mackey, C.A., Wilson, G.H., Stark, A.J., Flom, M.P., Gee, L.C., and Quarles, C.C. (2018). In vivo neuroimaging and behavioral correlates in a rat model of chemotherapy-induced cognitive dysfunction. Brain Imaging Behav 12, 87–95.

Baudino, B., D'agata, F., Caroppo, P., Castellano, G., Cauda, S., Manfredi, M., Geda, E., Castelli, L., Mortara, P., Orsi, L., et al. (2012). The chemotherapy long-term effect on cognitive functions and brain metabolism in lymphoma patients. Q J Nucl Med Mol Imaging 56, 559–568.

Bernacki, R.J., Bansal, S.K., and Gurtoo, H.L. (1987). Combinations of mesna with cyclophosphamide or adriamycin in the treatment of mice with tumors. Cancer research 47, 799-802.

Bertholdo, D., Watcharakorn, A., and Castillo, M. (2013). Brain proton magnetic resonance spectroscopy: introduction and overview. Neuroimaging clinics of North America 23, 359-380.

Bradford, M.M. (1976). A rapid and sensitive method for the quantitation of microgram quantities of protein utilizing the principle of protein-dye binding. Analytical biochemistry 72, 248-254.

Briones, T.L., and Woods, J. (2014). Dysregulation in Myelination Mediated by Persistent Neuroinflammation: Possible Mechanisms in Chemotherapy-related Cognitive Impairment. Brain Behav Immun 35.

Buchanan, R.J., Darrow, D.P., Meier, K.T., Robinson, J., Schiehser, D.M., Glahn, D.C., and Nadasdy, Z. (2014). Changes in GABA and glutamate concentrations during memory tasks in patients with Parkinson's disease undergoing DBS surgery. Front Hum Neurosci 8, 81.

Butterfield, D.A. (1997). beta-Amyloid-associated free radical oxidative stress and neurotoxicity: implications for Alzheimer's disease. Chem. Res. Toxicol. 10, 495–506.

Butterfield, D.A. (2014). The 2013 SFRBM discovery award: selected discoveries from the Butterfield laboratory of oxidative stress and its sequela in brain in cognitive disorders exemplified by Alzheimer disease and chemotherapy induced cognitive impairment. Free Radic Biol Med 74, 157-174.

Butterfield, D.A., and Lauderback, C.M. (2002). Lipid peroxidation and protein oxidation in Alzheimer's disease brain: potential causes and consequences involving amyloid beta-peptide-associated free radical oxidative stress. Free radical biology & medicine 32, 1050-1060.

Butterfield, D.A., Bader Lange, M.L., and Sultana, R. (2010). Involvements of the lipid peroxidation product, HNE, in the pathogenesis and progression of Alzheimer's disease. Biochim. Biophys. Acta 1801, 924–929.

Butterfield, D.A., Castegna, A., Lauderback, C.M., and Drake, J. (2002). Evidence that amyloid beta-peptide-induced lipid peroxidation and its sequelae in Alzheimer's disease brain contribute to neuronal death. Neurobiol. Aging 23, 655–664.

Butterfield, D.A., Perluigi, M., Reed, T., Muharib, T., Hughes, C.P., Robinson, R.A., and Sultana, R. (2012). Redox proteomics in selected neurodegenerative disorders: from its infancy to future applications. Antioxidants & redox signaling 17, 1610-1655.

Cacabelos, R. (2017). Parkinson's Disease: From Pathogenesis to Pharmacogenomics. Int J Mol Sci 18.

Cai, R., Zhang, Y., Simmering, J.E., Schultz, J.L., Li, Y., Fernandez-Carasa, I., Consiglio, A., Raya, A., Polgreen, P.M., Narayanan, N.S., et al. (2019). Enhancing glycolysis attenuates Parkinson's disease progression in models and clinical databases. J Clin Invest 129, 4539–4549.

Calabrese, V., Santoro, A., Trovato Salinaro, A., Modafferi, S., Scuto, M., Albouchi, F., Monti, D., Giordano, J., Zappia, M., Franceschi, C., et al. (2018). Hormetic approaches to the treatment of Parkinson's disease: Perspectives and possibilities. J. Neurosci. Res. 96, 1641–1662.

Calabrese, V., Scapagnini, G., Davinelli, S., Koverech, G., Koverech, A., De Pasquale, C., Salinaro, A.T., Scuto, M., Calabrese, E.J., and Genazzani, A.R. (2014). Sex hormonal regulation and hormesis in aging and longevity: role of vitagenes. J Cell Commun Signal 8, 369–384.

Cantuti-Castelvetri, I., Keller-McGandy, C., Bouzou, B., Asteris, G., Clark, T.W., Frosch, M.P., and Standaert, D.G. (2007). Effects of gender on nigral gene expression and parkinson disease. Neurobiol. Dis. 26, 606–614.

Car, H., Zendzian-Piotrowska, M., Fiedorowicz, A., Prokopiuk, S., Sadowska, A., and Kurek, K. (2012). [The role of ceramides in selected brain pathologies: ischemia/hypoxia,

Alzheimer disease]. Postepy Hig Med Dosw (Online) 66, 295-303.

Castegna, A., Drake, J., Pocernich, C., and Butterfield, D.A. (2003). Protein Carbonyl Levels—An Assessment of Protein Oxidation. In Methods in Biological Oxidative Stress, K. Hensley, and R.A. Floyd, eds. (Totowa, NJ: Humana Press), pp. 161–168.

Castegna, A., Lauderback, C.M., Mohmmad-Abdul, H., and Butterfield, D.A. (2004). Modulation of phospholipid asymmetry in synaptosomal membranes by the lipid peroxidation products, 4-hydroxynonenal and acrolein: implications for Alzheimer's disease. Brain Res. 1004, 193–197.

Castellino, S.M., Ullrich, N.J., Whelen, M.J., and Lange, B.J. (2014). Developing Interventions for Cancer-Related Cognitive Dysfunction in Childhood Cancer Survivors. J Natl Cancer Inst 106.

Chaiswing, L., St. Clair, W.H., and St. Clair, D.K. (2018). Redox Paradox: A Novel Approach to Therapeutics-Resistant Cancer. Antioxidants & Redox Signaling 29, 1237–1272.

Chandel, N.S., Trzyna, W.C., McClintock, D.S., and Schumacker, P.T. (2000). Role of oxidants in NF-kappa B activation and TNF-alpha gene transcription induced by hypoxia and endotoxin. J Immunol 165, 1013-1021.

Chaturvedi, R.K., and Flint Beal, M. (2013). Mitochondrial diseases of the brain. Free Radic Biol Med 63, 1-29.

Chaudhuri, K.R., Healy, D.G., Schapira, A.H.V., and National Institute for Clinical Excellence (2006). Non-motor symptoms of Parkinson's disease: diagnosis and management. Lancet Neurol 5, 235–245.

Chen, Y., Daosukho, C., Opii, W.O., Turner, D.M., Pierce, W.M., Klein, J.B., Vore, M., Butterfield, D.A., and St Clair, D.K. (2006). Redox proteomic identification of oxidized cardiac proteins in adriamycin-treated mice. Free radical biology & medicine 41, 1470-1477.

Chen, Y., Jungsuwadee, P., Vore, M., Butterfield, D.A., and St Clair, D.K. (2007). Collateral damage in cancer chemotherapy: oxidative stress in nontargeted tissues. Molecular interventions 7, 147-156.

Cheng, H., Li, W., Gong, L., Xuan, H., Huang, Z., Zhao, H., Wang, L.S., and Wang, K. (2017). Altered resting-state hippocampal functional networks associated with chemotherapy-induced prospective memory impairment in breast cancer survivors. Scientific Reports 7, 45135.

Cheung, Y.T., Ng, T., Shwe, M., Ho, H.K., Foo, K.M., Cham, M.T., Lee, J.A., Fan, G., Tan, Y.P., Yong, W.S., et al. (2015). Association of proinflammatory cytokines and

chemotherapy-associated cognitive impairment in breast cancer patients: a multi-centered, prospective, cohort study. Ann Oncol 26, 1446–1451.

Chinta, S.J., Rajagopalan, S., Butterfield, D.A., and Andersen, J.K. (2006). In vitro and in vivo neuroprotection by gamma-glutamylcysteine ethyl ester against MPTP: relevance to the role of glutathione in Parkinson's disease. Neurosci. Lett. 402, 137–141.

Christie, L.-A., Acharya, M.M., Parihar, V.K., Nguyen, A., Martirosian, V., and Limoli, C.L. (2012). Impaired cognitive function and hippocampal neurogenesis following cancer chemotherapy. Clin. Cancer Res. 18, 1954–1965.

Chuang, R.Y., and Chuang, L.F. (1979). Inhibition of chicken myeloblastosis RNA polymerase II activity by adriamycin. Biochemistry 18, 2069–2073.

Church, L.D., Hessler, G., Goodall, J.E., Rider, D.A., Workman, C.J., Vignali, D.A., Bacon, P.A., Gulbins, E., and Young, S.P. (2005). TNFR1-induced sphingomyelinase activation modulates TCR signaling by impairing store-operated Ca2+ influx. Journal of leukocyte biology 78, 266-278.

Ciszkowska-Lyson, B., Krolicki, L., Teska, A., Janowicz-Zebrowska, A., Krzakowski, M., and Tacikowska, M. (2003). [Brain metabolic disorders after chemotherapy in the study by magnetic resonance spectroscopy]. Neurologia i neurochirurgia polska 37, 783-798.

Clarke, J.R., Cammarota, M., Gruart, A., Izquierdo, I., and Delgado-Garcia, J.M. (2010). Plastic modifications induced by object recognition memory processing. Proceedings of the National Academy of Sciences of the United States of America 107, 2652-2657.

Cohen, B.M., Renshaw, P.F., Stoll, A.L., Wurtman, R.J., Yurgelun-Todd, D., and Babb, S.M. (1995). Decreased brain choline uptake in older adults. An in vivo proton magnetic resonance spectroscopy study. JAMA : the journal of the American Medical Association 274, 902-907.

Cole, P.D., Vijayanathan, V., Ali, N.F., Wagshul, M.E., Tanenbaum, E.J., Price, J., Dalal, V., and Gulinello, M.E. (2013). Memantine Protects Rats Treated with Intrathecal Methotrexate from Developing Spatial Memory Deficits. Clin Cancer Res 19, 4446–4454.

Conroy, S.K., McDonald, B.C., Smith, D.J., Moser, L.R., West, J.D., Kamendulis, L.M., Klaunig, J.E., Champion, V.L., Unverzagt, F.W., and Saykin, A.J. (2013). Alterations in brain structure and function in breast cancer survivors: effect of post-chemotherapy interval and relation to oxidative DNA damage. Breast Cancer Res. Treat. 137, 493–502.

Cucca, A., Biagioni, M.C., Sharma, K., Golomb, J., Gilbert, R.M., Di Rocco, A., and Fleisher, J.E. (2018). Comorbid Normal Pressure Hydrocephalus with Parkinsonism: A Clinical Challenge and Call for Awareness. Case Rep Neurol Med 2018, 2513474.

Cummings, J., Anderson, L., Willmott, N., and Smyth, J.F. (1991). The molecular

pharmacology of doxorubicin in vivo. European Journal of Cancer and Clinical Oncology 27, 532–535.

Dawson, T.M., Ko, H.S., and Dawson, V.L. (2010). Genetic animal models of Parkinson's disease. Neuron 66, 646–661.

de Ruiter, M.B., Reneman, L., Boogerd, W., Veltman, D.J., Caan, M., Douaud, G., Lavini, C., Linn, S.C., Boven, E., van Dam, F.S., et al. (2012). Late effects of high-dose adjuvant chemotherapy on white and gray matter in breast cancer survivors: converging results from multimodal magnetic resonance imaging. Human brain mapping 33, 2971-2983.

De Valck, D., Beyaert, R., Van Roy, F., and Fiers, W. (1993). Tumor necrosis factor cytotoxicity is associated with phospholipase D activation. Eur J Biochem 212, 491-497.

Deas, E., Plun-Favreau, H., and Wood, N.W. (2009). PINK1 function in health and disease. EMBO Mol Med 1, 152–165.

Deas, E., Plun-Favreau, H., Gandhi, S., Desmond, H., Kjaer, S., Loh, S.H.Y., Renton, A.E.M., Harvey, R.J., Whitworth, A.J., Martins, L.M., et al. (2011). PINK1 cleavage at position A103 by the mitochondrial protease PARL. Hum. Mol. Genet. 20, 867–879.

DeAtley, S.M., Aksenov, M.Y., Aksenova, M.V., Jordan, B., Carney, J.M., and Butterfield, D.A. (1999). Adriamycin-induced changes of creatine kinase activity in vivo and in cardiomyocyte culture. Toxicology 134, 51-62.

Debess, J., Riis, J.Ø., Engebjerg, M.C., and Ewertz, M. (2010). Cognitive function after adjuvant treatment for early breast cancer: a population-based longitudinal study. Breast Cancer Res. Treat. 121, 91–100.

Deprez, S., Amant, F., Smeets, A., Peeters, R., Leemans, A., Van Hecke, W., Verhoeven, J.S., Christiaens, M.-R., Vandenberghe, J., Vandenbulcke, M., et al. (2012). Longitudinal assessment of chemotherapy-induced structural changes in cerebral white matter and its correlation with impaired cognitive functioning. J. Clin. Oncol. 30, 274–281.

Deres, P., Halmosi, R., Toth, A., Kovacs, K., Palfi, A., Habon, T., Czopf, L., Kalai, T., Hideg, K., Sumegi, B., et al. (2005). Prevention of doxorubicin-induced acute cardiotoxicity by an experimental antioxidant compound. J. Cardiovasc. Pharmacol. 45, 36–43.

Desai, V.G., Herman, E.H., Moland, C.L., Branham, W.S., Lewis, S.M., Davis, K.J., George, N.I., Lee, T., Kerr, S., and Fuscoe, J.C. (2013). Development of doxorubicin-induced chronic cardiotoxicity in the B6C3F1 mouse model. Toxicology and applied pharmacology 266, 109-121.

Dezortova, M., and Hajek, M. (2008). (1)H MR spectroscopy in pediatrics. European journal of radiology 67, 240-249.

Di Domenico, F., Tramutola, A., and Butterfield, D.A. (2017). Role of 4-hydroxy-2-nonenal (HNE) in the pathogenesis of alzheimer disease and other selected age-related neurodegenerative disorders. Free Radic Biol Med 111, 253-261.

Dietrich, J., Prust, M., and Kaiser, J. (2015). Chemotherapy, cognitive impairment and hippocampal toxicity. Neuroscience 309, 224–232.

Drachtman, R.A., Cole, P.D., Golden, C.B., James, S.J., Melnyk, S., Aisner, J., and Kamen, B.A. (2002). Dextromethorphan is effective in the treatment of subacute methotrexate neurotoxicity. Pediatr Hematol Oncol 19, 319–327.

El-Agamy, S.E., Abdel-Aziz, A.K., Wahdan, S., Esmat, A., and Azab, S.S. (2018). Astaxanthin Ameliorates Doxorubicin-Induced Cognitive Impairment (Chemobrain) in Experimental Rat Model: Impact on Oxidative, Inflammatory, and Apoptotic Machineries. Mol. Neurobiol. 55, 5727–5740.

Engelborghs, S., Marescau, B., and De Deyn, P.P. (2003). Amino acids and biogenic amines in cerebrospinal fluid of patients with Parkinson's disease. Neurochem. Res. 28, 1145–1150.

Ennaceur, A., and Delacour, J. (1988). A new one-trial test for neurobiological studies of memory in rats. 1: Behavioral data. Behav Brain Res 31, 47-59.

Fang, J., Seki, T., and Maeda, H. (2009). Therapeutic strategies by modulating oxygen stress in cancer and inflammation. Advanced drug delivery reviews 61, 290-302.

Ferguson, R.J., McDonald, B.C., Saykin, A.J., and Ahles, T.A. (2007). Brain Structure and Function Differences in Monozygotic Twins: Possible Effects of Breast Cancer Chemotherapy. J Clin Oncol 25, 3866–3870.

Firbank, M.J., Harrison, R.M., and O'Brien, J.T. (2002). A comprehensive review of proton magnetic resonance spectroscopy studies in dementia and Parkinson's disease. Dement Geriatr Cogn Disord 14, 64–76.

Friday, S.C., and Fox, D.A. (2016). Phospholipase D enzymes facilitate IL-17- and TNFalpha-induced expression of proinflammatory genes in rheumatoid arthritis synovial fibroblasts (RASF). Immunol Lett 174, 9-18.

Furlanut, M., and Franceschi, L. (2003). Pharmacology of ifosfamide. Oncology 65 Suppl 2, 2–6.

Gaman, A.M., Uzoni, A., Popa-Wagner, A., Andrei, A., and Petcu, E.-B. (2016). The Role of Oxidative Stress in Etiopathogenesis of Chemotherapy Induced Cognitive Impairment (CICI)-"Chemobrain." Aging Dis 7, 307–317.

Gandhi, S., Wood-Kaczmar, A., Yao, Z., Plun-Favreau, H., Deas, E., Klupsch, K.,

Downward, J., Latchman, D.S., Tabrizi, S.J., Wood, N.W., et al. (2009). PINK1-associated Parkinson's disease is caused by neuronal vulnerability to calcium-induced cell death. Mol. Cell 33, 627–638.

Ganz, P.A., Kwan, L., Castellon, S.A., Oppenheim, A., Bower, J.E., Silverman, D.H.S., Cole, S.W., Irwin, M.R., Ancoli-Israel, S., and Belin, T.R. (2013). Cognitive Complaints After Breast Cancer Treatments: Examining the Relationship With Neuropsychological Test Performance. J Natl Cancer Inst 105, 791–801.

Gardoni, F., and Bellone, C. (2015). Modulation of the glutamatergic transmission by Dopamine: a focus on Parkinson, Huntington and Addiction diseases. Front Cell Neurosci 9, 25.

Geilen, C.C., Wieder, T., and Orfanos, C.E. (1997). Ceramide signalling: regulatory role in cell proliferation, differentiation and apoptosis in human epidermis. Archives of dermatological research 289, 559-566.

Gilgun-Sherki, Y., Melamed, E., and Offen, D. (2001). Oxidative stress induced-neurodegenerative diseases: the need for antioxidants that penetrate the blood brain barrier. Neuropharmacology 40, 959–975.

Glasl, L., Kloos, K., Giesert, F., Roethig, A., Di Benedetto, B., Kühn, R., Zhang, J., Hafen, U., Zerle, J., Hofmann, A., et al. (2012). Pink1-deficiency in mice impairs gait, olfaction and serotonergic innervation of the olfactory bulb. Exp. Neurol. 235, 214–227.

Goulart, B.K., de Lima, M.N., de Farias, C.B., Reolon, G.K., Almeida, V.R., Quevedo, J., Kapczinski, F., Schroder, N., and Roesler, R. (2010). Ketamine impairs recognition memory consolidation and prevents learning-induced increase in hippocampal brain-derived neurotrophic factor levels. Neuroscience 167, 969-973.

Gow, A.J., Duran, D., Malcolm, S., and Ischiropoulos, H. (1996). Effects of peroxynitrite-induced protein modifications on tyrosine phosphorylation and degradation. FEBS Lett 385, 63–66.

Gracy, R.W., Talent, J.M., and Zvaigzne, A.I. (1998). Molecular wear and tear leads to terminal marking and the unstable isoforms of aging. J. Exp. Zool. 282, 18–27.

Greenamyre, J.T. (2018). What's wrong with mitochondria in Parkinson's disease? Movement Disorders 33, 1515–1517.

Griscavage, J.M., Wilk, S., and Ignarro, L.J. (1996). Inhibitors of the proteasome pathway interfere with induction of nitric oxide synthase in macrophages by blocking activation of transcription factor NF-kappa B. Proceedings of the National Academy of Sciences of the United States of America 93, 3308-3312.

Groven, N., Fors, E.A., Iversen, V.C., White, L.R., and Reitan, S.K. (2018). Association

between cytokines and psychiatric symptoms in chronic fatigue syndrome and healthy controls. Nord J Psychiatry 1–5.

Groves, T.R., Farris, R., Anderson, J.E., Alexander, T.C., Kiffer, F., Carter, G., Wang, J., Boerma, M., and Allen, A.R. (2017). 5-Fluorouracil chemotherapy upregulates cytokines and alters hippocampal dendritic complexity in aged mice. Behavioural Brain Research 316, 215–224.

Grünewald, A., Kumar, K.R., and Sue, C.M. (2019). New insights into the complex role of mitochondria in Parkinson's disease. Prog. Neurobiol. 177, 73–93.

Gupta, R.K., Cloughesy, T.F., Sinha, U., Garakian, J., Lazareff, J., Rubino, G., Rubino, L., Becker, D.P., Vinters, H.V., and Alger, J.R. (2000). Relationships between choline magnetic resonance spectroscopy, apparent diffusion coefficient and quantitative histopathology in human glioma. Journal of neuro-oncology 50, 215-226.

Gutteridge, J.M. (1984). Lipid peroxidation and possible hydroxyl radical formation stimulated by the self-reduction of a doxorubicin-iron (III) complex. Biochemical pharmacology 33, 1725-1728.

Haddad, P.M., and Dursun, S.M. (2008). Neurological complications of psychiatric drugs: clinical features and management. Hum Psychopharmacol 23 Suppl 1, 15–26.

Halliwell, B., and Gutteridge, J.M. (1984). Free radicals, lipid peroxidation, and cell damage. Lancet 2, 1095.

Handa, K., and Sato, S. (1975). Generation of free radicals of quinone group-containing anti-cancer chemicals in NADPH-microsome system as evidenced by initiation of sulfite oxidation. Gan 66, 43–47.

Hansen, S.H., Andersen, M.L., Cornett, C., Gradinaru, R., and Grunnet, N. (2010). A role for taurine in mitochondrial function. J Biomed Sci 17, S23.

Hayslip, J., Dressler, E.V., Weiss, H., Taylor, T.J., Chambers, M., Noel, T., Miriyala, S., Keeney, J.T., Ren, X., Sultana, R., et al. (2015). Plasma TNF-alpha and Soluble TNF Receptor Levels after Doxorubicin with or without Co-Administration of Mesna-A Randomized, Cross-Over Clinical Study. PLoS One 10, e0124988.

Hermelink, K. (2015). Chemotherapy and Cognitive Function in Breast Cancer Patients: The So-Called Chemo Brain. J. Natl. Cancer Inst. Monographs 2015, 67–69.

Hipkiss, A.R. (2011). Energy metabolism and ageing regulation: metabolically driven deamidation of triosephosphate isomerase may contribute to proteostatic dysfunction. Ageing Res. Rev. 10, 498–502.

Hyka, N., Dayer, J.M., Modoux, C., Kohno, T., Edwards, C.K., 3rd, Roux-Lombard, P.,

and Burger, D. (2001). Apolipoprotein A-I inhibits the production of interleukin-1beta and tumor necrosis factor-alpha by blocking contact-mediated activation of monocytes by T lymphocytes. Blood 97, 2381-2389.

Ischiropoulos, H., and Beckman, J.S. (2003). Oxidative stress and nitration in neurodegeneration: Cause, effect, or association? J Clin Invest 111, 163–169.

Janelsins, M.C., Heckler, C.E., Peppone, L.J., Kamen, C., Mustian, K.M., Mohile, S.G., Magnuson, A., Kleckner, I.R., Guido, J.J., Young, K.L., et al. (2017). Cognitive Complaints in Survivors of Breast Cancer After Chemotherapy Compared With Age-Matched Controls: An Analysis From a Nationwide, Multicenter, Prospective Longitudinal Study. J. Clin. Oncol. 35, 506–514.

Jang, Y.H., Ahn, B.H., Namkoong, S., Kim, Y.M., Jin, J.K., Kim, Y.S., and Min do, S. (2008a). Differential regulation of apoptosis by caspase-mediated cleavage of phospholipase D isozymes. Cell Signal 20, 2198-2207.

Jang, Y.H., Namkoong, S., Kim, Y.M., Lee, S.J., Park, B.J., and Min, D.S. (2008b). Cleavage of phospholipase D1 by caspase promotes apoptosis via modulation of the p53-dependent cell death pathway. Cell death and differentiation 15, 1782-1793.

Jankovic, J. (2008). Parkinson's disease: clinical features and diagnosis. J. Neurol. Neurosurg. Psychiatry 79, 368–376.

Jansen, J.F., Backes, W.H., Nicolay, K., and Kooi, M.E. (2006). 1H MR spectroscopy of the brain: absolute quantification of metabolites. Radiology 240, 318-332.

Jean-Pierre, P., Winters, P.C., Ahles, T.A., Antoni, M., Armstrong, F.D., Penedo, F., Lipshultz, S.E., Miller, T.L., and Fiscella, K. (2012). Prevalence of Self-Reported Memory Problems in Adult Cancer Survivors: A National Cross-Sectional Study. J Oncol Pract 8, 30–34.

Jiang, P., and Dickson, D.W. (2018). Parkinson's disease: experimental models and reality. Acta Neuropathol. 135, 13–32.

Jiang, P., and Dickson, D.W. (2018). Parkinson's disease: experimental models and reality. Acta Neuropathologica. 135, 13–32.

Joshi, G., Aluise, C.D., Cole, M.P., Sultana, R., Pierce, W.M., Vore, M., St Clair, D.K., and Butterfield, D.A. (2010). Alterations in brain antioxidant enzymes and redox proteomic identification of oxidized brain proteins induced by the anti-cancer drug adriamycin: implications for oxidative stress-mediated chemobrain. Neuroscience 166, 796-807.

Joshi, G., Hardas, S., Sultana, R., St Clair, D.K., Vore, M., and Butterfield, D.A. (2007). Glutathione elevation by gamma-glutamyl cysteine ethyl ester as a potential therapeutic strategy for preventing oxidative stress in brain mediated by in vivo administration of

adriamycin: Implication for chemobrain. Journal of neuroscience research 85, 497-503.

Joshi, G., Sultana, R., Tangpong, J., Cole, M.P., St Clair, D.K., Vore, M., Estus, S., and Butterfield, D.A. (2005). Free radical mediated oxidative stress and toxic side effects in brain induced by the anti cancer drug adriamycin: insight into chemobrain. Free Radic Res 39, 1147-1154.

Jungsuwadee, P., Cole, M.P., Sultana, R., Joshi, G., Tangpong, J., Butterfield, D.A., St Clair, D.K., and Vore, M. (2006). Increase in Mrp1 expression and 4-hydroxy-2-nonenal adduction in heart tissue of Adriamycin-treated C57BL/6 mice. Molecular cancer therapeutics 5, 2851-2860.

Jungsuwadee, P., Nithipongvanitch, R., Chen, Y., Oberley, T.D., Butterfield, D.A., Clair, D.K.S., and Vore, M. (2009). Mrp1 Localization and Function in Cardiac Mitochondria after Doxorubicin. Mol Pharmacol 75, 1117–1126.

Jungsuwadee, P., Zhao, T., Stolarczyk, E.I., Paumi, C.M., Butterfield, D.A., St Clair, D.K., and Vre, M. (2012). The G671V variant of MRP1/ABCC1 links doxorubicin-induced acute cardiac toxicity to disposition of the glutathione conjugate of 4-hydroxy-2-trans-nonenal. Pharmacogenetics and genomics 22, 273-284.

Junjing, Z., Yan, Z., and Baolu, Z. (2010). Scavenging Effects of Dexrazoxane on Free Radicals. J. Clin. Biochem. Nutr. 47, 238–245.

Kawajiri, S., Saiki, S., Sato, S., and Hattori, N. (2011). Genetic mutations and functions of PINK1. Trends Pharmacol. Sci. 32, 573–580.

Keeney, J.T., Forster, S., Sultana, R., Brewer, L.D., Latimer, C.S., Cai, J., Klein, J.B., Porter, N.M., and Allan Butterfield, D. (2013a). Dietary vitamin D deficiency in rats from middle to old age leads to elevated tyrosine nitration and proteomics changes in levels of key proteins in brain: Implications for low vitamin D-dependent age-related cognitive decline. Free Radic Biol Med 65C, 324-334.

Keeney, J.T., Swomley, A.M., Forster, S., Harris, J.L., Sultana, R., and Butterfield, D.A. (2013b). Apolipoprotein A-I: insights from redox proteomics for its role in neurodegeneration. Proteomics Clin Appl 7, 109-122.

Keeney, J.T.R., Miriyala, S., Noel, T., Moscow, J.A., St Clair, D.K., and Butterfield, D.A. (2015). Superoxide induces protein oxidation in plasma and TNF-α elevation in macrophage culture: Insights into mechanisms of neurotoxicity following doxorubicin chemotherapy. Cancer Lett. 367, 157–161.

Keeney, J.T.R., Ren, X., Warrier, G., Noel, T., Powell, D.K., Brelsfoard, J.M., Sultana, R., Saatman, K.E., Clair, D.K.S., and Butterfield, D.A. (2018). Doxorubicin-induced elevated oxidative stress and neurochemical alterations in brain and cognitive decline: protection by MESNA and insights into mechanisms of chemotherapy-induced cognitive impairment

("chemobrain"). Oncotarget 9, 30324-30339.

Keeney, J.T.R., Swomley, A.M., Förster, S., Harris, J.L., Sultana, R., and Butterfield, D.A. (2013). Apolipoprotein A-I: Insights from redox proteomics for its role in neurodegeneration. PROTEOMICS – Clinical Applications 7, 109–122.

Kesler, S., Janelsins, M., Koovakkattu, D., Palesh, O., Mustian, K., Morrow, G., and Dhabhar, F.S. (2013). Reduced hippocampal volume and verbal memory performance associated with interleukin-6 and tumor necrosis factor-alpha levels in chemotherapy-treated breast cancer survivors. Brain Behav Immun 30 Suppl, S109-116.

Kesler, S.R. (2014). Default mode network as a potential biomarker of chemotherapy-related brain injury. Neurobiol Aging 35 Suppl 2, S11–S19.

Kesler, S.R., and Blayney, D.W. (2016). Neurotoxic Effects of Anthracycline- vs Nonanthracycline-Based Chemotherapy on Cognition in Breast Cancer Survivors. JAMA Oncol 2, 185–192.

Kesler, S.R., Watson, C.L., and Blayney, D.W. (2015). Brain network alterations and vulnerability to simulated neurodegeneration in breast cancer. Neurobiol Aging 36, 2429–2442.

Kitada, T., Pisani, A., Porter, D.R., Yamaguchi, H., Tscherter, A., Martella, G., Bonsi, P., Zhang, C., Pothos, E.N., and Shen, J. (2007). Impaired dopamine release and synaptic plasticity in the striatum of PINK1-deficient mice. Proc. Natl. Acad. Sci. U.S.A. 104, 11441–11446.

Kitamura, Y., Hattori, S., Yoneda, S., Watanabe, S., Kanemoto, E., Sugimoto, M., Kawai, T., Machida, A., Kanzaki, H., Miyazaki, I., et al. (2015). Doxorubicin and cyclophosphamide treatment produces anxiety-like behavior and spatial cognition impairment in rats: Possible involvement of hippocampal neurogenesis via brain-derived neurotrophic factor and cyclin D1 regulation. Behav Brain Res 292, 184-193.

Konat, G.W., Kraszpulski, M., James, I., Zhang, H.T., and Abraham, J. (2008). Cognitive dysfunction induced by chronic administration of common cancer chemotherapeutics in rats. Metab Brain Dis 23, 325-333.

Koppelmans, V., Breteler, M.M.B., Boogerd, W., Seynaeve, C., Gundy, C., and Schagen, S.B. (2012). Neuropsychological performance in survivors of breast cancer more than 20 years after adjuvant chemotherapy. J. Clin. Oncol. 30, 1080–1086.

Kwatra, M., Jangra, A., Mishra, M., Sharma, Y., Ahmed, S., Ghosh, P., Kumar, V., Vohora, D., and Khanam, R. (2016). Naringin and Sertraline Ameliorate Doxorubicin-Induced Behavioral Deficits Through Modulation of Serotonin Level and Mitochondrial Complexes Protection Pathway in Rat Hippocampus. Neurochem Res 41, 2352-2366.

Lange, K.W., Kornhuber, J., and Riederer, P. (1997). Dopamine/glutamate interactions in Parkinson's disease. Neuroscience & Biobehavioral Reviews 21, 393–400.

Lee, B.E., Choi, B.Y., Hong, D.K., Kim, J.H., Lee, S.H., Kho, A.R., Kim, H., Choi, H.C., and Suh, S.W. (2017). The cancer chemotherapeutic agent paclitaxel (Taxol) reduces hippocampal neurogenesis via down-regulation of vesicular zinc. Scientific Reports 7, 11667.

Lee, S.M., Choi, H.J., Oh, C.H., Oh, J.W., and Han, J.S. (2014). Leptin increases TNF-alpha expression and production through phospholipase D1 in Raw 264.7 cells. PLoS One 9, e102373.

Leibrock, C., Ackermann, T.F., Hierlmeier, M., Lang, F., Borgwardt, S., and Lang, U.E. (2013). Akt2 deficiency is associated with anxiety and depressive behavior in mice. Cell Physiol Biochem 32, 766-777.

Lien, Y.C., Noel, T., Liu, H., Stromberg, A.J., Chen, K.C., and St Clair, D.K. (2006). Phospholipase C-delta1 is a critical target for tumor necrosis factor receptor-mediated protection against adriamycin-induced cardiac injury. Cancer Res 66, 4329-4338.

Lira, F.S., Esteves, A.M., Pimentel, G.D., Rosa, J.C., Frank, M.K., Mariano, M.O., Budni, J., Quevedo, J., Santos, R.V., and de Mello, M.T. (2016). Sleep pattern and locomotor activity are impaired by doxorubicin in non-tumor-bearing rats. Sleep Sci 9, 232-235.

Liu, J., Desai, K., Wang, R., and Wu, L. (2013). Up-regulation of aldolase A and methylglyoxal production in adipocytes. Br. J. Pharmacol. 168, 1639–1646.

Liu, J., Head, E., Gharib, A.M., Yuan, W., Ingersoll, R.T., Hagen, T.M., Cotman, C.W., and Ames, B.N. (2002). Memory loss in old rats is associated with brain mitochondrial decay and RNA/DNA oxidation: partial reversal by feeding acetyl-L-carnitine and/or R-alpha -lipoic acid. Proc. Natl. Acad. Sci. U.S.A. 99, 2356–2361.

Liu, L., Zuo, Z., Lu, S., Wang, L., Liu, A., and Liu, X. (2018). Silencing of PINK1 represses cell growth, migration and induces apoptosis of lung cancer cells. Biomed. Pharmacother. 106, 333–341.

Liu, R.-Y., Zhang, Y., Coughlin, B.L., Cleary, L.J., and Byrne, J.H. (2014). Doxorubicin Attenuates Serotonin-Induced Long-Term Synaptic Facilitation by Phosphorylation of p38 Mitogen-Activated Protein Kinase. J Neurosci 34, 13289–13300.

Lomeli, N., Di, K., Czerniawski, J., Guzowski, J.F., and Bota, D.A. (2017). Cisplatin-induced mitochondrial dysfunction is associated with impaired cognitive function in rats. Free Radical Biology and Medicine 102, 274–286.

Mallampalli, R.K., Ryan, A.J., Salome, R.G., and Jackowski, S. (2000). Tumor necrosis factor-alpha inhibits expression of CTP:phosphocholine cytidylyltransferase. The Journal

of biological chemistry 275, 9699-9708.

Manchon, J.F.M., Dabaghian, Y., Uzor, N.-E., Kesler, S.R., Wefel, J.S., and Tsvetkov, A.S. (2016). Levetiracetam mitigates doxorubicin-induced DNA and synaptic damage in neurons. Sci Rep 6, 25705.

Marras, C., Beck, J.C., Bower, J.H., Roberts, E., Ritz, B., Ross, G.W., Abbott, R.D., Savica, R., Van Den Eeden, S.K., Willis, A.W., et al. (2018). Prevalence of Parkinson's disease across North America. NPJ Parkinsons Dis 4, 21.

Mashiach, E., Sela, S., Weinstein, T., Cohen, H.I., Shasha, S.M., and Kristal, B. (2001). Mesna: a novel renoprotective antioxidant in ischaemic acute renal failure. Nephrology, dialysis, transplantation : official publication of the European Dialysis and Transplant Association - European Renal Association 16, 542-551.

Matsuda, N., Sato, S., Shiba, K., Okatsu, K., Saisho, K., Gautier, C.A., Sou, Y.-S., Saiki, S., Kawajiri, S., Sato, F., et al. (2010). PINK1 stabilized by mitochondrial depolarization recruits Parkin to damaged mitochondria and activates latent Parkin for mitophagy. J. Cell Biol. 189, 211–221.

Mattiazzi, M., D'Aurelio, M., Gajewski, C.D., Martushova, K., Kiaei, M., Beal, M.F., and Manfredi, G. (2002). Mutated human SOD1 causes dysfunction of oxidative phosphorylation in mitochondria of transgenic mice. The Journal of biological chemistry 277, 29626-29633.

Mattson, M.P., Goodman, Y., Luo, H., Fu, W., and Furukawa, K. (1997). Activation of NF-kappaB protects hippocampal neurons against oxidative stress-induced apoptosis: evidence for induction of manganese superoxide dismutase and suppression of peroxynitrite production and protein tyrosine nitration. J. Neurosci. Res. 49, 681–697.

McDonald, B.C., and Saykin, A.J. (2013). Alterations in brain structure related to breast cancer and its treatment: chemotherapy and other considerations. Brain Imaging Behav 7, 374–387.

McDonald, B.C., Conroy, S.K., Ahles, T.A., West, J.D., and Saykin, A.J. (2010). Gray matter reduction associated with systemic chemotherapy for breast cancer: a prospective MRI study. Breast Cancer Res. Treat. 123, 819–828.

McDonald, B.C., Conroy, S.K., Smith, D.J., West, J.D., and Saykin, A.J. (2013). Frontal gray matter reduction after breast cancer chemotherapy and association with executive symptoms: a replication and extension study. Brain Behav. Immun. 30 Suppl, S117-125.

Meck, W.H., Church, R.M., and Matell, M.S. (2013). Hippocampus, time, and memory-A retrospective analysis. Behavioral neuroscience 127, 642-654.

Merzoug, S., Toumi, M.L., and Tahraoui, A. (2014). Quercetin mitigates Adriamycin-

induced anxiety- and depression-like behaviors, immune dysfunction, and brain oxidative stress in rats. Naunyn Schmiedebergs Arch Pharmacol 387, 921-933.

Miller, I.N., and Cronin-Golomb, A. (2010). GENDER DIFFERENCES IN PARKINSON'S DISEASE: CLINICAL CHARACTERISTICS AND COGNITION. Mov Disord 25, 2695–2703.

Miller, W., Siegel, R.L., Lin, C.C., Mariotto, A.B., Kramer, J.L., Rowland, J.H., Stein, K.D., Alteri, R., and Jemal, A. (2016). Cancer treatment and survivorship statistics, 2016. CA: A Cancer Journal for Clinicians 66, 271–289.

Miquel, S., Champ, C., Day, J., Aarts, E., Bahr, B.A., Bakker, M., Bánáti, D., Calabrese, V., Cederholm, T., Cryan, J., et al. (2018). Poor cognitive ageing: Vulnerabilities, mechanisms and the impact of nutritional interventions. Ageing Res. Rev. 42, 40–55.

Mischley, L.K., Standish, L.J., Weiss, N.S., Padowski, J.M., Kavanagh, T.J., White, C.C., and Rosenfeld, M.E. (2016). Glutathione as a Biomarker in Parkinson's Disease: Associations with Aging and Disease Severity. Oxid Med Cell Longev 2016, 9409363.

Mohamed, R.H., Karam, R.A., and Amer, M.G. (2011). Epicatechin attenuates doxorubicin-induced brain toxicity: critical role of TNF-alpha, iNOS and NF-kappaB. Brain Res Bull 86, 22-28.

Moon, H.M., and Wynshaw-Boris, A. (2013). Cytoskeleton in action: lissencephaly, a neuronal migration disorder. WIREs Developmental Biology 2, 229–245.

Moore, H.C.F. (2014). An overview of chemotherapy-related cognitive dysfunction, or "chemobrain." Oncology (Williston Park, N.Y.) 28, 797–804.

Moore, H.C.F., Parsons, M.W., Yue, G.H., Rybicki, L.A., and Siemionow, W. (2014). Electroencephalogram power changes as a correlate of chemotherapy-associated fatigue and cognitive dysfunction. Support Care Cancer 22, 2127–2131.

Moruno-Manchon, J.F., Uzor, N.-E., Kesler, S.R., Wefel, J.S., Townley, D.M., Nagaraja, A.S., Pradeep, S., Mangala, L.S., Sood, A.K., and Tsvetkov, A.S. (2016). TFEB ameliorates the impairment of the autophagy-lysosome pathway in neurons induced by doxorubicin. Aging (Albany NY) 8, 3507–3519.

Moruno-Manchon, J.F., Uzor, N.-E., Kesler, S.R., Wefel, J.S., Townley, D.M., Nagaraja, A.S., Pradeep, S., Mangala, L.S., Sood, A.K., and Tsvetkov, A.S. (2018). Peroxisomes contribute to oxidative stress in neurons during doxorubicin-based chemotherapy. Molecular and Cellular Neuroscience 86, 65–71.

Murata, H., Sakaguchi, M., Jin, Y., Sakaguchi, Y., Futami, J., Yamada, H., Kataoka, K., and Huh, N. (2011). A New Cytosolic Pathway from a Parkinson Disease-associated Kinase, BRPK/PINK1. J Biol Chem 286, 7182–7189.

Nakashima, S., and Nozawa, Y. (1999). Possible role of phospholipase D in cellular differentiation and apoptosis. Chemistry and physics of lipids 98, 153-164.

Naressi, A., Couturier, C., Castang, I., de Beer, R., and Graveron-Demilly, D. (2001). Java-based graphical user interface for MRUI, a software package for quantitation of in vivo/medical magnetic resonance spectroscopy signals. Comput Biol Med 31, 269-286.

Nithipongvanitch, R., Ittarat, W., Velez, J.M., Zhao, R., St Clair, D.K., and Oberley, T.D. (2007). Evidence for p53 as guardian of the cardiomyocyte mitochondrial genome following acute adriamycin treatment. The journal of histochemistry and cytochemistry : official journal of the Histochemistry Society 55, 629-639.

Nozawa, Y. (2002). Roles of phospholipase D in apoptosis and pro-survival. Biochimica et biophysica acta 1585, 77-86.

Oprins, J.C., van der Burg, C., Meijer, H.P., Munnik, T., and Groot, J.A. (2002). Tumour necrosis factor alpha potentiates ion secretion induced by histamine in a human intestinal epithelial cell line and in mouse colon: involvement of the phospholipase D pathway. Gut 50, 314-321.

Pickrell, A.M., and Youle, R.J. (2015). The Roles of PINK1, Parkin and Mitochondrial Fidelity in Parkinson's Disease. Neuron 85, 257–273.

Pinares-Garcia, P., Stratikopoulos, M., Zagato, A., Loke, H., and Lee, J. (2018). Sex: A Significant Risk Factor for Neurodevelopmental and Neurodegenerative Disorders. Brain Sciences 8, 154.

Poewe, W., Seppi, K., Tanner, C.M., Halliday, G.M., Brundin, P., Volkmann, J., Schrag, A.-E., and Lang, A.E. (2017). Parkinson disease. Nature Reviews Disease Primers 3, 17013.

Poly, C., Massaro, J.M., Seshadri, S., Wolf, P.A., Cho, E., Krall, E., Jacques, P.F., and Au, R. (2011). The relation of dietary choline to cognitive performance and white-matter hyperintensity in the Framingham Offspring Cohort. The American journal of clinical nutrition 94, 1584-1591.

Prestel, J., Gempel, K., Hauser, T.K., Schweitzer, K., Prokisch, H., Ahting, U., Freudenstein, D., Bueltmann, E., Naegele, T., Berg, D., et al. (2008). Clinical and molecular characterisation of a Parkinson family with a novel PINK1 mutation. J Neurol 255, 643–648.

Provencher, S.W. (1993). Estimation of metabolite concentrations from localized in vivo proton NMR spectra. Magnetic Resonance in Medicine 30, 672–679.

Przedborski, S., Vila, M., and Jackson-Lewis, V. (2003). Series Introduction: Neurodegeneration: What is it and where are we? J Clin Invest 111, 3–10.

Pun, P.B.L., Lu, J., and Moochhala, S. (2009). Involvement of ROS in BBB dysfunction. Free Radical Research 43, 348–364.

Qin, S., Ding, J., Kurosaki, T., and Yamamura, H. (1998). A deficiency in Syk enhances ceramide-induced apoptosis in DT40 lymphoma B cells. FEBS letters 427, 139-143.

Raffa, R.B. (2010). Is a picture worth a thousand (forgotten) words?: neuroimaging evidence for the cognitive deficits in 'chemo-fog'/'chemo-brain'. Journal of Clinical Pharmacy and Therapeutics 35, 1–9.

Raffa, R.B. (2011). A proposed mechanism for chemotherapy-related cognitive impairment ('chemo-fog'). Journal of clinical pharmacy and therapeutics 36, 257-259.

Raffa, R.B., and Tallarida, R.J. (2010). Chemo fog: cancer chemotherapy-related cognitive impairment. Preface. Advances in experimental medicine and biology 678, vii-viii.

Ransohoff, R.M., and Perry, V.H. (2009). Microglial Physiology: Unique Stimuli, Specialized Responses. Annu. Rev. Immunol. 27, 119–145.

Reich, S.D., Steinberg, F., Bachur, N.R., Riggs, C.E., Goebel, R., and Berman, M. (1979). Mathematical model for adriamycin (Doxorubicin) pharmacokinetics. Cancer Chemother. Pharmacol. 3, 125–131.

Ren, X., Boriero, D., Chaiswing, L., Bondada, S., St Clair, D.K., and Butterfield, D.A. (2019a). Plausible biochemical mechanisms of chemotherapy-induced cognitive impairment ("chemobrain"), a condition that significantly impairs the quality of life of many cancer survivors. Biochim Biophys Acta Mol Basis Dis 1865, 1088–1097.

Ren, X., Hinchie, A., Swomley, A., Powell, D.K., and Butterfield, D.A. (2019b). Profiles of brain oxidative damage, ventricular alterations, and neurochemical metabolites in the striatum of PINK1 knockout rats as functions of age and gender: Relevance to Parkinson disease. Free Radic. Biol. Med. 143, 146–152.

Ren, X., Keeney, J.T.R., Miriyala, S., Noel, T., Powell, D.K., Chaiswing, L., Bondada, S., St Clair, D.K., and Butterfield, D.A. (2018). The triangle of death of neurons: Oxidative damage, mitochondrial dysfunction, and loss of choline-containing biomolecules in brains of mice treated with doxorubicin. Advanced insights into mechanisms of chemotherapy induced cognitive impairment ("chemobrain") involving TNF-α. Free Radic. Biol. Med. 134, 1–8.

Ren, X., St Clair, D.K., and Butterfield, D.A. (2017). Dysregulation of cytokine mediated chemotherapy induced cognitive impairment. Pharmacol Res 117, 267-273.

Requejo-Aguilar, R., Lopez-Fabuel, I., Fernandez, E., Martins, L.M., Almeida, A., and Bolaños, J.P. (2014). PINK1 deficiency sustains cell proliferation by reprogramming glucose metabolism through HIF1. Nature Communications 5, 1–9.

Reuter-Lorenz, P.A., and Cimprich, B. (2013). Cognitive function and breast cancer: promise and potential insights from functional brain imaging. Breast Cancer Res. Treat. 137, 33–43.

Rizzo, F.R., Musella, A., De Vito, F., Fresegna, D., Bullitta, S., Vanni, V., Guadalupi, L., Stampanoni Bassi, M., Buttari, F., Mandolesi, G., et al. (2018). Tumor Necrosis Factor and Interleukin-1β Modulate Synaptic Plasticity during Neuroinflammation. Neural Plast. 2018, 8430123.

Runowicz, C.D., Leach, C.R., Henry, N.L., Henry, K.S., Mackey, H.T., Cowens-Alvarado, R.L., Cannady, R.S., Pratt-Chapman, M.L., Edge, S.B., Jacobs, L.A., et al. (2016). American Cancer Society/American Society of Clinical Oncology Breast Cancer Survivorship Care Guideline. CA: A Cancer Journal for Clinicians 66, 43–73.

Saeed, U., Compagnone, J., Aviv, R.I., Strafella, A.P., Black, S.E., Lang, A.E., and Masellis, M. (2017). Imaging biomarkers in Parkinson's disease and Parkinsonian syndromes: current and emerging concepts. Translational Neurodegeneration 6, 8.

Santos, J.C., and Pyter, L.M. (2018). Neuroimmunology of Behavioral Comorbidities Associated With Cancer and Cancer Treatments. Front. Immunol. 9, 1195.

Sarkisyan, G., and Hedlund, P.B. (2009). The 5-HT7 receptor is involved in allocentric spatial memory information processing. Behavioural brain research 202, 26-31.

Sauerbeck, A., Gao, J., Readnower, R., Liu, M., Pauly, J.R., Bing, G., and Sullivan, P.G. (2011). Pioglitazone attenuates mitochondrial dysfunction, cognitive impairment, cortical tissue loss, and inflammation following traumatic brain injury. Exp. Neurol. 227, 128–135.

Saykin, A.J., Ahles, T.A., and McDonald, B.C. (2003). Mechanisms of chemotherapy-induced cognitive disorders: neuropsychological, pathophysiological, and neuroimaging perspectives. Seminars in clinical neuropsychiatry 8, 201-216.

Schaffer, S.W., Azuma, J., and Mozaffari, M. (2009). Role of antioxidant activity of taurine in diabetes. Can. J. Physiol. Pharmacol. 87, 91–99.

Scheele, C., Nielsen, A.R., Walden, T.B., Sewell, D.A., Fischer, C.P., Brogan, R.J., Petrovic, N., Larsson, O., Tesch, P.A., Wennmalm, K., et al. (2007). Altered regulation of the PINK1 locus: a link between type 2 diabetes and neurodegeneration? FASEB J. 21, 3653–3665.

Schoch, K.M., Evans, H.N., Brelsfoard, J.M., Madathil, S.K., Takano, J., Saido, T.C., and Saatman, K.E. (2012). Calpastatin overexpression limits calpain-mediated proteolysis and behavioral deficits following traumatic brain injury. Exp Neurol 236, 371-382.

Seigers, R., Schagen, S.B., Van Tellingen, O., and Dietrich, J. (2013). Chemotherapy-related cognitive dysfunction: current animal studies and future directions. Brain Imaging and Behavior 7, 453–459.

Sheng-Huang, C., Chieh-Hsin, C., Mu-Chun, Y., Wen-Tung, H., Chia-Ying, H., Ya-Ting, H., Wan-Ling, S., Jiuan-Jen, S., Chih-Yang, H., And Jer-Yuh, L. (2015). Effects of estrogen on glutathione and catalase levels in human erythrocyte during menstrual cycle. Biomed Rep 3, 266–268.

Shi, D.-D., Huang, Y.-H., Lai, C.S.W., Dong, C.M., Ho, L.C., Wu, E.X., Li, Q., Wang, X.-M., Chung, S.K., Sham, P.C., et al. (2019). Chemotherapy-Induced Cognitive Impairment Is Associated with Cytokine Dysregulation and Disruptions in Neuroplasticity. Mol. Neurobiol. 56, 2234–2243.

Siegel, G.J. (2006). Basic neurochemistry : molecular, cellular, and medical aspects, 7th edn (Amsterdam ; Boston: Elsevier).

Simo, M., Rifa-Ros, X., Rodriguez-Fornells, A., and Bruna, J. (2013). Chemobrain: A systematic review of structural and functional neuroimaging studies. Neuroscience and biobehavioral reviews 37, 1311-1321.

Smith, S.M. (2002). Fast robust automated brain extraction. Hum Brain Mapp 17, 143–155.

Soares, D.P., and Law, M. (2009). Magnetic resonance spectroscopy of the brain: review of metabolites and clinical applications. Clinical radiology 64, 12-21.

Sterrenberg, L., Julicher, R.H., Bast, A., and Noordhoek, J. (1984). Adriamycin stimulates NADPH-dependent lipid peroxidation in liver microsomes not only by enhancing the production of O2 and H2O2, but also by potentiating the catalytic activity of ferrous ions. Toxicology letters 22, 153-159.

Subramaniam, R., Roediger, F., Jordan, B., Mattson, M.P., Keller, J.N., Waeg, G., and Butterfield, D.A. (1997). The lipid peroxidation product, 4-hydroxy-2-trans-nonenal, alters the conformation of cortical synaptosomal membrane proteins. J Neurochem 69, 1161-1169.

Sultana, R., and Butterfield, D.A. (2008). Slot-blot analysis of 3-nitrotyrosine-modified brain proteins. Meth. Enzymol. 440, 309–316.

Sultana, R., Perluigi, M., and Allan Butterfield, D. (2013). Lipid peroxidation triggers neurodegeneration: a redox proteomics view into the Alzheimer disease brain. Free radical biology & medicine 62, 157-169.

Tabaczar, S., Czepas, J., Koceva-Chyla, A., Kilanczyk, E., Piasecka-Zelga, J., and Gwozdzinski, K. (2017). The effect of the nitroxide pirolin on oxidative stress induced by doxorubicin and taxanes in the rat brain. J Physiol Pharmacol 68, 295-308.

Tanaka, T., Serneo, F.F., Higgins, C., Gambello, M.J., Wynshaw-Boris, A., and Gleeson, J.G. (2004a). Lis1 and doublecortin function with dynein to mediate coupling of the nucleus to the centrosome in neuronal migration. J Cell Biol 165, 709–721.

Tangpong, J., Cole, M.P., Sultana, R., Estus, S., Vore, M., St Clair, W., Ratanachaiyavong, S., St Clair, D.K., and Butterfield, D.A. (2007). Adriamycin-mediated nitration of manganese superoxide dismutase in the central nervous system: insight into the mechanism of chemobrain. J Neurochem 100, 191-201.

Tangpong, J., Cole, M.P., Sultana, R., Joshi, G., Estus, S., Vore, M., St. Clair, W., Ratanachaiyavong, S., St. Clair, D.K., and Butterfield, D.A. (2006). Adriamycin-induced, TNF-α-mediated central nervous system toxicity. Neurobiology of Disease 23, 127–139.

Tangpong, J., Sompol, P., Vore, M., St Clair, W., Butterfield, D.A., and St Clair, D.K. (2008). Tumor necrosis factor alpha-mediated nitric oxide production enhances manganese superoxide dismutase nitration and mitochondrial dysfunction in primary neurons: an insight into the role of glial cells. Neuroscience 151, 622-629.

Tibar, H., El Bayad, K., Bouhouche, A., Ait Ben Haddou, E.H., Benomar, A., Yahyaoui, M., Benazzouz, A., and Regragui, W. (2018). Non-Motor Symptoms of Parkinson's Disease and Their Impact on Quality of Life in a Cohort of Moroccan Patients. Front Neurol 9, 170.

Trask, P.C., Esper, P., Riba, M., and Redman, B. (2000). Psychiatric side effects of interferon therapy: prevalence, proposed mechanisms, and future directions. J. Clin. Oncol. 18, 2316–2326.

Triplett, J.C., Zhang, Z., Sultana, R., Cai, J., Klein, J.B., Büeler, H., and Butterfield, D.A. (2015). Quantitative expression proteomics and phosphoproteomics profile of brain from PINK1 knockout mice: insights into mechanisms of familial Parkinson's disease. Journal of Neurochemistry 133, 750–765.

Trompier, D., Vejux, A., Zarrouk, A., Gondcaille, C., Geillon, F., Nury, T., Savary, S., and Lizard, G. (2014). Brain peroxisomes. Biochimie 98, 102–110.

Urbahn, M.A., Kaup, S.C., Reusswig, F., Kruger, I., Spelleken, M., Jurk, K., Klier, M., Lang, P.A., and Elvers, M. (2018). Phospholipase D1 regulation of TNF-alpha protects against responses to LPS. Sci Rep 8, 10006.

Vijayanathan, V., Gulinello, M., Ali, N., and Cole, P.D. (2011). Persistent cognitive deficits, induced by intrathecal methotrexate, are associated with elevated CSF concentrations of excitotoxic glutamate analogs and can be reversed by an NMDA antagonist. Behav. Brain Res. 225, 491–497.

Villeneuve, L.M., Purnell, P.R., Boska, M.D., and Fox, H.S. (2016). Early Expression of Parkinson's Disease-Related Mitochondrial Abnormalities in PINK1 Knockout Rats. Mol. Neurobiol. 53, 171–186.

Vitali, M., Ripamonti, C.I., Roila, F., Proto, C., Signorelli, D., Imbimbo, M., Corrao, G., Brissa, A., Rosaria, G., de Braud, F., et al. (2017). Cognitive impairment and chemotherapy:

a brief overview. Critical Reviews in Oncology/Hematology 118, 7–14.

Walker, K.R., and Tesco, G. (2013). Molecular mechanisms of cognitive dysfunction following traumatic brain injury. Front Aging Neurosci 5, 29.

Wang, G., Dinkins, M., He, Q., Zhu, G., Poirier, C., Campbell, A., Mayer-Proschel, M., and Bieberich, E. (2012). Astrocytes secrete exosomes enriched with proapoptotic ceramide and prostate apoptosis response 4 (PAR-4): potential mechanism of apoptosis induction in Alzheimer disease (AD). The Journal of biological chemistry 287, 21384-21395.

Wang, H., Pang, H., Bartlam, M., and Rao, Z. (2005). Crystal Structure of Human E1 Enzyme and its Complex with a Substrate Analog Reveals the Mechanism of its Phosphatase/Enolase Activity. Journal of Molecular Biology 348, 917–926.

Weber, C., and Noels, H. (2011). Atherosclerosis: current pathogenesis and therapeutic options. Nature medicine 17, 1410-1422.

Wefel, J.S., Kesler, S.R., Noll, K.R., and Schagen, S.B. (2015). Clinical characteristics, pathophysiology, and management of noncentral nervous system cancer-related cognitive impairment in adults. CA Cancer J Clin 65, 123–138.

Wefel, J.S., Saleeba, A.K., Buzdar, A.U., and Meyers, C.A. (2010). Acute and late onset cognitive dysfunction associated with chemotherapy in women with breast cancer. Cancer 116, 3348–3356.

Wood-Kaczmar, A., Gandhi, S., Yao, Z., Abramov, A.Y., Abramov, A.S.Y., Miljan, E.A., Keen, G., Stanyer, L., Hargreaves, I., Klupsch, K., et al. (2008). PINK1 is necessary for long term survival and mitochondrial function in human dopaminergic neurons. PLoS ONE 3, e2455.

Wu, Y.Q., Dang, R.L., Tang, M.M., Cai, H.L., Li, H.D., Liao, D.H., He, X., Cao, L.J., Xue, Y., and Jiang, P. (2016). Long Chain Omega-3 Polyunsaturated Fatty Acid Supplementation Alleviates Doxorubicin-Induced Depressive-Like Behaviors and Neurotoxicity in Rats: Involvement of Oxidative Stress and Neuroinflammation. Nutrients 8, 243.

Yang, M., Kim, J.-S., Kim, J., Jang, S., Kim, S.-H., Kim, J.-C., Shin, T., Wang, H., and Moon, C. (2012). Acute treatment with methotrexate induces hippocampal dysfunction in a mouse model of breast cancer. Brain Res. Bull. 89, 50–56.

Yang, Y., Tang, B.-S., and Guo, J.-F. (2016). Parkinson's Disease and Cognitive Impairment. Parkinsons Dis 2016, 6734678.

Yen, H.C., Oberley, T.D., Vichitbandha, S., Ho, Y.S., and St Clair, D.K. (1996). The protective role of manganese superoxide dismutase against adriamycin-induced acute cardiac toxicity in transgenic mice. The Journal of clinical investigation 98, 1253-1260.

Yin, K., Deng, X., Mo, Z.C., Zhao, G.J., Jiang, J., Cui, L.B., Tan, C.Z., Wen, G.B., Fu, Y., and Tang, C.K. (2011). Tristetraprolin-dependent post-transcriptional regulation of inflammatory cytokine mRNA expression by apolipoprotein A-I: role of ATP-binding membrane cassette transporter A1 and signal transducer and activator of transcription 3. The Journal of biological chemistry 286, 13834-13845.

Zhang, F., Zhao, G., and Dong, Z. (2001). Phosphatidylcholine-specific phospholipase C and D in stimulation of RAW264.7 mouse macrophage-like cells by lipopolysaccharide. Int Immunopharmacol 1, 1375-1384.

Zhang, Y., Brady, M., and Smith, S. (2001). Segmentation of brain MR images through a hidden Markov random field model and the expectation-maximization algorithm. IEEE Transactions on Medical Imaging 20, 45–57.

Zhang, Y., Kawedia, J.D., Myers, A.L., McIntyre, C.M., Anderson, P.M., Kramer, M.A., and Culotta, K.S. (2014). Physical and chemical stability of high-dose ifosfamide and mesna for prolonged 14-day continuous infusion. J Oncol Pharm Pract 20, 51–57.

Zhuang, H., Qiang, Z., Shao, X., Wang, H., Dang, Y., Wang, Z., Wu, F., Wei, W., and Li, Y. (2019). Integration of metabolomics and expression of enolase-phosphatase 1 links to hepatocellular carcinoma progression. Theranostics 9, 3639–3652.

VITA

Xiaojia Ren was born in Xi An, Shaanxi, China, where she spent her childhood life. She moved to Beijing, China in 2002. She graduated from Beijing No.2 Middle School in 2008, and then achieved her undergraduate degree at East China University of Science and Technology (ECUST) in Shanghai, China, in 2012. She is familiar with biomolecular and cellular techniques learned during undergraduate time, and familiar with biochemistry and proteomics techniques learned during Ph.D. studies.

SCIENTIFIC PUBLICATIONS FROM THE UNIVERSITY OF KENTUCKY

J. Hayslip, E.V. Dressler, H. Weiss, T.J. Taylor, M. Chambers, T. Noel, S. Miriyala, J.T.R. Keeney, X. Ren, R. Sultana, M. Vore, D.A. Butterfield, D. St Clair, J.A. Moscow, Plasma TNF-α and Soluble TNF Receptor Levels after Doxorubicin with or without Co-Administration of Mesna-A Randomized, Cross-Over Clinical Study, PloS One. 10 (2015) e0124988.

X. Ren, D.K. St. Clair, D.A. Butterfield, Dysregulation of cytokine mediated chemotherapy induced cognitive impairment, Pharmacol. Res. 117 (2017) 267–273.

J.T.R. Keeney, X. Ren* (co-first author), G. Warrier, T. Noel, D.K. Powell, J.M. Brelsfoard, R. Sultana, K.E. Saatman, D.K.S. Clair, D.A. Butterfield, Doxorubicin-induced elevated oxidative stress and neurochemical alterations in brain and cognitive decline: protection by MESNA and insights into mechanisms of chemotherapy-induced cognitive impairment ("chemobrain"), Oncotarget. 9 (2018) 30324–30339.

X. Ren, J.T.R. Keeney, S. Miriyala, T. Noel, D.K. Powell, L. Chaiswing, S. Bondada, D.K. St. Clair, D.A. Butterfield, The triangle of death of neurons: Oxidative damage, mitochondrial dysfunction, and loss of choline-containing biomolecules in brains of mice treated with doxorubicin. Advanced insights into mechanisms of chemotherapy-induced cognitive impairment ("chemobrain") involving TNF-α, Free Radic. Biol. Med. 134 (2019) 1–8.

X. Ren, D. Boriero, L. Chaiswing, S. Bondada, D.K. St. Clair, D.A. Butterfield, Plausible biochemical mechanisms of chemotherapy-induced cognitive impairment ("chemobrain"),

a condition that significantly impairs the quality of life of many cancer survivors, Biochim. Biophys. Acta BBA - Mol. Basis Dis. 1865 (2019) 1088–1097.

X. Ren, A. Hinchie, A. Swomley, D.K. Powell, D.A. Butterfield, Profiles of brain oxidative damage, ventricular alterations, and neurochemical metabolites in the striatum of PINK1 knockout rats as functions of age and gender: Relevance to Parkinson disease, Free Radic. Biol. Med. 143 (2019) 146–152.

X. Ren, D.K. Powell, J. Cai, J.B. Klein, D.A. Butterfield, The proteome of brain of PINK1 KO rats as a function of age. Manuscript in preparation (2020).

X. Ren, Sarah Goebel, Eric Vogt, Angela Hinchie, Martha Mortell, D.A. Butterfield, The mTOR pathway in the brain of PINK1 KO rats. Manuscript in preparation (2020).